

Copyright
by
Vladimir Roznyatovskiy
2011

The Dissertation Committee for Vladimir Roznyatovskiy Certifies that this is the approved version of the following dissertation:

From old porphyrins to novel materials

Committee:

Jonathan L. Sessler, Supervisor

Christopher W. Bielawski

Dionicio Siegel

Bradley J. Holliday

Sean M. Kerwin

From old porphyrins to novel materials

by

Vladimir Roznyatovskiy, B. S.

Dissertation

Presented to the Faculty of the Graduate School of

The University of Texas at Austin

in Partial Fulfillment

of the Requirements

for the Degree of

Doctor of Philosophy

The University of Texas at Austin

August 2011

Dedication

This dissertation is based on the research work that was emotionally supported by my caring and much beloved grandparents, mom, dad and my mentor sister. These chemistry-minded three generations of close relatives were and are truly inspiring examples of persistence, pursuit and perseverance. With the best hope this contribution is very much dedicated to the chemical sciences, and research in general, as a lifetime commitment.

Acknowledgements

The author greatly appreciates the mentorship and scientific freedom provided by Professor Jonathan L. Sessler. The author would also like to thank Professor Zeev Gross, who hosted me in his group in Technion, Israel during my short internship in the Fall 2008. He helped me to start looking at chemistry outside of the box. Professor Christopher W. Bielawski was very helpful in numerous scientific discussions.

From old porphyrins to novel materials

Vladimir Roznyatovskiy, PhD.

The University of Texas at Austin, 2011

Supervisor: Jonathan L. Sessler

The fascinating role that porphyrins play in natural processes such as photosynthesis and respiration, continues to provide a compelling motivation to study these chromophores and to design new analogues with improved functions.

This dissertation describes the interdisciplinary study of several classes of compounds that include π -extended porphyrins, expanded porphyrins, porphycenes, polypyrroles and porphyrins.

Dictated by the need to capture efficiently red and near-infrared light, the so-called π -extension approach has been established as a powerful tool in the synthesis of large aromatic chromophores. Many of these artificial systems demonstrate properties similar to natural porphyrins. Often, however, a reduced bandgap is seen due to a greater π -system. Synthetic challenges associated with the preparation of the linearly annulated porphyrins have long been recognized. Many of these have now been overcome as the result of a newly developed synthetic protocol described in Chapter 1. This protocol allows for the synthesis of a pyrrolic building block under milder conditions. As a continuation of this work, naphthobipyrroles were obtained *via* the π -extension strategy applied to a benzobipyrrole. The utility of this new building block was demonstrated with the syntheses of an electrochromic polynaphthobipyrrolic polymer (Chapter 3) and a dinaphthoporphyrene (Chapter 2), a chromophore isomeric to porphyrin.

Chapter 4 describes a different approach to porphyrin functionalization. Here, the goal was to effect substitution at the so-called β pyrrolic positions with using two bithiophene groups. Although, the resulting product is not completely rigid, enhancement in the sensitizing properties of the basic porphyrin chromophore was seen in a dye sensitized solar cell (DSSC) assembly, as studied by scanning electrochemical microscopy (SECM). The synthetic contributions concerning this work, carried in collaboration with Bard group, are expected to lay the groundwork for the development future photovoltaic materials.

Expanded porphyrins are the more diverse group of porphyrinic derivatives. In effort to develop new conjugated expanded porphyrin systems and to understand their spectroscopic behavior in greater detail, a set of expanded porphyrins, based on the direct electrochemical oxidation of terpyrrole-like fragments, was developed in conjunction with the Bucher group (Grenoble, France). This effort is described in Chapter 5. Specifically it is shown that trithiacyclo[9]pyrrole may be prepared by means of an electrochemical synthesis.

Table of Contents

List of Tables	xi
List of Figures	xii
Introduction.....	1
Chapter One. Linearly Annulated Porphyrins, π -Extension Approach.	2
Synthetic routes to linearly annulated π -extended porphyrins.	6
Template condensation.	6
Retro-Diels-Alder route.	7
Tetrahydroisindole approach.	8
Dihydroisindole in the synthesis of π -extended systems.	9
Experimental section.....	17
4-Chloro-5-(phenylthio)-cyclohexene (1.16):	17
4-Chloro-5-(phenylsulfonyl)-cyclohexene (1.17):.....	18
(1,4-Cyclohexadien-1-ylsulfonyl)-benzene (1.18):	18
2H-Isoindole-1-carboxylic acid, 4,7-dihydro-, ethyl ester (1.20a):	19
Octamethyl calix[4]4,7-dihydroisindole 1.45:	19
Chapter Two: π -Extension in Porphyrin Analogs.	21
π -extended boron-dipyrromethanes.	21
π -extended sapphyrins.	25
π -extended porphycenes.	29
Dinaphthoporphycenes	32
Experimental section.....	41
General procedure for the synthesis of ethyl α -oxocarboxylates 2.51a and 2.51b:	41
Ethyl 2-oxo-4-ethyl-octanoate 2.51a.	42
Ethyl 2-oxo-4-methyl-pentanoate 2.51b.	42
General procedure for the synthesis 2,3-(Ethyl alkynoate-2)- naphthelenehydrazone 2.53a-c.....	42
2,3-(Ethyl 4-ethyl-octanoate-2)-naphthelenehydrazone 2.53a. ..	42
2,3-(Ethyl 4-methylpentanoate-2)-naphthelenehydrazone 2.53b.	43
2,3-(Ethyl propanoate-2)-naphthelenehydrazone 2.53c.....	43

General procedure for the synthesis of diethyl 3,8-dialkyl-1,10-dihydro-benzo[e]pyrrolo[3,2-g]indole-2,9-dicarboxylates 2.54a-c.....	44
Diethyl 3,8-di-1-ethylpentyl-1,10-dihydro-benzo[e]pyrrolo[3,2-g]indole-2,9-dicarboxylate 2.54a.....	44
Diethyl 3,8-diisopropyl-1,10-dihydro-benzo[e]pyrrolo[3,2-g]indole-2,9-dicarboxylate 2.54b.	45
Diethyl 1,10-dihydro-benzo[e]pyrrolo[3,2-g]indole-2,9-dicarboxylate 2.54c.	45
General procedure for the synthesis of 3,8-dialkyl-1,10-dihydro-benzo[e]pyrrolo[3,2-g]indole 2.50a-c.....	45
3,8-Di-1-ethylpentyl-1,10-dihydro-benzo[e]pyrrolo[3,2-g]indole 2.50a.....	45
3,8-Diisopropyl-1,10-dihydro-benzo[e]pyrrolo[3,2-g]indole 2.50b.	46
General procedure for the synthesis of 2,9-diformyl-3,8-dialkyl-1,10-dihydro-benzo[e]pyrrolo[3,2-g]indoles 2.55a,b	46
2,9-diformyl-3,8-di-1-ethylpentyl-1,10-dihydro-benzo[e]pyrrolo[3,2-g]indole 2.55a.	46
2,9-diformyl-3,8-diisopropyl-1,10-dihydro-benzo[e]pyrrolo[3,2-g]indole 2.55b.	47
General procedure for the synthesis of 2,7,12,17-tetraalkylporphycenes 2.56a,b.	47
2,7,12,17-Tetra-1-ethylpentylporphycene 2.56a.....	48
2,7,12,17-Tetraisopropylporphycene 2.56b.	48
Chapter Three. Polynaphthobipyrrole	49
Electrochemistry.	55
Morphology of the polymer film	59
Spectroelectrochemistry.....	61
Experimental section.....	66
2,3-(Ethyl pentanoate-2)-naphthalenehydrazone 3.5.	66
3,8-Diethyl-1,10-dihydro-benzo[e]pyrrolo[3,2-g]indole-2,9-dicarboxylic acid, 2,9-diethyl ester 3.6.	67
3,8-Diethyl-1,10-dihydro-benzo[e]pyrrolo[3,2-g]indole 3.1	67

Chapter Four. A Method for Rapid Screening of Photosensitizers by Scanning Electrochemical Microscopy (SECM) and the Synthesis and Testing of a Porphyrin Sensitizer	69
Sensitizer design considerations	71
Synthesis of the porphrin-based sensitizers	72
Photoelectrochemistry	73
Experimental Section	84
Porphyrin 4.2	84
Diiodoporphyrin 4.6	85
Porphyrin 4.1	86
Preparation of TiO ₂ nanotubes/Ti foil substrate.	86
Preparation of photosensitizer arrays	87
Screening of the array	87
Preparation and photoelectrochemical measurements of bulk samples ..	88
Chapter Five. Electrochemical Synthesis of a Thiophene-containing Cyclo[9]pyrrole	89
Experimental Section	105
Synthesis of 2,5-bis(3,4-diethyl-2-pyrrolyl)thiophene (5.5H ₂)	105
Electrosynthesis of the bis protonated dodecaethyl-substituted thiophene-containing cyclo[9]pyrrole [5.4H ₆]•2TFA	105
References	107

List of Tables

Table 3.1. UV-Vis spectral features of selected polypyrrole polymers.....	64
Table 4.1. Spectroscopic data for porphyrin 4.1 , control porphyrin 4.2 , and N719 recorded in DCE.	83
Table 5.1. Optical and electrochemical properties of [5.1H₆]•2Cl, [5.2H₇]•2Cl, [5.3H₈]•2Cl, and [5.4H₆]•2TFA.	98

List of Figures

Figure 1.1: UV-vis absorption spectra of a series of expanded porphyrins with different number of pyrrolic units.....	2
Figure 1.2. General structures of the linearly annulated π -extended porphyrins.....	4
Figure 1.3. Light absorption spectra of π -extended zinc <i>meso</i> -tetraphenyl porphyrins: black line – parent porphyrin, red line – tetrabenzoporphyrin, green line – tetranaphthoporphyrin.....	4
Figure 1.4. Schematic representation of the energy transfer (ET) processes underlying in the triplet-triplet annihilation (TTA) and up conversion events.....	5
Figure 1.5: Templated synthesis of linearly annulated porphyrins.....	6
Figure 1.6. Retro-Diels-Alder approach to the synthesis of π -extended porphyrins.....	7
Figure 1.7: Synthesis of monobenzoporphyrin by oxidative aromatization.	8
Figure 1.8. Synthesis of tetrabenzoporphyrins from tetrahydroisindole precursors.	9
Figure 1.9. Early attempt in the synthesis of dihydroisindole.	9
Figure 1.10. Synthesis of dihydroisindole.	11
Figure 1.11. Equilibrium between allyl and vinyl sulfones.....	12
Figure 1.12. Synthesis of dihydroisindole by Cheprakov and coworkers.	12
Figure 1.13. Synthesis of symmetrical tetrabenzoporphyrins from dihydroisindole.	13
Figure 1.14. Synthesis of π -extended dipyrromethane precursors.	13
Figure 1.15. Synthesis of unsymmetric tetrabenzoporphyrins.....	14
Figure 1.16. Dihydroxylation of the dihydroisindole precursor 1.20b	15
Figure 1.17. Porphyrin synthesis using diacetoxytetrahydroisindole.	15
Figure 1.19. The use of dihydroisindole in the synthesis of calixpyrrole.....	16

Figure 1.18. An inverse Diels-Alder reaction in the functionalization of dihydroisindole and its role in the π -extended porphyrin synthesis.	16
Figure 2.1: Normalized fluorescence emission spectra of a series BODIPY dyes as recorded in methanol: 1 - FL, 2 - R6G, 3 - TMR, 4 - 581/591, 5 - TR, 6 - 630/650, 7 - 650/665.	22
Figure 2.2: Synthesis of π -extended boron-dipyrromethene (BODIPY) dyes.	22
Figure 2.3. BODIPY dyes containing fluorantho[8,9- <i>f</i>]isindole unites.	23
Figure 2.4. a. Normalized absorption spectra of the 2.9a , 2.9b , 2.8a , 2.9c , 2.9d , 2.11a , 2.11d and 2.11c (from left to right). b. Colors of the dyes under ambient (top) and UV (bottom) light.	23
Figure 2.5. Variously substituted aza-BODIPY dyes and their corresponding absorption maxima given in nm.	24
Figure 2.6. Synthesis of a monoisindole saphyrin.	25
Figure 2.7. Synthesis of the diisindole saphyrin.	26
Figure 2.8. Synthesis of the π -extended trithiasaphyrins.	28
Figure 2.9. Synthesis of benzosaphyrin.	29
Figure 2.10. Synthesis of linearly annulated porphycenes.	30
Figure 2.11. Synthesis of naphthobipyrroles. Structure 2.50 shows accepted position numeration.	32
Figure 2.12. ^1H NMR spectra of the two different isomers of 2.53c . (A) corresponds to the more polar conformer and (B) corresponds to the less symmetrical and less polar fraction.	34
Figure 2.13 ^1H NMR spectra (low field portion) of porphycene 2.54a recorded in DMSO- d_6 at 27 °C (bottom) and 100 °C (top).	35
Figure 2.14. Synthesis of naphthobipyrroles.	37
Figure 2.15. ^1H NMR spectra (low field portion) of porphycene 2.56a in toluene- d_8 at 27 °C (bottom) and 100 °C (top).	38

Figure 2.16. UV-vis spectra for 2.56a and 2.56b recorded in dichloromethane (0.11 mM).....	39
Figure 2.17. Three orthogonal views of the X-ray structure of 2.56b . All hydrogen atoms bound to carbon atoms are omitted for clarity. Thermal ellipsoids were scaled to the 50% probability level.	41
Figure 3.1. Formation of polynaphthobipyrroles. A. Coupling reactions proposed by Nadeau and Swager; B. Alternative structures that could arise from reaction of 3.2 or 3.3 ; C. Regiocontrolled electropolymerization. ...	53
Figure 3.2 Synthesis of the 3,8-diethyl-1,10-dihydro-benzo[e]pyrrolo[3,2-g]indole	54
Figure 3.3. Cyclic voltammograms of 3.1 oxidation (1st cycle) and polymer growth observed during repeated oxidation cycles (1-4th cycles – thick line; after this, every 5th cycle up to the 40th cycle is shown) vs. Ag/Ag ⁺ . The scan rate is 50 mV/s. Arrows denote the evolution of voltammograms as the cycle number increases	56
Figure 3.4. Absorption spectra of 5 mM solutions 3.1 in 0.1 M LiClO ₄ recorded in MeCN before electrooxidation (dashed line) and after electropolymerization under conditions of cyclic voltammetry (solid line). Because of its high optical density, the sample obtained via electropolymerization was subject to a 20-fold dilution with background electrolyte solution prior to recording the spectrum.	57
Figure 3.5. Typical cyclic voltammograms recorded for films of poly3.1 deposited on an ITO substrate (0.1 M LiClO ₄ , MeCN) vs. Ag/Ag ⁺ at (a) 5, (b) 20, (c) 50, (d) 100 mV/s.	59
Figure 3.6. Scanning electron microscopy images of poly3.1 film deposited on an ITO electrode taken after equilibration of the film in a background electrolyte solution (0.1 M LiClO ₄ , MeCN). Enlargement is (a) 500x, (b) 2000x.....	60

Figure 3.7. Results of spectroelectrochemical studies of **poly3.1** film deposited on an ITO electrode. The measurements were conducted in MeCN, 0.1 M LiClO₄ with 100 mV steps between +0.9 V and -0.6 V vs. a Ag pseudo reference electrode (each step is 60 s long). Inserts show photographs of the polymer films as obtained at potentials of (a) -0.6 V, (b) 0.0, (c) +0.3 and (d) +0.9 V. Arrows denote changes in the spectra associated with a decrease in the applied potential.62

Figure 3.8. Current transients and changes in the absorbance features of **poly3.1** film supported on an ITO electrode (solid lines) at 700 nm observed upon repetitive switching of the applied potential between -0.7 and +1.0 V (dotted line) in 0.1 M LiClO₄, MeCN.65

Figure 4.1. Synthesis of the porphyrin-based sensitizers.72

Figure 4.2. Top and side views of a single crystal X-ray diffraction structure of porphyrin **4.1** showing two orientations of the bithiophene substituents. All hydrogen atoms are omitted for clarity. Thermal ellipsoids are scaled to the 50% probability level.73

Figure 4.3. SEM image of TiO₂ nanotubes anodized at 20 V in ethylene glycol/water (99:1, volume ratio) with the addition of 0.5 wt.% NH₄F.74

Figure 4.4. (a) Dispensed pattern of a **N719** sensitizer array. Shown are number of drops dispensed at a given location. SECM images of **N719** sensitizer on TiO₂ nanotubes/Ti foil at an applied potential of 0.2 V vs AgQRE (quasi reference electrode) under (b) UV-visible and (c) visible light ($\lambda > 420$ nm). Scan rate: 500 $\mu\text{m/s}$ (SECM setting 50 $\mu\text{m}/0.1$ s); solution, 0.1 M TBAI in MeCN.76

Figure 4.5. (a) Dispensed pattern of three different kinds of dye arrays. SECM images of three different kinds of dyes on TiO₂ nanotubes/Ti foil at applied potential of 0.5 V vs an AgQRE under (b) UV-visible and (c) visible light. Scan rate: 500 μm/s (SECM setting 50 μm/0.1 s); solution, 0.1 M TBAI in MeCN.77

Figure 4.6. (a) Dispensed pattern of dye arrays. The first spot in the first row is 100% **N719**. The first and second numbers inside each circle represent the number of drops of **N719** and porphyrin **4.1**, respectively. (b) SECM image of dyes on TiO₂ nanotubes/Ti foil at an applied potential of 0.2 V vs an AgQRE under visible light. Scan rate: 500 μm/s (SECM setting 50 μm/0.1 s); solution, 0.1 M TBAI in MeCN.80

Figure 4.7. Linear sweep voltammograms (LSVs) of (a) control porphyrin **4.2** and (b) porphyrin **4.1** and (c) **N719** bulk films in MECN with 0.1 M TBAI as the sacrificial reagent under dark, visible, and UV-visible light irradiation. Scan rate: 20 mV/s. Exposed electrode area, ~ 0.2 cm².81

Figure 4.8. UV-visible absorption spectra of porphyrin **4.1**, control porphyrin **4.2**, and dye **N719** measured in dichloroethane.....82

Figure 5.1. Representation of the previously reported cyclo[n]pyrroles [**5.1H₆**]²⁺, [**5.2H₇**]²⁺, [**5.3H₈**]²⁺ and of the novel thiophene-containing cyclo[9]pyrrole [**5.4H₆**]²⁺ as well as its bispyrrolylthiophene precursor **5.5H₂**.90

Figure 5.2. Cyclic voltammograms of 1 mM solution of **5.5H₂** in 0.1 M TBAP/CH₂Cl₂ recorded at. r.t. using a glassy carbon working electrode (Ø = 3 mm, Ag/AgNO₃ reference electrode, scan rate 100 mV/s). Full line: **5.5H₂**; dashed line: **5.5H₂** after adding 1 molar equivalence of sym-collidine; inset: First oxidation wave of **5.5H₂**.....91

Figure 5.3. Cyclic voltammogram (solid line) and voltammogram at a rotating disk (dashed line) of 5.5H₂ and 1 molar equivalence of decamethylferrocene recorded in 0.1 M TBAP/CH ₂ Cl ₂	92
Figure 5.4. Schematic representation of the coupled electrochemical-chemical coupled processes leading to the formation of [5.4H₆] •SO₄ from three molecules of 5.5H₂	93
Figure 5.5. Time-dependent evolution of the UV/Vis spectra observed during an analytical scale electrolysis of 5.5H₂	95
Figure 5.6. UV/Vis/NIR absorption spectrum of [5.4H₆] •2TFA in CH ₂ Cl ₂ (11 μM, l = 1 cm).	97
Figure 5.9. Cyclic voltammogram (continued line) and voltammogram at a rotating disk (dashed line) recorded at r.t. of 0.135 mM solution of [5.4H₆] •2TFA (left) and [5.4H₆] •2TFA neutralized by 1200 molar equivalents of <i>sym</i> -collidine (right) in 0.1 M TBAP/CH ₃ CN, Pt metal wire counter and Ag/AgNO ₃ 0.01 M in 0.1 M TBAP/CH ₃ CN reference electrodes. CV: 2-mm Pt disk working electrode, 100 mV/s. RDE: 3-mm glassy disk carbon tip working electrode, 10 mV/s, 500 rd/min.	100
Figure 5.10. UV-Vis-NIR spectroelectrochemical signatures for [5.4H₆] ²⁺ recorded periodically during CV scans conducted in 0.1 M TBAP/CH ₃ CN in the presence of TFA (> 20 molar equivalents) on a platinum gauze (WE) inserted in a 1 mm slit inside a quartz electrochemical cell. Scan rate: 100 mV/s. (a) monoreduced form, [5.4H₆] ⁺ , recorded upon scanning the WE potential from 0 to -140 mV and electrolysis at -140 mV for 45 s, (b) monooxidized form, [5.4H₆] ³⁺ , recorded upon scanning from 0 to +230 mV followed by an electrolysis at +230 mV for 45 s, (c) doubly oxidized form, [5.4H₆] ⁴⁺ , recorded upon scanning from 0 to +475 mV followed by an electrolysis at 475 mV for 45 s.	103

Introduction

Porphyryns, cyclic, conjugated systems containing pyrroles, have been one of the major research foci of chemists over the course of the last two centuries. Hans Fischer, 1930 Nobel Prize awardee, elucidated the chemical structure of various porphyryns, including heme, the pigment responsible for oxygen binding in erythrocytes. This early 20th century work on red cell active species and Fischers contributions to our understanding of the structure and properties of the other porphyryns, e.g. bile pigments and chlorophyll, serves as an historical landmark. Since then, numerous porphyryns and porphyryns-like biomolecules have been discovered and studied. Their biosynthesis, metabolism and functions have been studied in great detail, not to mention a great variety of synthetic and artificial analogs that were also designed and prepared. Another motivation for work in the area of porphyryns research that may allow a more detailed understanding of photosynthesis, cell respiration and oxygen transport processes is effectiveness and ingenuity with which these processes operate in nature. Indeed, at present considerable effort is being devoted to the design of artificial solar cells, water splitting catalysts, etc. that are based on porphyryns and porphyryns analogues. Considerable work in the Sessler group has been focused on expanded porphyryns. The goal of this dissertation has been to contribute to this body of understanding and develop functional systems that exploit the unique features of porphyryns and expanded porphyryns.

Chapter One. Linearly Annulated Porphyrins, π -Extension Approach.

Porphyrins and expanded porphyrins have been studied in conjunction with hydrocarbon aromatic molecules.^{1,2} Initially this was done in an effort to understand Huckel aromaticity. More recently, this work has been motivated by a desire to make and understand Mobius conjugated belts. Following the $4n+2$ rule, the original porphyrin core with 18 π electrons has been expanded through synthesis. This has led to a number of novel systems with a greater number of pyrrolic units (5 or more) and varying quantity of

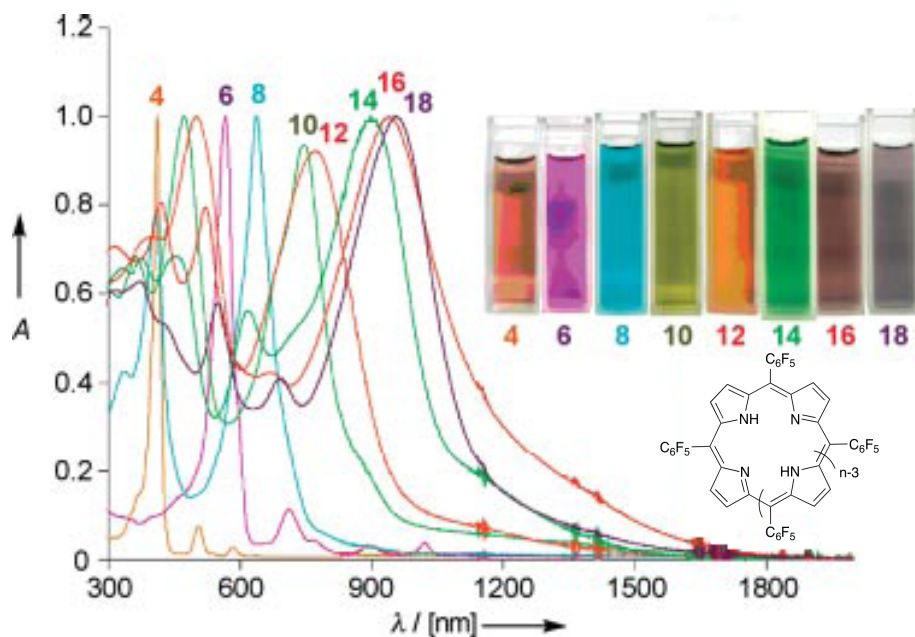
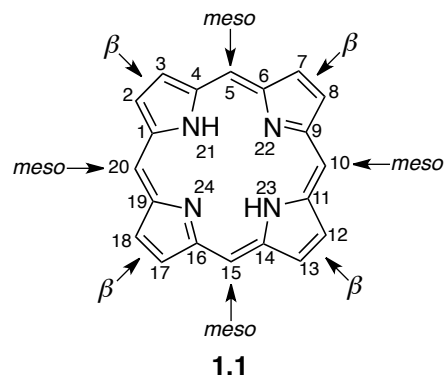


Figure 1.1: UV-vis absorption spectra of a series of expanded porphyrins with different number of pyrrolic units.

connecting carbon atoms between them, the so-called *meso* groups. This approach to

larger size macrocycles proved effective in the design and synthesis of highly colored compounds,³ whose excitation energies cover the entire solar spectrum (at the earth surface), including near IR frequencies (Figure 1.1). These chromophores commonly exhibit nonlinear absorption behavior; this feature, coupled with their redox behavior, has led to a variety of proposed applications in medicine and materials research. Unfortunately, with a larger number of electrons in a formally conjugated molecular circuit and as the ring size of the porphyrinoids in question increases, the stability under ambient conditions decreases. This represents a serious drawback. Compounding the problem are synthetic challenges associated with the synthesis of target porphyrinoids. Moreover, it is now apparent that upon reaching a certain ring size, further expansion does not result in a decrease in the excitation energy (bathochromic shift).⁴ In other words the π -system becomes saturated (Figure 1.1). Geometrical distortions are also more prominent in expanded systems and thus additionally reduce the diatropic current.

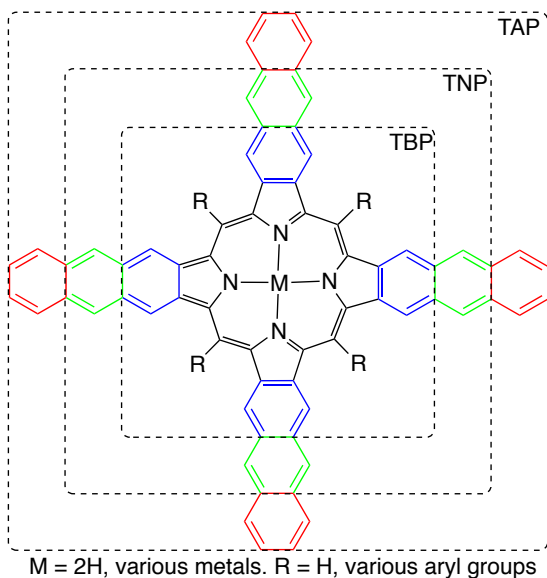


Figure 1.2. General structures of the linearly annulated π -extended porphyrins.

relatively high chemical stability, together with a reduced HOMO-LUMO gap (Figure 1.3), has made this family of so-called π -extended porphyrins very attractive for use in certain applications. As a result, an increasing number of reports have been devoted in literature to these macrocycles, including several major reviews.⁵⁻⁷

Alternatively, formal annulations of benzo-, naphtha- and anthro fragments at the so-called β -positions of the pyrrole units in the parent porphyrin **1.1** produces benzo- (TBP), naphtho- (TNP) and anthraporphyrins (TAP), respectively (Figure 1.2). Such porphyrin derivatization preserves the size of the macrocycle, and therefore its stability, compared to the expanded porphyrins. Nevertheless, significant bathochromic shifts have been observed upon formal addition of each phenyl ring. The

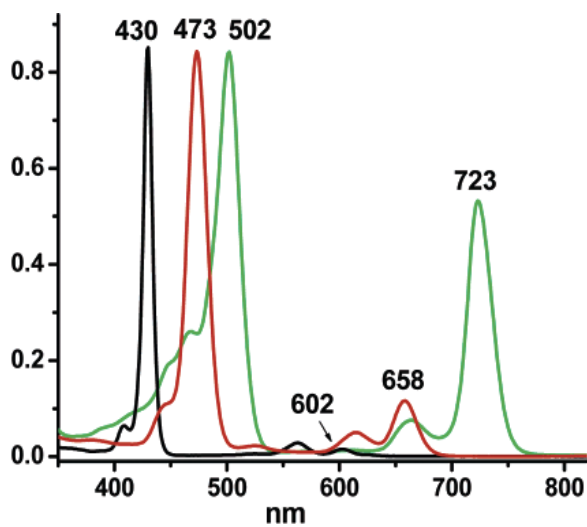


Figure 1.3. Light absorption spectra of π -extended zinc *meso*-tetraphenyl porphyrins: black line – parent porphyrin, red line – tetrabenzoporphyrin, green line – tetranaphthoporphyrin.

Several photophysical features of the π -extended porphyrins are important to mention in order to explain and justify all the synthetic efforts undertaken in the development of general and simple routes to these systems. As expected, decreasing the band-gap (a consequence of π -extension) results in a red-shift in the absorption spectra, with some reports reaching near IR energies (800 nm for ZnTAP). Linearly annulated porphyrins also show significantly larger emission quantum yields, e.g. 41% for the TBPs, while for typical non-extended porphyrins this value is no larger than 1%. Platinum and palladium complexes of these systems are also unique due to their relatively increased phosphorescence intensity. The latter process is sensitive to the presence of oxygen. This led to the construction of dendrimer-encapsulated platinum π -extended porphyrin complexes for the sensing of oxygen *in vivo*.^{8,9} This energy transfer from the excited porphyrin triplet state to oxygen molecules, as well as tunable absorptions in the red portion of the visible region are necessities in photodynamic therapy (PDT) applications. Altogether, these findings led to the use of the platinum and

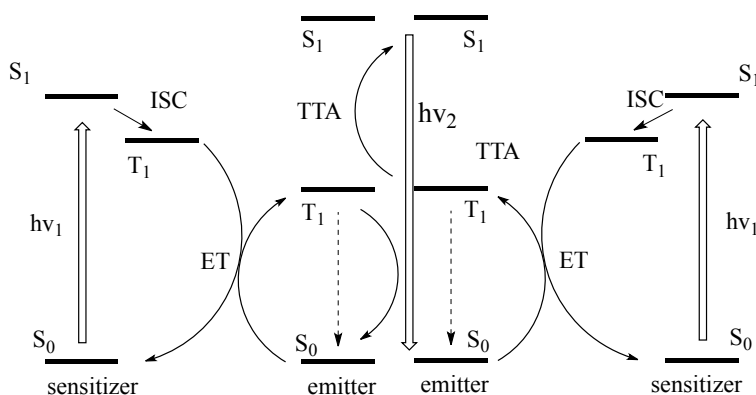


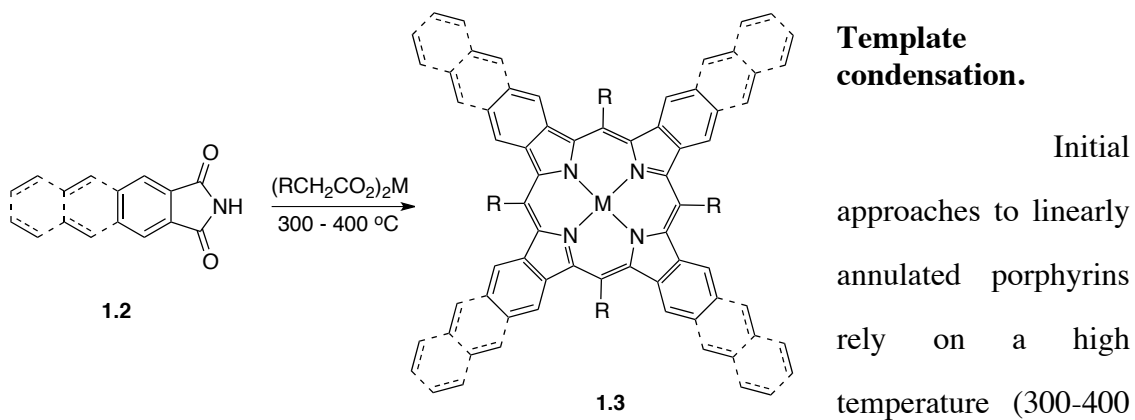
Figure 1.4. Schematic representation of the energy transfer (ET) processes underlying in the triplet-triplet annihilation (TTA) and up conversion events.

palladium porphyrins, especially those with extended π -systems, in triplet-triplet annihilation up-conversion experiments (Figure 1.4). Due to effective formation of the triplet excited state, porphyrin complexes act as sensitizers, which through

an energy transfer event convert emitter molecules (typically oligoarenes such as rubrene and perylene) into their excited triplet states. The latter states, *via* triplet-triplet annihilation, produce an excited singlet state of the emitter molecule. Final relaxation to

the ground state results in an emission of higher energy than the initial excitation frequency (Figure 1.4). The advantages of this process include the use of low excitation power and a noncoherent light source. The red shifted absorption typical of linearly annulated porphyrin complexes allows for greater energy up-conversion. Tetrabenzo- and tetranaphthoporphyrins, in the form of their platinum and palladium complexes, in combination with perylene and tetracene, respectively, characterized by a hypsochromic shift in emission by ~ 0.8 eV compared to the excitation energy (conversion of the red light in the 640-700 nm region into blue light of the 450-480 nm region). In order to take advantage of these promising physical and chemical properties, the requisite chromophore needs to be available on large scale. Therefore, all synthetic challenges associated with their preparation need to be met. A key challenge is thus to develop more efficient routes to π -extended porphyrin chromophores, including intermediate synthons.

SYNTHETIC ROUTES TO LINEARLY ANNULATED π -EXTENDED PORPHYRINS.



Template condensation.

Initial approaches to linearly annulated porphyrins rely on a high temperature (300-400 °C) reaction between phthalimide, or its

Figure 1.5: Templated synthesis of linearly annulated porphyrins. Despite the fact that this protocol consists of only one step, extremely harsh conditions limit the use

of functionalized reagents. Furthermore, yields of the products are typically low, and isolation commonly requires several chromatographic purifications.

Retro-Diels-Alder route.

Ono and coworkers reported a general procedure for preparing π -extended porphyrins, that exploits the presence of an ethano-bridge in the bicyclic pyrrolic reagents

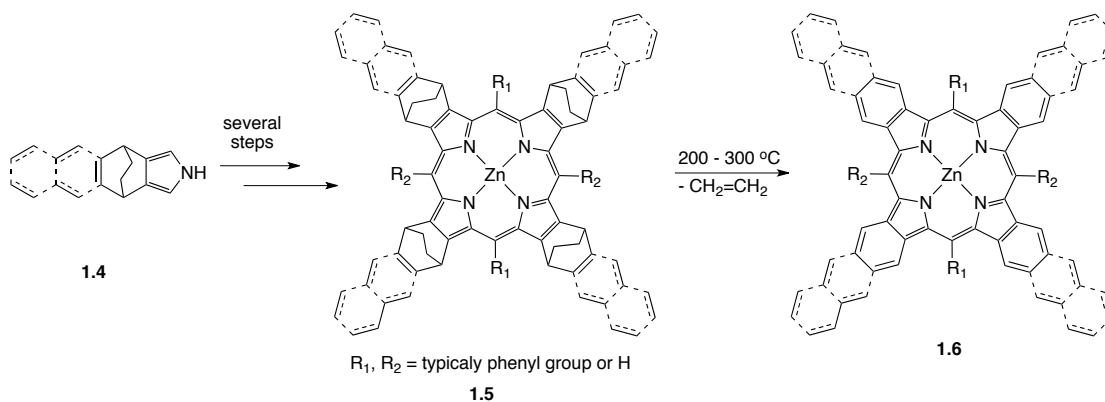


Figure 1.6. Retro-Diels-Alder approach to the synthesis of π -extended porphyrins.

and takes advantage of a retro-Diels-Alder reaction.⁷ This method allows the construction of various substituted (both symmetrically and asymmetrically) porphyrins. The ethano bridge acts as a protecting group in this approach by preventing unwanted oxidation from occurring during the early steps. A final retro-Diels-Alder reaction deprotects the masked isoindole fragment and leads to a fully aromatized system in excellent yield. Unfortunately, the very high temperature in the final step limits the number of compatible substituents (in both the *meso* positions and on the fused arene groups). Nevertheless, this procedure is useful for the *in situ* generation of layers of the annulated product on a surface. This is especially advantageous in the case of non-soluble compounds that cannot be otherwise processed. One clear downside to this strategy is that the synthesis of the starting bicyclic pyrroles often requires several steps and includes tedious purification procedures.

Tetrahydroisoidole approach.

In 1993 Lash showed that a saturated cyclohexane ring fused to a porphyrin core can be aromatized to produce the corresponding monobenzoporphyrin containing isoidole fragment by treatment with dichlorodicyanoquinone (DDQ) in toluene solution

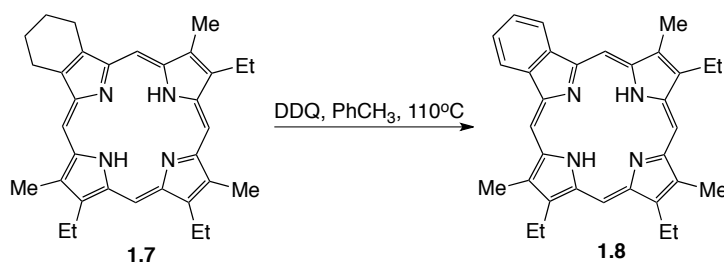


Figure 1.7: Synthesis of monobenzoporphyrin by oxidative aromatization.

under refluxing conditions (Figure 1.7).¹⁰ This finding received little note in the porphyrin community until recently, when Cheprakov and coworkers proved this synthetic tool useful in the synthesis of tetrabenzoporphyrins (Figure 1.8).¹¹ While, the partially-saturated free base porphyrin **1.9** (no metal coordinated inside the core) did not lead to the desired product, the corresponding Ni, Pd and Cu complexes could be readily produced in their fully aromatized forms. It is worth mentioning that although zinc is one of the most commonly used cations in synthetic porphyrin chemistry, its application in the aforementioned transformation proved unproductive. Presumably this reflects competitive demetalation during the key DDQ-mediated oxidation step. Another limitation of this chemistry is that only the copper tetrabenzoporphyrin could be demetalated to form the corresponding free base tetrabenzoporphyrin **1.11** (Figure 1.8). The generally greater stability of metalated π -extended porphyrins compared to the metal-free forms became apparent as the copper complex was subject to demetalation. Specifically, treatment with warm sulfuric or polyphosphoric acids gave only a low yield of **1.11**, presumably because the metal-free form produced *in situ* is actually unstable under the reaction conditions.

In search of a better protocol, naphthalene was tested as the solvent for free base porphyrin **1.9** aromatization and found effective. Alternately, it was found that tetraphenylcyclopentadienone **1.10** could be used as both an oxidant and as a solvent in

the same transformation. Despite this latter success, it is important to appreciate that these aromatization reactions require extremely high temperatures. Therefore tetrabenzoporphyrins with only robust substituents can be prepared *via* this method. However, if only the simplest Ni or Pd aryl-substituted chromophores are required, the low cost and synthetic availability of the requisite tetrahydroisoindole precursor are certainly attractive factors.

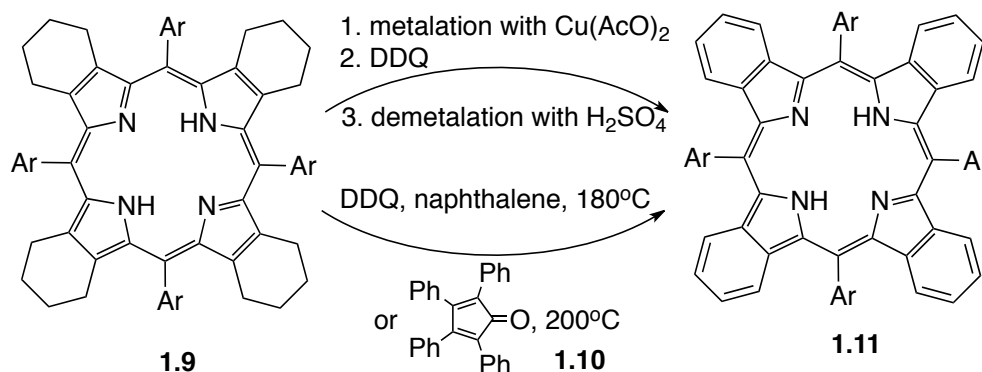


Figure 1.8. Synthesis of tetrabenzoporphyrins from tetrahydroisoindole precursors.

DIHYDROISOINDOLE IN THE SYNTHESIS OF π -EXTENDED SYSTEMS.

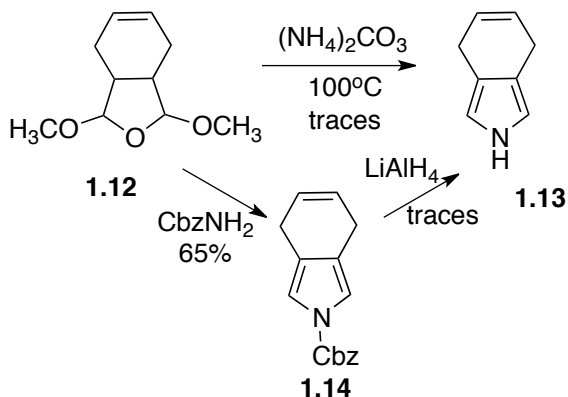


Figure 1.9. Early attempt in the synthesis of dihydroisoindole.

Harsh conditions (during at least the aromatization step) in the previous preparations of linearly annulated porphyrins are a recognized problem that may have precluded the further development of these chromophores. Given their origins in nature, it is perhaps not surprising porphyrins, including alkyl

substituted derivatives, are relatively sensitive compounds. Therefore, precursors to the fully conjugated targets need to be energetically as close to the products as possible in

order to avoid harsh reaction conditions and decomposition of any incipient product. On the other hand, the precursor materials must be sufficiently stable so as to avoid decomposition. Dihydroisindole **1.13** is an obvious choice. Its stability, which lies in between the stable tetrahydroisindole and the extremely unstable isindole, is attractive. Nevertheless, the seeming lability of dihydroisindole left this bicycle relatively understudied. In fact very few reports concerning its synthesis and properties have appeared. For example, Fuhrhop and coworkers investigated the synthesis of **1.13** (Figure 1.9).¹² Here, 1,3,3a,4,7,7a-hexahydro-1,3-dimethoxyisobenzofuran was used to form the corresponding dihydroisindole, *via* both 1) reaction with ammonium carbonate at 100 °C, and 2) using the carbobenzyloxy protected derivative. In either strategy only a trace amount of target molecule was seen. Harsh reaction conditions that most likely facilitate product decomposition led the authors to deem dihydroisindole as unstable and therefore not a valuable precursor.

In spite of the above precedent, the candidate succeeded in preparing dihydroisindole. Starting with 1,4-cyclohexadiene we constructed a pyrrole ring using five steps. None of these steps require chromatographic purification. Moreover the first three of which can be run in one pot (Figure 1.10). Here, phenyl sulfenyl chloride was first reacted with 1,4-cyclohexadiene in dry dichloromethane at r.t. Even though the two double bonds in 1,4-cyclohexadiene are not conjugated, addition of 1.1 equiv. of sulfenyl chloride when added slowly to the reaction mixture, produced the desired precursor **1.16** in quantitative yield. This intermediate was treated with meta-chloroperbenzoic acid (mCPBA) to convert the thioether group into the corresponding sulfonyl. Even a slight excess (2.2 equiv.) of mCPBA in this step resulted in quantitative formation of the compound **1.17**. Although the double bond present in **1.17** can be oxidized to the corresponding epoxide,^{13,14} under our conditions the sulfur atom most likely reacted relatively faster. Elimination of hydrogen chloride from **1.17** led to the vinylsulfone derivative **1.18**. Although 1,8-diazabicyclo[5.4.0]undec-7-ene (DBU) worked very well

as a base in this latter step, triethylamine, a considerably cheaper base, was also tested successfully. It too gave product. Unfortunately, under the unoptimized experimental conditions used to produce **1.18**, chromatographic purification of the product was

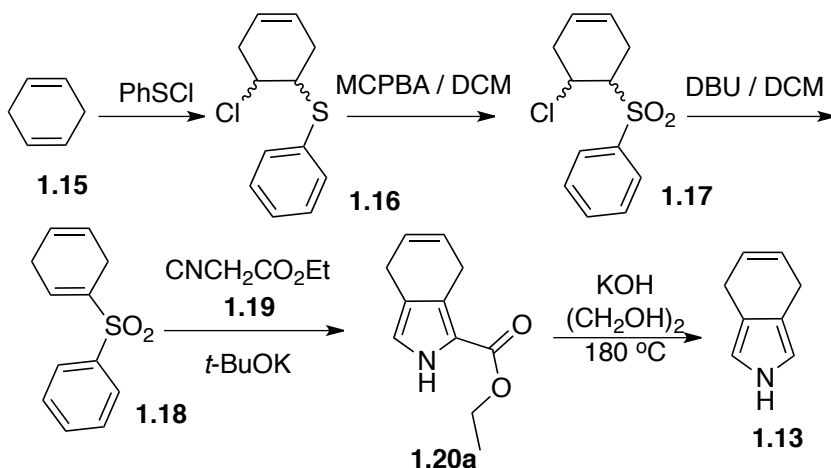


Figure 1.10. Synthesis of dihydroisoindole.

required. Vinylsulfones, similar to nitroalkenes, act as Michael acceptors, and are found to be particularly important in the so-called Barton-Zard reaction,¹⁵ in which ethyl isocyanoacetate typically reacts with a nitroalkene under basic conditions, resulting in the formation of a pyrrolic ring. Therefore, using this approach the ethyl 4,7-dihydroisoindolecarboxylate **1.20a** could be obtained. This precursor demonstrates the stability, characteristic of pyrroles in general. Further, it can be stored under ambient conditions for several months. Saponification and decarboxylation, conducted in one pot, resulted in formation of the 4,7-dihydroisoindole in excellent yield. Bicycle **1.13** can be stored in a freezer in the absence of light for several weeks without major decomposition. The stability of **1.13** is rationalized in terms of the greater reactivity of the pyrrolic ring, compared to a simple alkene functional group. However under normal conditions and with exposure to air, this compound undergoes darkening over the course of a few days, concomitantly degrading, most likely *via* oxidation to unstable isoindole fragments.

It is worth noting that vinyl sulfone exists in equilibrium with its isomeric allylic sulfone **1.21**.^{16,17} As evident from the ¹H NMR spectrum, a ratio of **1.18** to **1.21** (Figure 1.11) (the vinyl form to the allyl isomer) is close to 2:1. Elimination reaction conducted

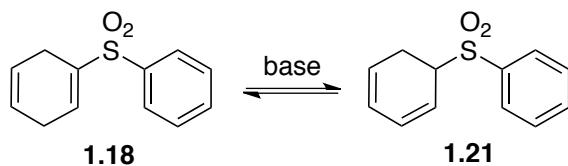


Figure 1.11. Equilibrium between allyl and vinyl sulfones.

at lower temperature (-40 °C) yielded the same proportion of the isomers compared to the r.t. experiment. This finding supports the existence of an equilibrium, as opposed to the formation of two products

independently. The former sulfone does not react as Michael acceptor in the Barton-Zard reaction. However, the basic conditions required for this transformation favors conversion of the allylic form into the corresponding vinyl isomer.

Support for the utility of our proposed strategy, came in the form of an independent synthesis of dihydroisindole (Figure 1.10), reported by Cheprakov and coworkers (Figure 1.12) while this project was ongoing.¹⁸ In both approaches, ours and

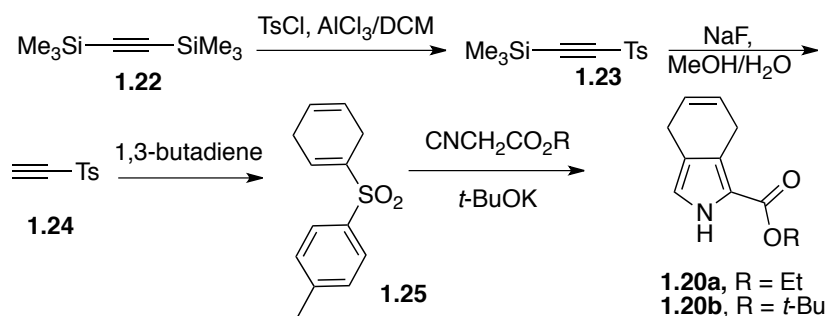


Figure 1.12. Synthesis of dihydroisindole by Cheprakov and coworkers.

Cheprakov's, the Barton-Zard reaction was employed to effect pyrrole ring formation; however, the synthetic route to the vinyl sulfone

precursors was qualitatively different. The vinyl sulfone, shown in Figure 1.10, is generated from an individual double bond. This synthetic approach, developed during this dissertation work, is general and can be applied in the synthesis of bicyclic pyrroles of varying ring size.^{19,20} On the other hand, the Cheprakov's protocol depicted in Figure

1.12 is suitable only for the pyrroles with a six-member ring annulated to the backbone. It also relies on a Diels-Alder cyclo-addition step, which requires a large excess of 1,3-butadiene that acts both as a reagent and the reaction medium.

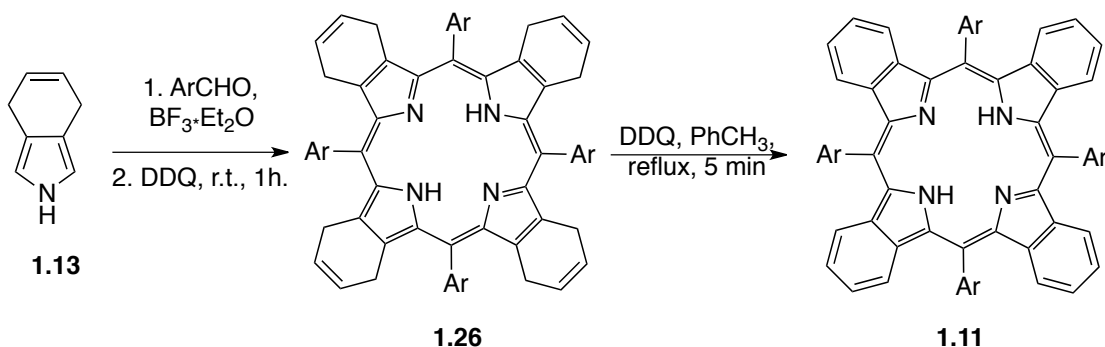


Figure 1.13. Synthesis of symmetrical tetrabenzoporphyrins from dihydroisoindole.

Using well-developed porphyrin chemistry, the dihydroisoindole discussed above (e.g. **1.13**) could be carried on to yield symmetrical octahydrotetrabenzoporphyrins of general structure **1.26** (Figure 1.13).^{18,21} Oxidative aromatization of the latter

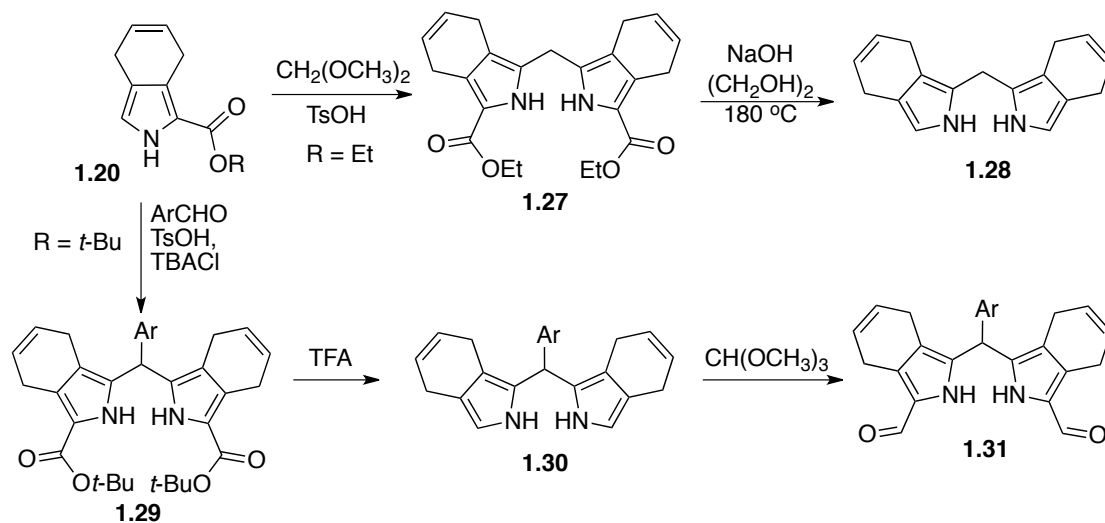


Figure 1.14. Synthesis of π -extended dipyrromethane precursors.

chromophore can be effected under much milder conditions, than are required for **1.9**. In

fact, nearly quantitative conversion takes place after just a few minutes when heated in boiling toluene. This ease of oxidation, in conjunction with the relatively high stability of ester **1.20**, spurred work in this field. In fact, to date, various substituted derivatives have been synthesized, **1.27 – 1.31** (Figure 1.14). Stepwise construction of the porphyrin ring allows for the preparation of unsymmetric products containing a different number of *meso*-substituents. Starting from the tetrahydroisoindeole, the resultant intermediate saturated precursors could not be oxidized to produce the corresponding π -extended porphyrins. This proved true whether the metal complexes or free bases forms were used. Even under harsh conditions, degradation products dominated in the reaction mixtures. This drawback was eliminated when dihydroisoindeole was used instead (Figure 1.15). In this way, the partially substituted **1.33** could be obtained as the free base under relatively mild oxidation conditions.

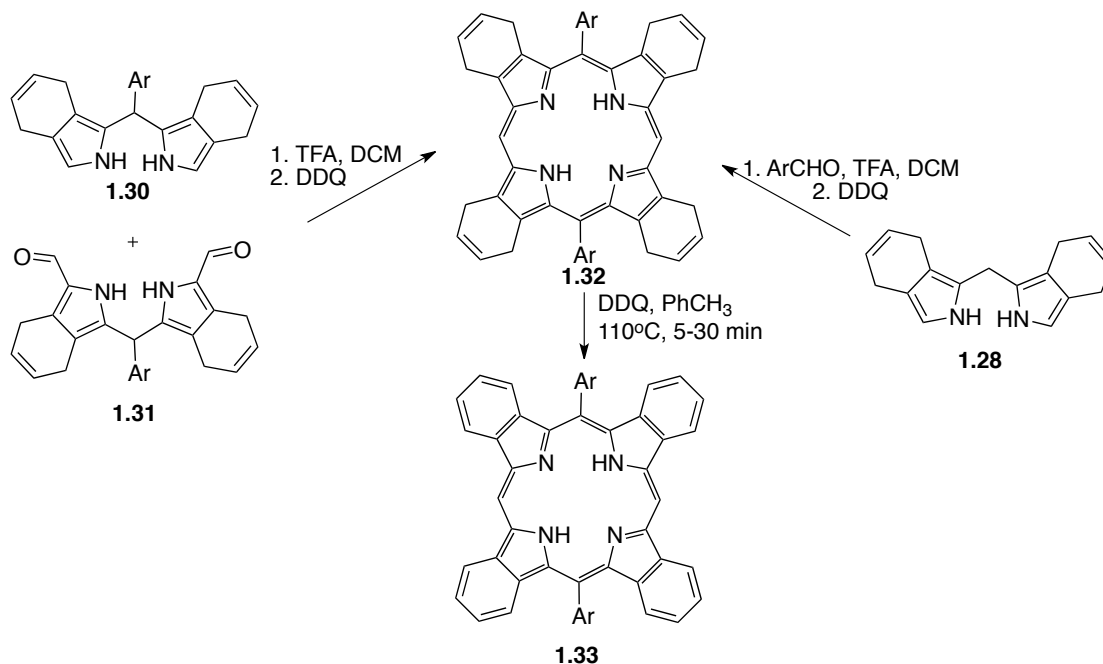


Figure 1.15. Synthesis of unsymmetric tetrabenzoporphyrins.

In addition to serving to adjust between the stability and reactivity seen in the case of **1.20** and **1.13**, the double bond of the annulated ring present in these species provides

a powerful synthetic tool. While the 5-position of ester **1.20** can be selectively iodinated or formylated (candidate's unpublished findings), the double bond of the cyclohexene ring can also be selectively modified.

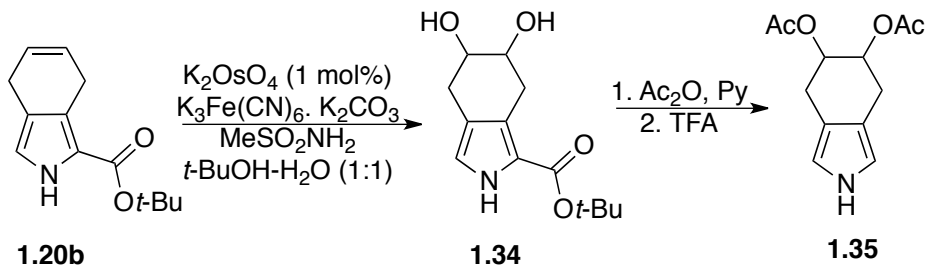


Figure 1.16. Dihydroxylation of the dihydroisindole precursor **1.20b**.

For instance, osmium-mediated potassium ferricyanide oxidation was shown^{22,23} to convert **1.20b** efficiently into its corresponding diol form **1.34** (Figure 1.16). Protection and decarboxylation yielded the diacetoxytetrahydroisindole **1.35**.

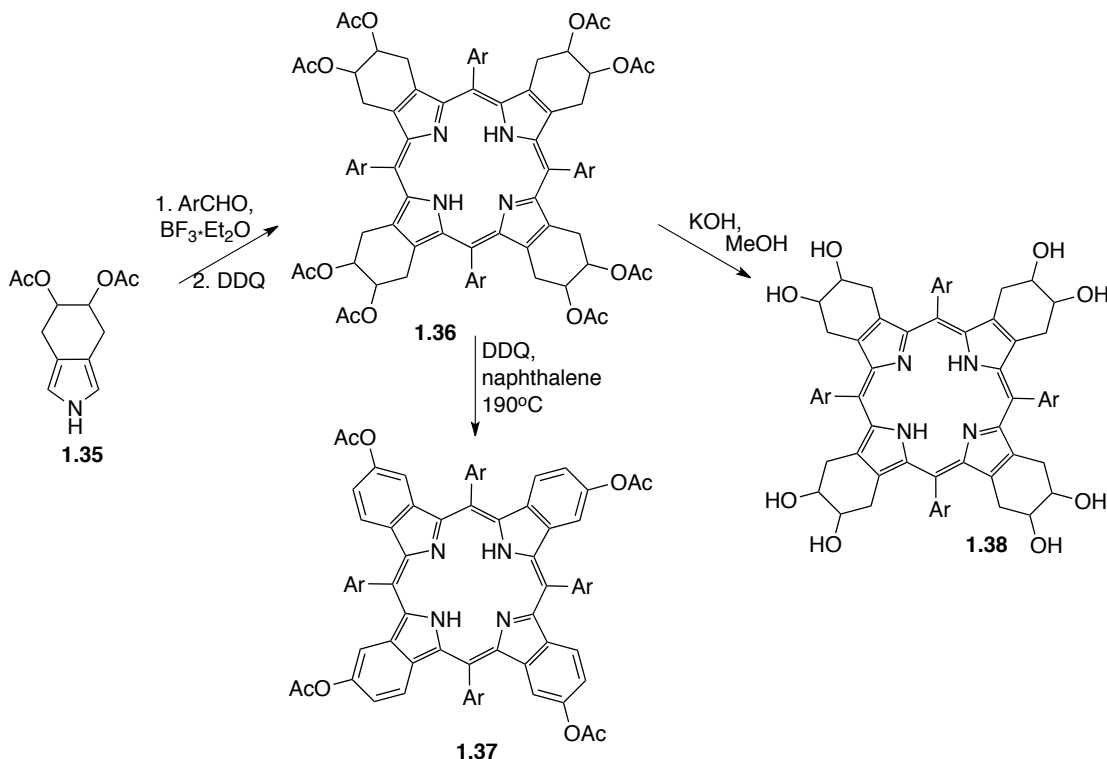


Figure 1.17. Porphyrin synthesis using diacetoxytetrahydroisindole.

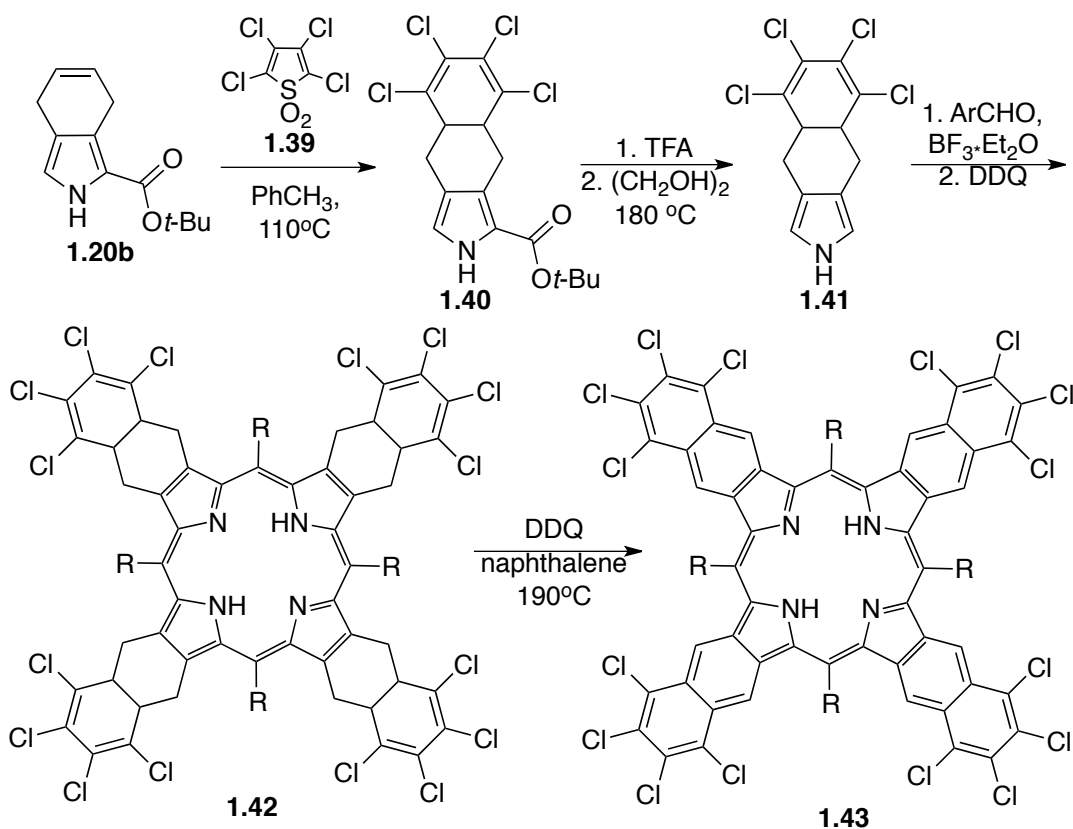


Figure 1.18. An inverse Diels-Alder reaction in the functionalization of dihydroisindole and its role in the π -extended porphyrin synthesis.

The utility of **1.35** as a synthon was demonstrated through its conversion to the tetraacetoxy tetrabenzoporphyrin **1.37** and the hydroxylated porphyrin **1.38** (Figure 1.17).

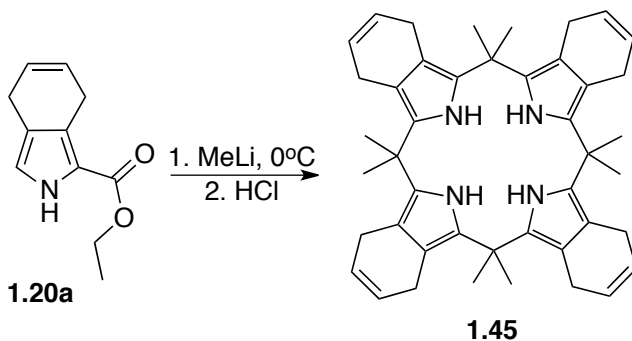


Figure 1.19. The use of dihydroisindole in the synthesis of calixpyrrole.

The latter is of potential interest due to its relatively small size and water solubility – highly desirable properties for biomedical applications.

Conventional [2+4] Diels-Alder reactions require an electron deficient alkene (dienophile) and an electron rich

diene. On the other hand, the less common inverse Diels-Alder cycloaddition reaction takes place between an electron rich dienophile and a diene with electron withdrawing groups. The ester **1.20b** contains an electron rich double bond. It was reacted with tetrachlorothiophene dioxide **1.39**. The resulting tetrachlorinated pyrrole **1.40** serves as a precursor for the tetranaphthoporphyrin **1.43** in accord with the synthetic sequence shown in Figure 1.18.⁶

Such chemical flexibility, as evident from Cheprakov's work, renders dihydroisindole useful as a building block for the preparation of π -extended porphyrins. The synthetic route independently developed in this work (Figure 1.10) and alternative the protocol reported by Cheprakov and coworkers (Figure 1.12) set the stage for future work devoted to the preparation of new porphyrin analogues. Indeed, in work that was carried out and published by the candidate, it was shown that dihydroisindole provides a convenient pathway to uniquely functionalized calix[4]pyrroles (Figure 1.19).¹⁹ These new calixpyrroles possess four double bonds, thus allowing for additional modifications, orthogonal to NH functionalization, to be conceived.

EXPERIMENTAL SECTION.

4-Chloro-5-(phenylthio)-cyclohexene (**1.16**):

A solution of phenylsulfenylchloride (11.03 g, 76.3 mmol) in 15 ml of dry dichloromethane was added over 2 hrs to a solution of 1,4-cyclohexdiene (7.22 ml, 76.3 mmol) in 75 ml of dry dichloromethane with stirring. The temperature was maintained at 0° C throughout the addition. The reaction mixture was then allowed to warm to r.t. while being stirred overnight. At this point, all volatiles were removed under reduced pressure with the aid of a rotary evaporator. The resulting white solid product, **1.16** (obtained as diastereomeric mixture), was dried under high vacuum and was used in the ensuing steps without any additional purification. ¹H NMR (400 MHz, CDCl₃) δ 7.48 (m, 2H), 7.33 (m,

3H), 5.69 (m, 1H), 5.63 (m, 1H), 4.21 (m, 1H), 3.62 (m, 1H), 3.03 (m, 1H), 2.89 (m, 1H), 2.43 (m, 1H), 2.30 (m, 1H). MS ESI (+) 225 m/z, [M+H]⁺, 189 m/z [M-Cl]⁺.

4-Chloro-5-(phenylsulfonyl)-cyclohexene (1.17):

mCPBA (3.73 g., 16.21 mmol, 75% aq.) was added dropwise into a solution of compound **1.16** (1.82 g., 8.11 mmol) in 100 ml of dichloromethane chilled with an ice bath. Caution: the reaction is exothermic and therefore slow addition is advised. It also allows for better control of the process. After 2 hrs of stirring (without refilling the ice bath) the reaction was complete as evident from TLC analysis (silica gel/DCM). The reaction solution was then washed with a saturated solution of sodium bicarbonate to remove the 3-chloro-benzoic acid by-product. The resulting solution was dried over Na₂SO₄, filtered and the volatiles removed under reduced pressure using a rotary evaporator. This yielded the compound **1.17** as a colorless oil. The product was of sufficient purity, based on ¹H NMR spectral analysis, to be carried forward without additional purification. ¹H NMR (400 MHz, CDCl₃) δ 7.92 (m, 2H), 7.67 (m, 1H), 7.58 (t, J = 7.7, 2H), 5.65 (t, J = 9.3, 2H), 4.62 (dd, J = 9.5, 4.8, 1H), 3.57 (dd, J = 11.3, 4.5, 1H), 2.93 (d, J = 18.6, 1H), 2.51 (dd, J = 58.9, 17.9, 3H). MS ESI (+) 257 m/z, [M+H]⁺, 221 m/z [M-Cl]⁺

(1,4-Cyclohexadien-1-ylsulfonyl)-benzene (1.18):

1,8-Diazabicyclo[5.4.0]undec-7-ene (DBU) (144 μl, 0.964 mmol) was added dropwise to an ice cooled solution of sulfone **1.17** (0.21 g., 0.803 mmol) in 25 ml of dry dichloromethane. The reaction solution was then stirred without cooling until deemed complete, typically 5-6 hrs, as inferred from the disappearance of the starting material per TLC analysis (silica gel/CH₂Cl₂ eluent). The reaction mixture was then washed with 1M HCl aq. followed by H₂O. After drying the organic layer over Na₂SO₄, the solvent was removed in vacuo. This produced a colorless oil, which proved to be a mixture of **1.18** and **1.21** based on ¹H NMR spectroscopic analysis. Yield 100%. ¹H NMR (400 MHz,

CDCl₃) δ 7.80 (dd, J = 9.1, 7.8, 2H), 7.55 (dd, J = 10.6, 4.2, 1H), 7.46 (m, 2H), 5.60 (t, J = 10.5, 2H), 5.46 (d, J = 6.8, 1H), 2.87 (s, 2H), 2.75 (d, J = 8.7, 2H). MS ESI (+) 221 m/z, [M+H]⁺.

2H-Isoindole-1-carboxylic acid, 4,7-dihydro-, ethyl ester (1.20a):

Potassium tert-butoxide (7.30 g., 65.2 mmol) was added to a solution of ethyl isocyanoacetate (7.30 g. 65.2 mmol) and sulfone **1.18** (mixture with **1.21**, 14.33 g. 65.2 mmol) in 500 ml of dry THF. The reaction mixture was stirred overnight, after which point the solvent volume was reduced to ~50 ml. Dichloromethane (100 ml) was then added. The resulting organic solution was washed with 1 M HCl aq. and then dried over Na₂SO₄. All of the volatiles were removed in vacuo, providing crude pyrrole **1.20a** in the form of gooey substance. Filtration through a short silica gel pad while washing with dichloromethane served to remove any impurities. Evaporation of the solvent and drying under high vacuum yielded pure product **1.20a** in 65% yield. ¹H NMR (400 MHz, CDCl₃) δ 9.31 (s, 1H), 6.72 (d, J = 2.8, 1H), 5.87 (m, 2H), 4.32 (q, J = 7.1, 2H), 3.45 (d, J = 2.6, 2H), 3.22 (s, 2H), 1.35 (dd, J = 7.4, 6.8, 3H). ¹³C NMR (101 MHz, CDCl₃) δ 162.64, 128.55, 125.33, 124.74, 119.76, 119.58, 118.39, 60.80, 25.03, 23.32, 15.47. MS ESI (+) 192 m/z [M+H]⁺. HiRes MS (CI+) m/z found 192.1017, calc. 192.1019 for C₁₁H₁₄NO₂⁺.

Octamethyl calix[4]4,7-dihydroisoindole 1.45:

A 1.6 M solution of methyl lithium in diethyl ether (1 ml, 1.57 mmol, 3 equiv.) was added via syringe to the clear colorless solution produced by dissolving the pyrrolic ester **1.20a** (100 mg, 0.52 mmol) in dry diethyl ether (30 ml) at 0° C; this was done with stirring over the course of 5 min. The reaction mixture was then stirred without refilling the cooling bath for two hours. After diluting the reaction mixture with dry diethyl ether (30 ml), a 2 M solution of HCl in diethyl ether (1 ml, 4 equiv.) was added drop-wise with stirring. This led to the formation of a white precipitate. The reaction was then stirred for an additional 30 min before being filtered through a sintered glass funnel. The filtrate was

collected and taken to dryness on a rotary evaporator. The product was purified by the flash chromatography over silica gel using a mixture of ethyl acetate and hexane in a 1:9 ratio as the eluent. Rf = 0.50 (silica gel, ethyl acetate:hexane = 1:9), 20% yield. ^1H NMR (CDCl_3): δ , ppm 1.63 (s, 6H, CH_3); 3.23 (s, 4H, CH_2); 5.81 (s, 2H, $-\text{CH}=\text{CH}-$); 7.12 (br. s, 1H, NH). ^{13}C NMR (CDCl_3): 25.4; 28.7; 38.4; 112.9; 124.9; 129.4. MS (ESI+) 637 m/z ($\text{M}+\text{H}$) $^+$. HRMS (CI+) m/z calc. for $\text{C}_{44}\text{H}_{53}\text{N}_4$ ($\text{M}+\text{H}$) $^+$: 637.4270, found: 637.4264.

Chapter Two: π -Extension in Porphyrin Analogs.

As research in natural porphyrin chemistry has advanced, increased attention has been devoted to expanded porphyrins and their analogs. For example, development of a convenient and rather simple scalable route to 2,2'-bipyrroles triggered contributions to the chemistry of expanded porphyrins, including the synthesis of a variety of cyclic polypyrroles - such as sapphyrin (a pentapyrrolic macrocycle), amethyrin and isoamethyrin, both of which contain six pyrrolic subunits.³ In another example, progress in the synthetic methodology of porphyrins and a greater basic understanding of their properties resulted in the design of sophisticated fully conjugated oligoporphyrin ribbons with large two-photon absorption coefficients and negative first oxidation potentials, properties that rendered this group of compounds promising as materials for use in photoelectronic applications.²⁴ Similarly, the discovery of relatively easy procedures for the synthesis of annulated pyrroles inspired the porphyrin community to create new pyrrolic chromophores that differ from porphyrins and contain these particular building blocks. Detailed below are some of these accomplishments reported up to date.

Π -EXTENDED BORON-DIPYRRROMETHANES.

Dipyrromethenes with boron coordinated to the nitrogen atoms have attracted a great deal of attention due to their highly fluorescent nature and chemical versatility. The emission efficiency for the simplest, unsubstituted BODIPY reaches 90% in a polar solvent such as water.²⁵ The BODIPY scaffold contains several positions amenable to modification (three positions at each pyrrolic ring, one *meso* carbon, and two additional ligands coordinated to boron), which has allowed for the creation of a vast number of dyes,²⁶ some of which are commercially available, and whose absorption/emission maxima cover a large portion of the solar spectrum (Figure 2.1). Not surprisingly, boron-dipyrromethene derivatives based on the use of π -annulated pyrroles started to appear in

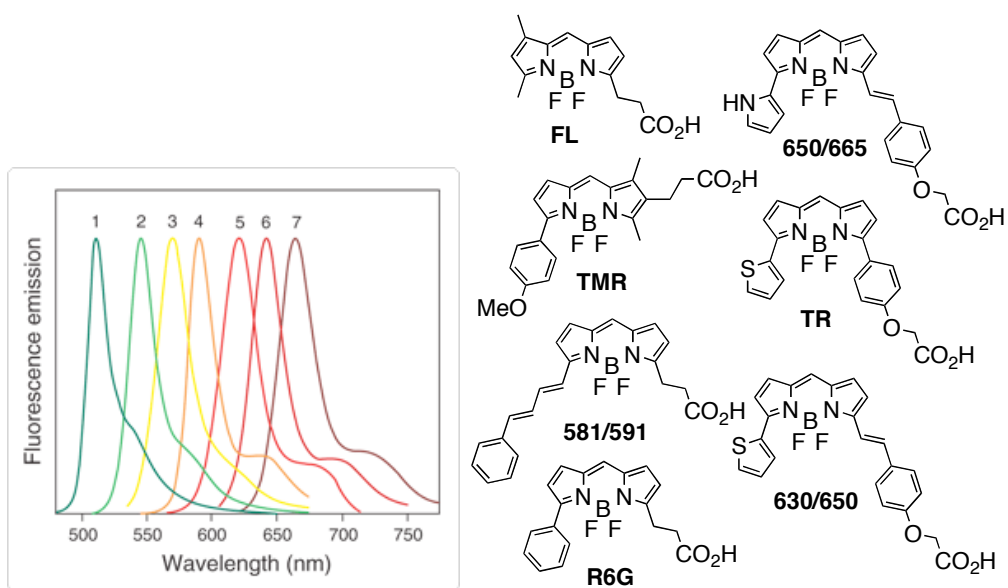


Figure 2.1: Normalized fluorescence emission spectra of a series BODIPY dyes as recorded in methanol: 1 - FL, 2 - R6G, 3 - TMR, 4 - 581/591, 5 - TR, 6 - 630/650, 7 - 650/665.

the literature soon after the corresponding porphyrins containing the respective building blocks were reported.

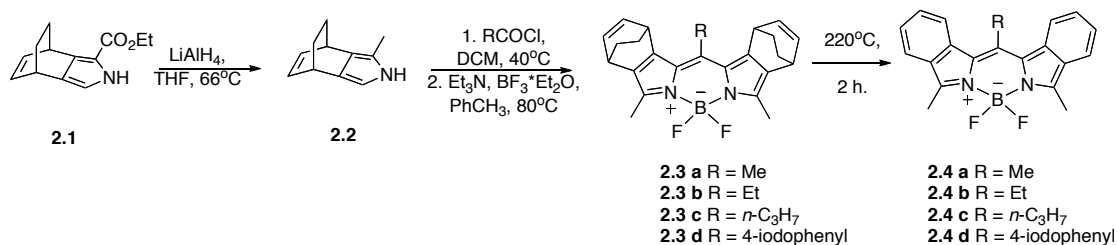


Figure 2.2: Synthesis of π -extended boron-dipyrromethene (BODIPY) dyes.

For example, using a retro Diels-Alder transformation Ono and coworkers prepared a series of BODIPYs containing diisoindole moieties (Figure 2.2).²⁷ Starting with the bicyclic pyrrolic ester **2.1**, which was used to develop corresponding π -extended porphyrin chemistry, these Japanese scientists were able to obtain the series of boron-dipyrromethene derivatives **2.3 a-d** that collectively encompass various substituents.

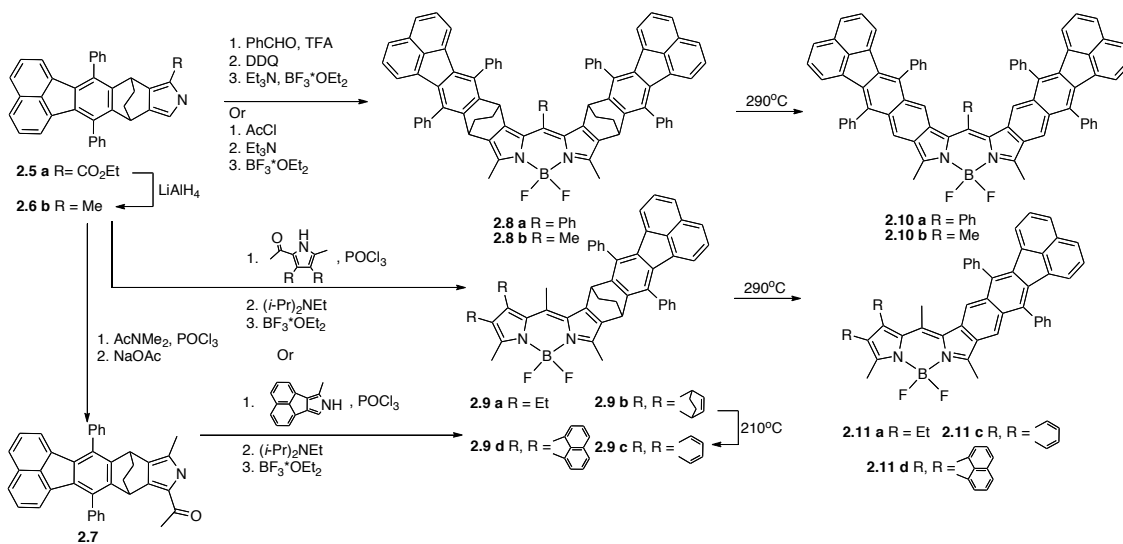


Figure 2.3. BODIPY dyes containing fluorantho[8,9-*f*]isoindole unites.

The final thermal aromatization step proceeds quantitatively and results in the series of compounds **2.4 a-d**, whose absorption maxima, as expected and in analogy to what is seen in the case of the corresponding porphyrins, are significantly red shifted, when compared to its precursors **2.3 a-d**. Such spectroscopic differences are especially evident in passing from **2.3a** to **2.4a**. Here λ_{max} shifts from 530 to 603 nm.

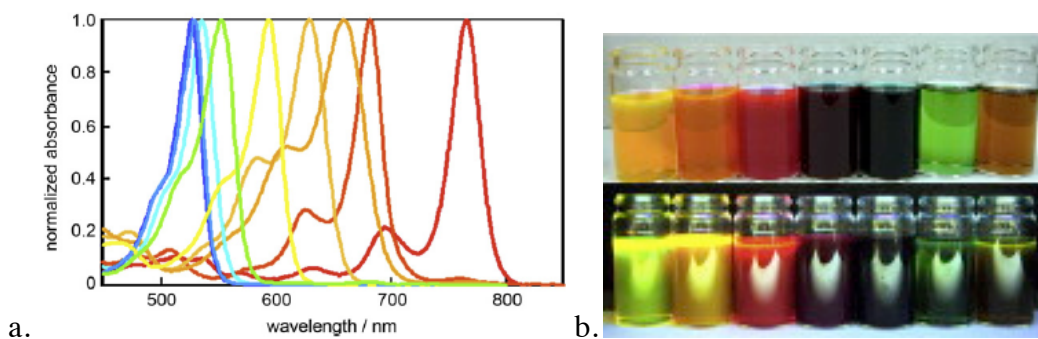


Figure 2.4. a. Normalized absorption spectra of the **2.9a**, **2.9b**, **2.8a**, **2.9c**, **2.9d**, **2.11a**, **2.11d** and **2.11c** (from left to right). b. Colors of the dyes under ambient (top) and UV (bottom) light.

Further elaborating on the theme of π -extended BODIPYs, Okujima *et al.* reported a multistep synthesis of a group of dyes containing fluorantho[8,9-*f*]isoindole subunits (Figure 2.3).²⁸ In this case, the authors tested a variety of substituents, including

both alkyl and aryl groups, in order to compare their effect on the corresponding absorption and emission properties. Both of these optical features were strongly pronounced across the series. However, clear substituent effects were seen. Some of these were quite dramatic. For instance, upon thermal aromatization of **2.8a** and conversion to **2.10a**, a 230 nm bathochromic shift in the absorption maxima was induced. In fact, the basic BODIPY absorption band reached the near-IR region. Such an unprecedented change in λ_{max} was attributed to the presence of the large, conjugated aromatic substituents.

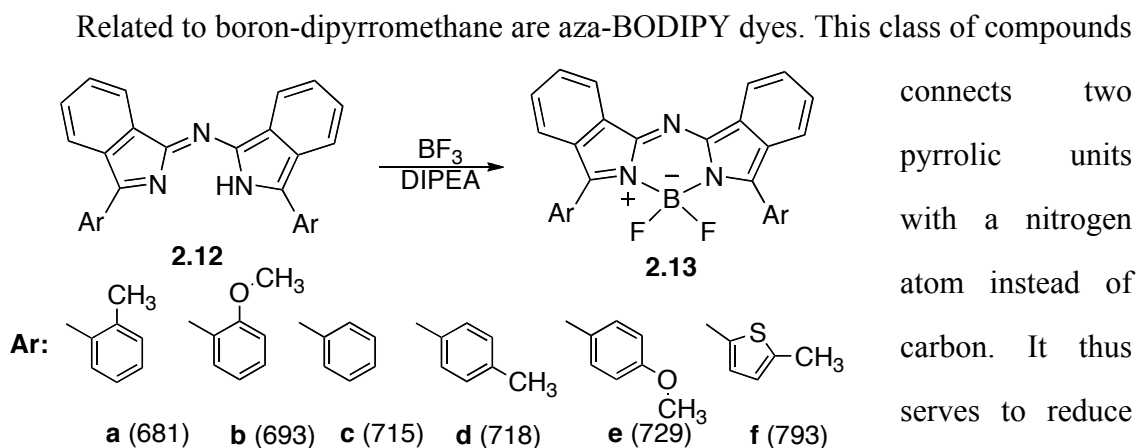


Figure 2.5. Various substituted aza-BODIPY dyes and their corresponding absorption maxima given in nm.

Nevertheless, aza-BODIPYs have been intensively studied,²⁶ due to the fact that they display intense absorption and emission properties similar to regular BODIPYs. Gresser and coworkers studied an effect of various aryl substituents on benzannulated aza-BODIPY dyes **2.13** and its precursors, aza-diisoidolemethines **2.12**.²⁹ In general, highly fluorescent chromophores were obtained, a finding consistent with the notion that more electron rich substituents tend to shift the absorption maxima bathochromically (Figure 2.5).

II-EXTENDED SAPPHYRINS.

Sapphyrin is a porphyrin analog with 5 pyrrole rings and 4 connecting *meso* carbons arranged to give a 22 π aromatic system. This electronic arrangement is thought responsible for the bluish-green sapphire-like color of the sapphyrins. This class of compounds has been tested *in vitro* and *in vivo* and shown to have anticancer activity.³⁰ Not surprisingly, therefore, efforts been made to prepare π -extended sapphyrins.

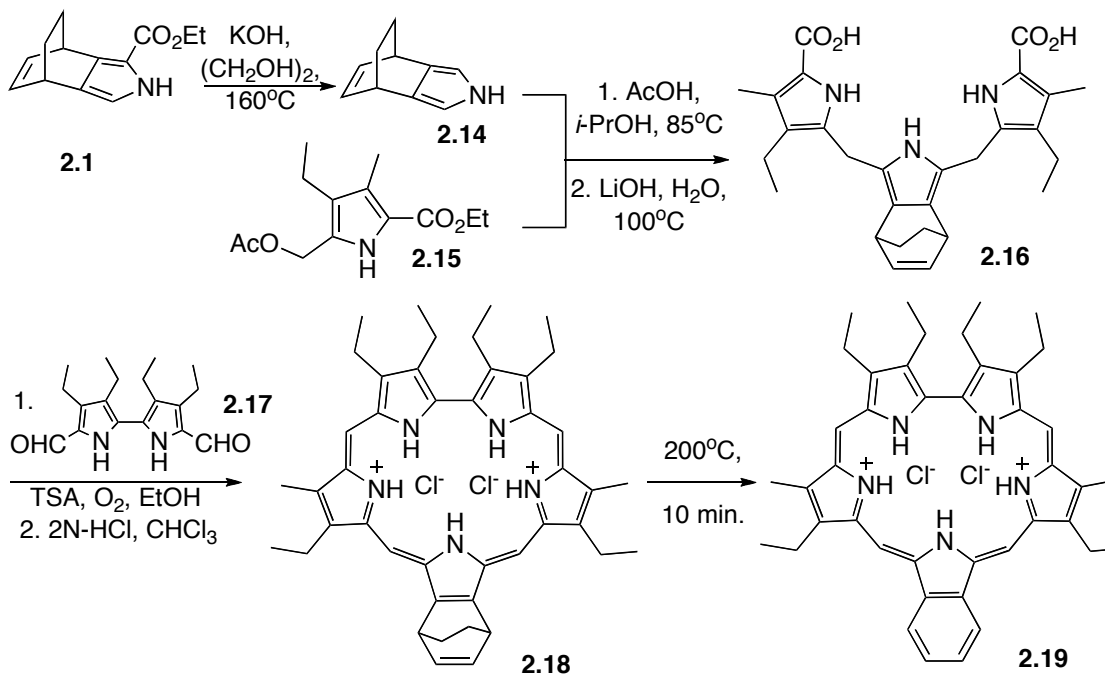


Figure 2.6. Synthesis of a monoisoindole sapphyrin.

Ono and coworkers applied their retro Diels-Alder approach, originally applied to the synthesis of π -extended porphyrins (Chapter 1), to the design and synthesis of π -expanded sapphyrins.³¹ Starting with ester **2.1**, tripyrromethane **2.16** was prepared in two steps (Figure 2.6). The latter precursor was subjected to a [2+3] type condensation with 5,5'-diformyl-3,3',4,4'-tetraethyl-2,2'-bipyrrrole **2.17** yielding sapphyrin **2.18**. The novelty of this approach was that chromophore **2.18** underwent a thermal retro Diels-Alder reaction to produce the desired π -expanded sapphyrin **2.19**.

In the same report,³¹ diisoidole sapphyrin **2.29** was described. In order to synthesize this latter target, bipyrrrole **2.24** had to be prepared. Although obtained using a synthetic route commonly used to prepare bipyrrroles, **2.24** appears to be the first bipyrrrole containing a masked π -extended substituents. Once **2.24** was in hand the Ono group removed the diacid groups to generate the 5,5'-unsubstituted bipyrrrole. This was done by subjecting **2.24** to an *in situ* decarboxylation, brought about by the combination of acid and heat. They were then able to react the product with tripyrrromethane dialdehyde **2.27**. The resulting sapphyrin **2.28**, with nearly identical absorption properties to its mono-functionalized analog **2.18**, was then thermally transformed into the corresponding diisoidole sapphyrin **2.29**. A red shift of 12 and 22 nm in the absorption maxima was seen in the case of **2.19** and **2.29**, respectively, as compared to their precursors **2.18** and **2.28**. These differences were attributed to the effect of π -extension.

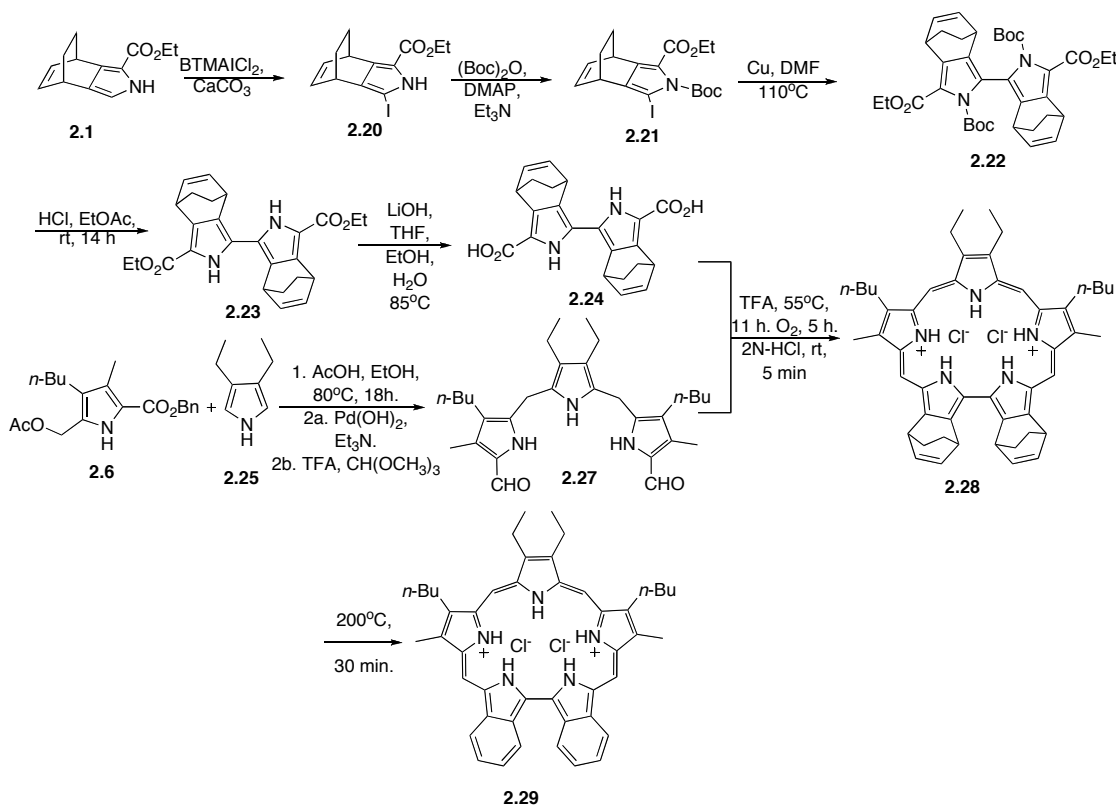


Figure 2.7. Synthesis of the diisoidole sapphyrin.

In continuation of their work on π -extension in expanded porphyrins, Okujima and Ono published pentabenzosapphyrins, albeit a trithia version thereof (Figure 2.8).³² Specifically, these Japanese scientists prepared sapphyrin **2.34** *via* a typical [3+2] condensation. The resulting product demonstrated interesting thermal properties. For instance, if sapphyrin **2.34** is subject to thermolysis for a brief period at 145 °C, only two ethylene molecules dissociate from the chromophore. Under harsher, more prolonged conditions, such as heating at 230 °C for an hour, all bicyclic substituents release ethylene to yield sapphyrin **2.36**. Based on an X-ray analysis, UV-vis spectroscopy and a theoretical study of macrocycles **2.34** – **2.36** the 22 π -electron circuit involving the 19 inner atoms was considered responsible for the observed properties. In other words, the annulated benzene rings hardly contribute to the electronic features of these new sapphyrin derivatives.

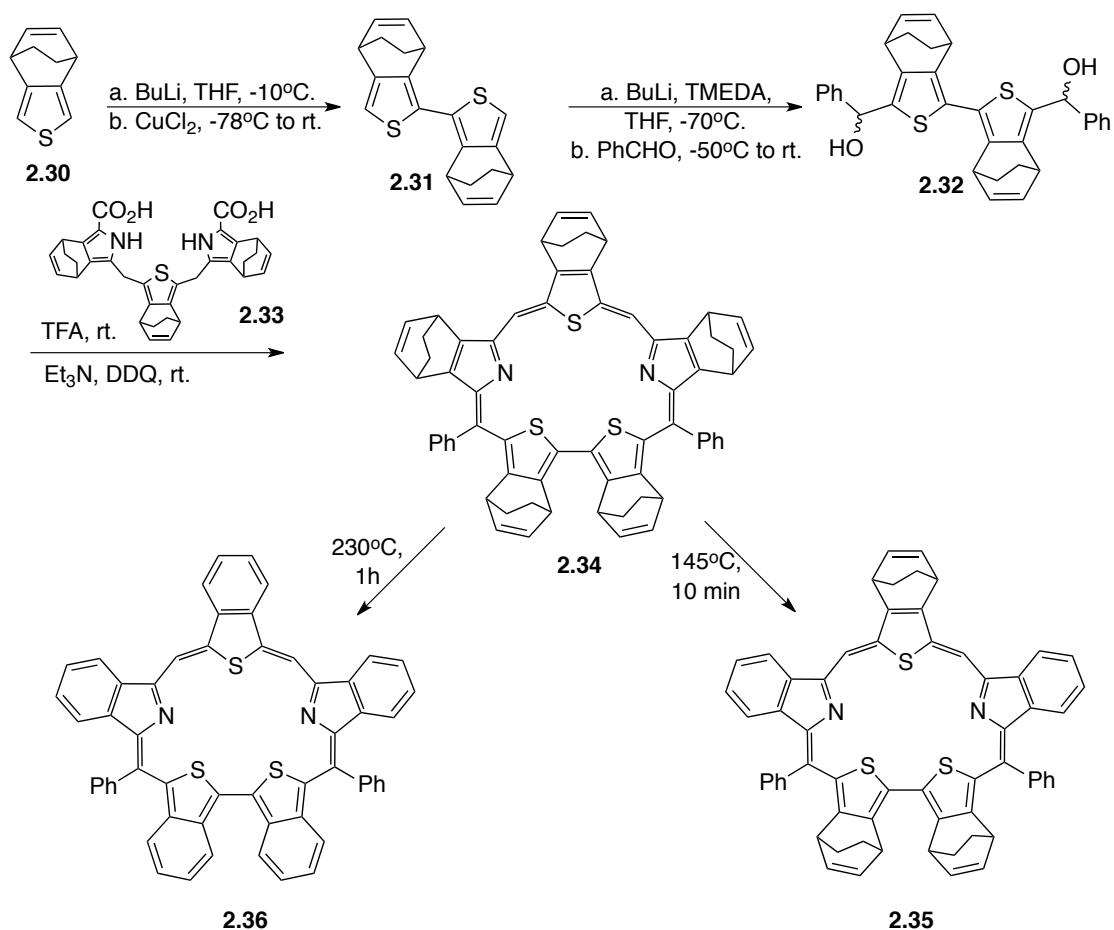


Figure 2.8. Synthesis of the π -extended trithiasaphyrins.

Lee and coworkers have explored a qualitatively different approach to achieving π -extension in expanded porphyrin chemistry. Specifically they have explored the use of benzobipyrrole **2.37** as a building block and synthetic precursor (Figure 2.9).³³ These researchers noted that the unsubstituted benzobipyrrole **2.38**, possesses ambiguous reactivity, in which both so-called α and β positions of the pyrrolic rings can undergo reaction depending on the specific conditions. Therefore, the authors first subjected this unsubstituted species to Vilsmeier-Haack formylation conditions. This produced predominantly the dialdehyde **2.39**. Subsequent reduction resulted in the two methyl groups present in **2.40**. A second formylation step furnished dialdehyde **2.37**. This precursor is attractive because it possesses both good solubility and the carbonyl groups

in the desired positions. Using it and the tripyrrane **2.41**, the benzosapphyrin **2.42** was obtained in the form of its salt, by means of a [3+2] condensation, promoted by two equivalents of p-toluensulfonic acid. In **2.42**, the Q-band-like absorption band was red-shifted, compared to the parent decaalkyl substituted sapphyrin. The authors further described the effect of such π -extension as following: “It appears that incorporation of the benzene ring into the sapphyrin has a stronger effect on the electronic properties of

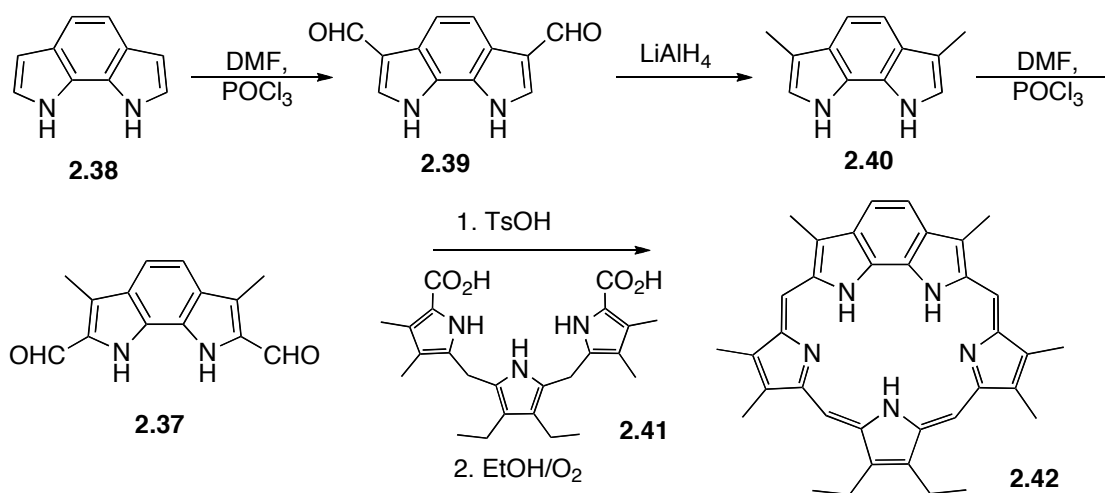


Figure 2.9. Synthesis of benzosapphyrin.

the molecule than in benzo-extended analogues by extension of overall π -electron conjugation (aromaticity) through the use of the diene part of the fused benzene unit.”³³ Thus, the effect of π -extension in at least this expanded porphyrin is both noticeable and real.

Π -EXTENDED PORPHYCENES.

Porphycenes are structural isomers of porphyrins consisting of two bipyrrrolic fragments and two ethylene units, the so-called *meso* carbons. Analogous to porphyrins, porphycenes possess an 18 π -electron aromaticity. However, periphery and displayed

features associated with the porphycenes, as compared to porphyrins, generally have greater fluorescence quantum yields and due to a smaller inter cavity, demonstrate different metal coordinating properties.

The synthesis of porphycenes relies on the intermolecular McMurry coupling of dialdehyde precursors. This route is general for most of the porphycenes and was pioneered by Vogel.³⁴ The problem thus is one of preparing the appropriate annulated diformylated π -extended bipyrrole.

Yamada, Kobayashi and coworkers studied the effect of substitution and π -extension in porphycenes.^{35,36} To prepare their target systems, formylation or acylation reactions were used to obtain dicarbonyl compounds **2.44 a-c** (Figure 2.10). These intermediates were subjected to McMurry condensations (Zn, TiCl₄, CuCl). Self-

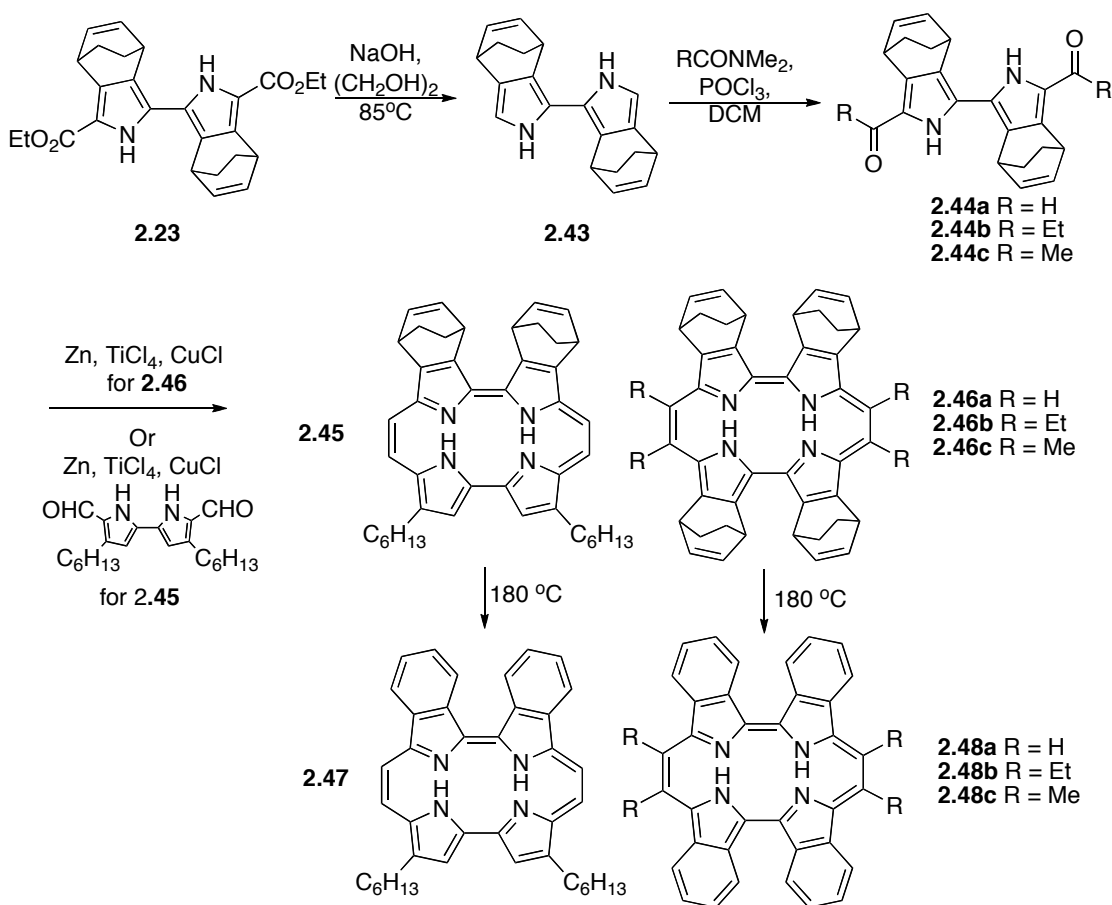
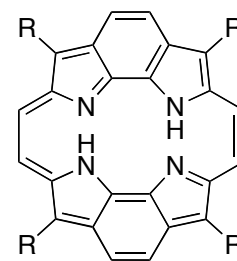


Figure 2.10. Synthesis of linearly annulated porphycenes.

condensation of **2.44** under these conditions resulted in a series of porphycenes **2.46**, while a mixed coupling reaction provided **2.45** among other products. It was revealed that conversion of compounds **2.45** and **2.46** into chromophores **2.47** and **2.48**, respectively, gave rise to the expected bathochromic shift in the absorption bands, presumably as the result of the π -extension. It was also found that the so-called *meso* substituents had a profound influence on the structure and properties of this porphycene series. For instance, it was determined that meso groups favor a rectangular shape for the macrocycle,³⁷ while a lack of *meso* substituents and the presence of groups on bipyrrole fragment enforces a more square-like geometry.³⁸ Porphycenes **2.46b,c** and **2.48b,c** proved nonfluorescent. In contrast, the unsubstituted analogs **2.46a** and **2.48a**, were strong emitters.

The Waluk and Vogel groups studied another type of extended porphycenes, namely dibenzoporphycenes **2.49**. These compounds contain two benzene rings fused to both bipyrrolic subunits.³⁹⁻⁴¹ The results of spectroscopic studies, particularly those relating to the interconversion between the internal NH *cis* – *trans* forms, were published in depth.



2.49. R = Me, *t*-Bu

Even with increasing research efforts being devoted to the area, π -extension of expanded and isomeric porphyrinoids remains a field that is still in its infancy. Systems with higher degrees of π -extension (e.g. containing fused naphtha- and anthra- groups), remain largely understudied.²⁸ On the other hand, naphtho and anthraporphyrins displayed remarkable properties due to their near infra-red absorption and intense phosphorescence. Such photophysical features provide an incentive to study further the effects of π -extension in the area of expanded and isomeric porphyrins, as well as to create larger annulated derivatives. Work in this direction, carried out by the candidate, resulted in synthesis and detailed characterization of novel dinaphthoporphycenes described below.

DINAPHTHOPORPHYCENES.⁴²

Naphthobipyrrole is another attractive building block for the preparation of larger annulated porphycenes. One potential naphthobipyrrole for use as an annulated porphycene precursor is the unsubstituted derivative **2.50c** (Figure 2.11). This particular bipyrrole is a known compound.⁴³ However, it has been shown to react with various electrophiles (diazonium salts, Vilsmeier-Haack formylation, aminomethylation reagents,

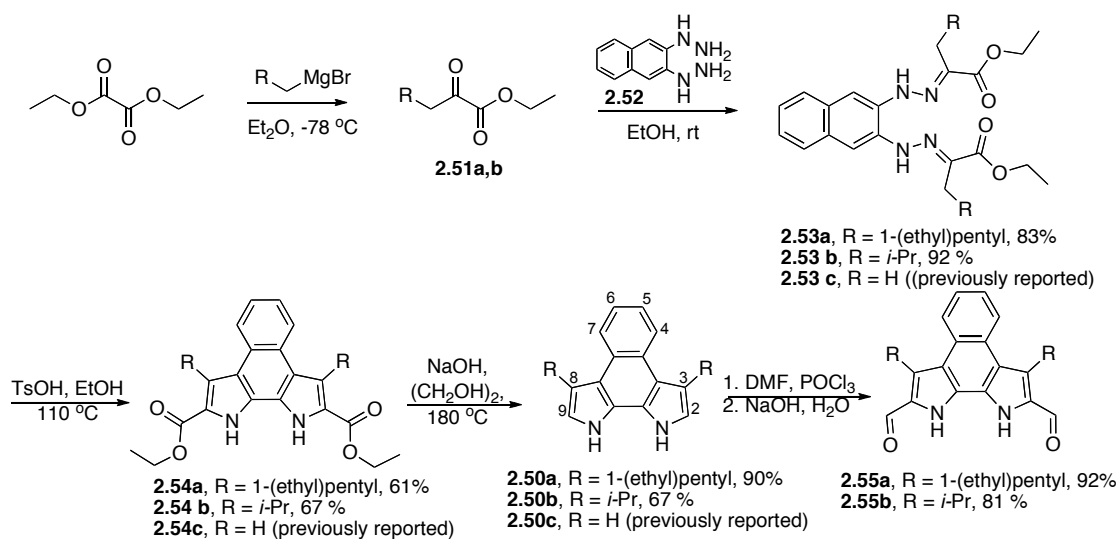


Figure 2.11. Synthesis of naphthobipyrroles. Structure **2.50** shows accepted position numeration.

etc.) predominantly at the so-called β positions (i.e., at carbons 3 and 8),⁴⁴⁻⁴⁶ this makes it less than ideal for the purpose of creating the dialdehyde derivatives needed to prepare porphycenes. Therefore, an alternative approach, developed by the candidate, was used to produce desired diformylated naphthobipyrroles, e.g. **2.55 a** and **b**, wherein the reactive β positions are blocked by alkyl groups. Here, an ancillary consideration was that the judicious choice of β -substituents would provide a means of modulating the solubility of these intermediates, as well as that of the final porphycene targets.

To create systems with high solubility in organic media, branched alkyl chains are attractive as β -substituents. Such branched species have been used as solubilizing groups in, for example, polymer chemistry;^{47,48} further, one particular branched system, 2-

ethylhexane, functionalized at carbon 1 as both the halide and corresponding Grignard reagent, is commercially available. Therefore, our initial efforts focused on creating a bipyrrrole containing this particular β -substituent. As a complement to this work, the synthesis of analogue bearing the smaller *i*-propyl substituents was also targeted.

With the above considerations in mind, diethyl oxalate was reacted with the requisite Grignard reagents at -78°C in accord with literature procedures.⁴⁹⁻⁵¹ This gave the corresponding ethyl α -oxocarboxylates **2.51a,b** in good yields. Ethyl pyruvate, used to produce unsubstituted naphthobipyrrrole, is commercially available.

Subsequent reaction with 2,3-naphthalene bishydrazine^{52,53} in ethanolic media at rt. led to the nearly quantitative conversion to the corresponding bishydrazones **2.53a-c**. Compounds **2.53a,b** are new compounds. However, the bishydrazone **2.53c** was reported as an intermediate leading to the synthesis of **2.50c** (*vide supra*). However, full characterization data were lacking, with only melting point and elemental analysis results being provided.⁴³

Interestingly, compounds **2.53a-c** exist in two different geometrically isomeric forms. The individual species in question can be isolated via column chromatography

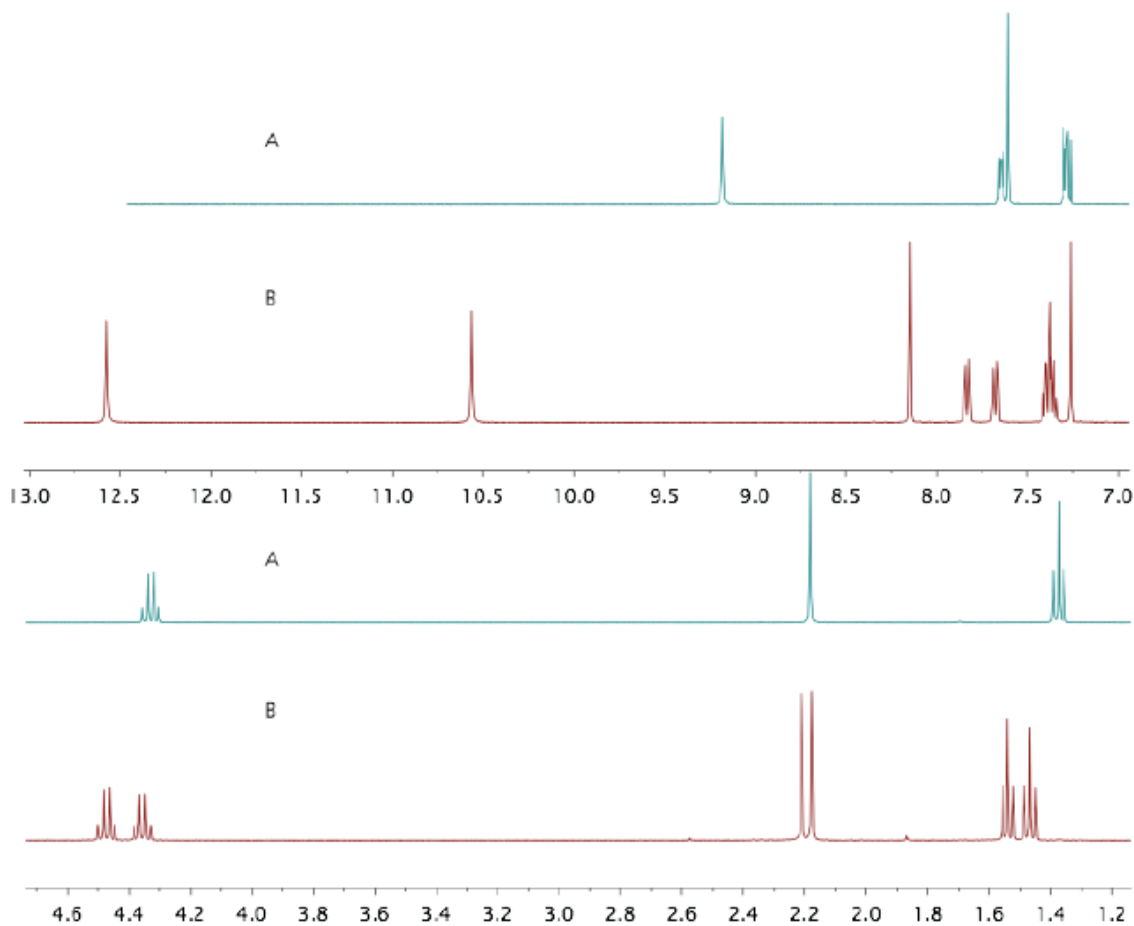


Figure 2.12. ^1H NMR spectra of the two different isomers of **2.53c**. (A) corresponds to the more polar conformer and (B) corresponds to the less symmetrical and less polar fraction.

over silica gel if desired. Based on ^1H NMR spectroscopic analysis, these isomeric forms possess different degrees of symmetry. The more polar (slower eluting) isomer gives rise to the simpler spectrum, while the faster eluting isomer (chromatography over normal silica gel) resulted in a more complex group of signals (Figure 2.12). However, these compounds behave identically in the subsequent synthetic step, namely the Fischer indole synthesis. This proved true whether the isomers were reacted separately or combined. Thus, they were generally used without further purification.

Subjecting **2.53a-c** to a ten-fold excess of *p*-toluenesulfonic acid hydrate in ethanol under reflux gave the diethyl 3,8-dialkyl-1,10-dihydro-benzo[*e*]pyrrolo[3,2-*g*]indole-2,9-dicarboxylate derivatives **2.54 a-c** in good to excellent yields after purification *via* recrystallization or filtration through a short silica gel column. We found these conditions⁵⁴ to be superior to the use of polyphosphoric ester in unspecified concentration as originally used for the preparation **2.54c**.⁴³

It is worth noting that the diesters **2.54a, b** are also formed as a mixture of isomers; presumably different conformers arising from the restricted rotation of the alkyl substituents. The interconversion rate between the various isomers was such that in some

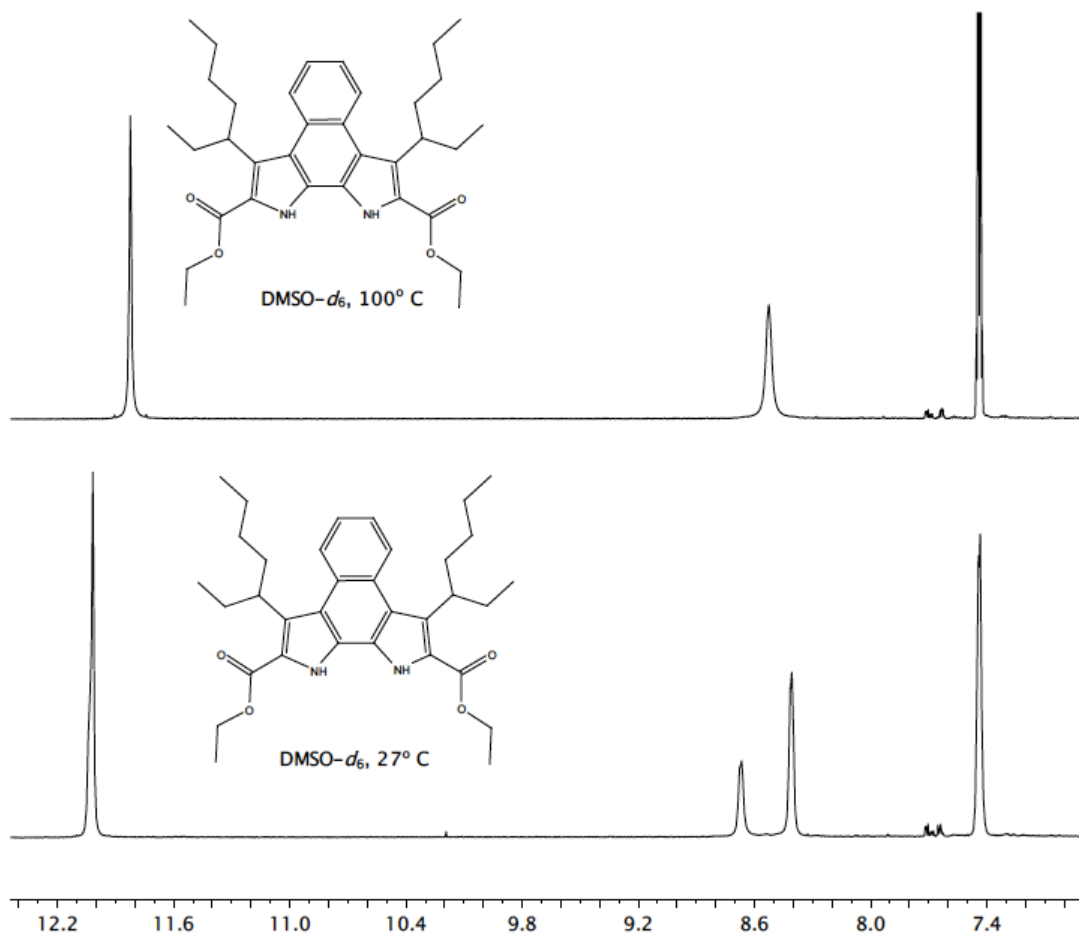


Figure 2.13 ¹H NMR spectra (low field portion) of porphycene **2.54a** recorded in DMSO-*d*₆ at 27 °C (bottom) and 100 °C (top).

cases the ^1H NMR signals were broadened and in others more than one species could be observed at rt. In the case of the test system **2.54a**, heating the sample to 100°C served to simplify the spectrum, producing one corresponding to a time-averaged symmetric species (Figure 2.13).

Diesters **2.54a** and **b** were saponified and decarboxylated to produce the α -free species **2.50a** and **b**. This was done using a standard one-pot procedure that involves heating at reflux in ethylene glycol under an inert atmosphere.⁵⁵ This gave **2.50a** and **b** in 90% and 83% yield respectively.

Vilsmeier-Haack formylation served to convert **2.50a**, **b** to **2.55a**, **b** in almost quantitative yield. As expected, **2.55a** had the highest solubility and proved soluble in most common organic solvents. The isopropyl substituted dialdehyde **2.55b** showed moderate solubility, which allowed for crystallization from halogenated solvents, such as dichloroethane.

Diformylbipyrroles **2.55a** and **2.55b** were subject to McMurry coupling (Figure 2.14).⁵⁵ Here, THF solutions of each aldehyde were added dropwise to the preformed titanium reagent in THF at reflux. This was done under an inert atmosphere over the course of 6 hours by means of a syringe pump. The reaction mixtures were then maintained at reflux overnight. A basic work-up then yielded a yellow-green fluorescent solution that was assumed to be dihydroporphycene (porphycenogen). This assignment was made on the basis of what was seen in the case of **2.49** ($\text{R} = t\text{-Bu}$); here, it was found that the corresponding porphycenogen is rather stable and can be isolated.¹

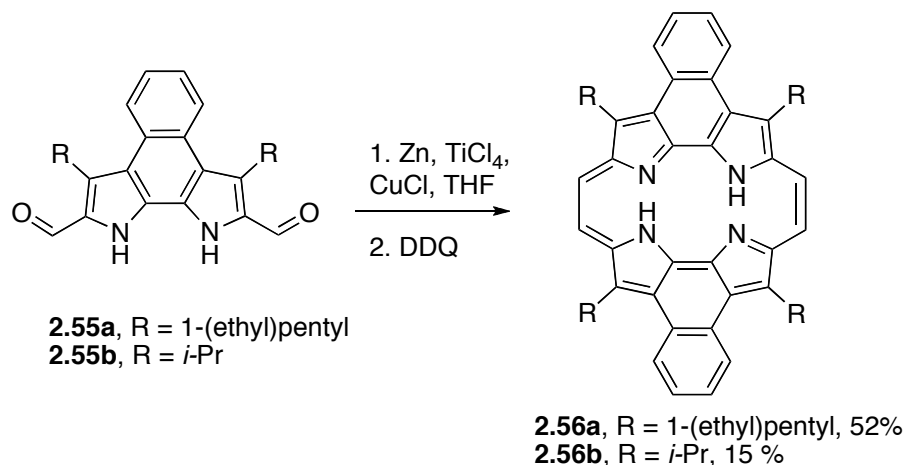


Figure 2.14. Synthesis of naphthobipyrroles.

Oxidation of the presumed porphycenogens was expected to give the desired porphycenes. To facilitate this process, 1 equiv. of DDQ was added. This caused the solution to turn dark blue, as would be expected were the oxidation successful. After chromatographic purification over silica gel, porphycenes **2.56a** and **2.56b** were isolated in 52% and 15% yield, respectively.

As proved true for the intermediate bipyrrole derivatives **2.54a** and **2.55a**, porphycene **2.56a** bearing branched alkyl substituents gave rise to poorly resolved ¹H NMR spectral features at rt. While not established unequivocally, this broadening is ascribed to hindered rotation of the branched alkyl groups and the existence of two or more tautomeric species at room temperature. In the event, an increase in spectral

resolution could be achieved by heating the sample to 100°C in toluene- d_8 (Figure 2.15).

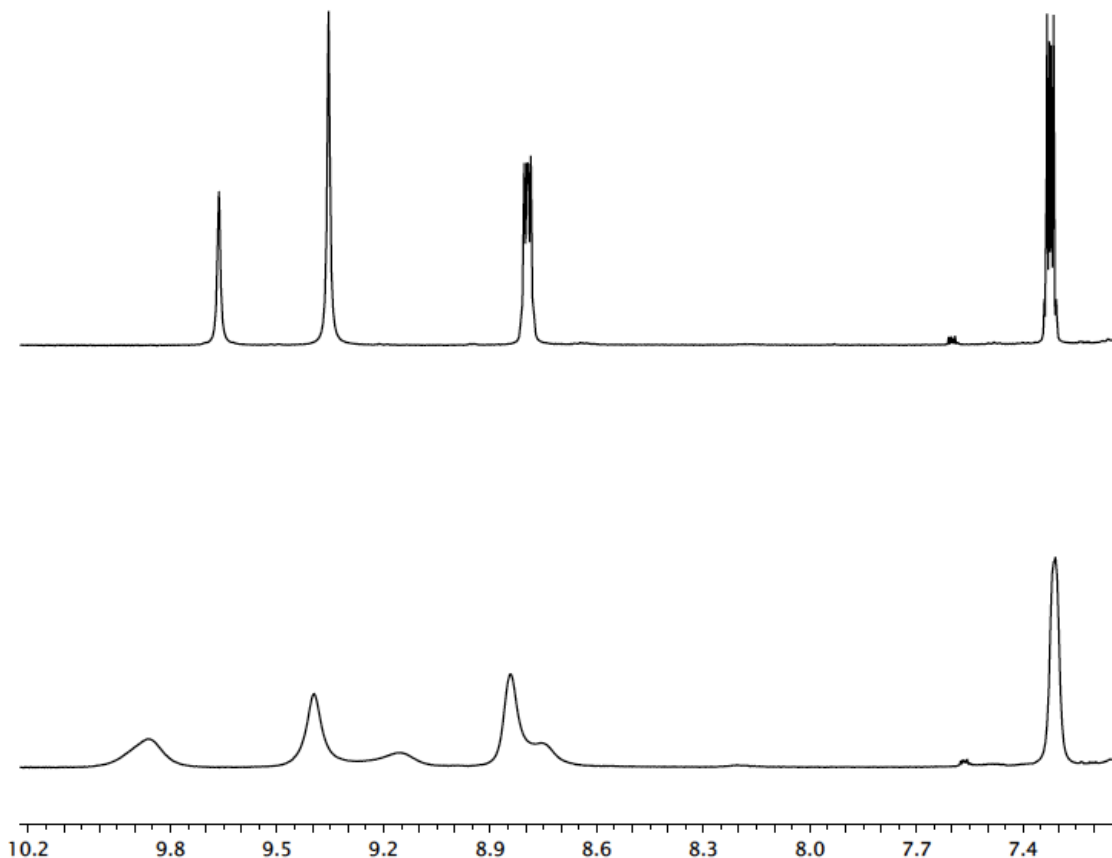


Figure 2.15. ^1H NMR spectra (low field portion) of porphycene **2.56a** in toluene- d_8 at 27 °C (bottom) and 100 °C (top).

Both porphycenes **2.56a** and **2.56b** display NH proton resonances at ca. 9.3 ppm (CDCl_3 , rt., 400 MHz). This is in marked contrast to the original unsubstituted porphycene (NH resonance at 3.2 ppm, CDCl_3 , 300 MHz).³⁴ However, it is in agreement with what is seen for the dibenzoporphycene **2.49** (R = *t*-Bu) (NH signal at 10.6 ppm; CDCl_3).⁵⁶

Both **2.56a** and **b** showed identical features in their respective UV-Vis spectra (dichloromethane). In particular, Q bands were seen at 725, 671, 556 nm, and a Soret band was observed at 404 nm with shoulder at 389 nm (Figure 2.16). Qualitatively, these spectral features are typical for porphycenes and are thought to reflect a lower symmetry than typically found in porphyrins. In accord with design expectations, however, the

visible portion of the spectrum is somewhat red-shifted as compared to non-annulated porphycenes (e.g., 2,7,12,17-tetrapropylporphycene for which Q bands at 634, 602, 562

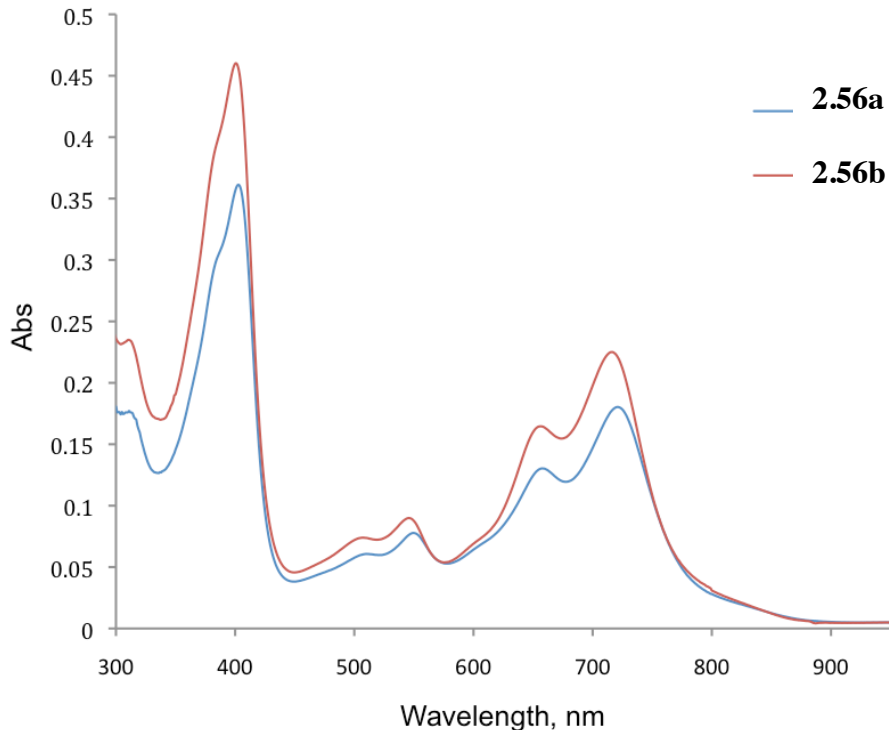


Figure 2.16. UV-vis spectra for **2.56a** and **2.56b** recorded in dichloromethane (0.11 mM).

nm are seen).⁵⁷ These differences are attributed to the bipyrrrole-fused naphthalene groups and to the resulting extension of the π -electron framework. Although further analyses are required, these structural changes relative to non-annulated porphycenes may also give rise to an appearance of an additional excited state, perhaps, due to imposing a greater molecular rigidity,³⁹ reflected in a weak transition at ca. 505 nm. Compound **2.56b** proved weakly fluorescent in dichloromethane.

Due to its higher crystallinity (and corresponding greater ease in handling) relative to **2.56a**, porphycene **2.56b** was subject to more detailed analysis using cyclic voltammetry. This particular annulated porphycene displays a reversible 2-step oxidation

process, which is characterized by peak potentials at 0.89 and 1.24 V (cyclic voltammetry, 1.5 mM/0.1 M TBAPF₆/DCM vs. SCE; 100 mV/s). The fact that oxidation is more facile with respect to the tetrapropyl porphycene parent is considered consistent with a larger π -electron framework being present in **2.56**.⁵⁸ The observation of a reversible, anodically shifted reduction wave at -0.78 V (vs. -1.04 V for the tetrapropyl system) provides further support for this conclusion. However, in contrast to what is seen in the case of the parent tetrapropyl porphycene, a second cathodic wave could not be observed in the case of **2.56b**.

This same, less soluble, isopropyl-substituted porphycene (i.e., **2.56b**) also yielded X-ray diffraction grade single crystals upon recrystallization from chloroform/hexane. The resulting structure revealed that this particular naphthoporphycene is nearly planar (Figure 2.17). The average deviation for the nitrogen atoms from the mean plane (excluding isopropyl groups) is ± 0.15 Å. On the basis of this structural parameter, **2.56b** is slightly more distorted than tetrapropylporphycene for which the corresponding deviation is ± 0.04 Å.³⁴ The shortest N-N distance in **2.56b** is 2.49 Å, whereas the corresponding separation in the parent, non-annulated porphycenes is typically 2.63 Å.³⁴ These structural differences, together with the NMR spectroscopic data discussed above, provide support for the notion that the N-H-N hydrogen bonds in the π -extended porphycenes reported here are stronger than those present in the original, non-annulated porphycenes.

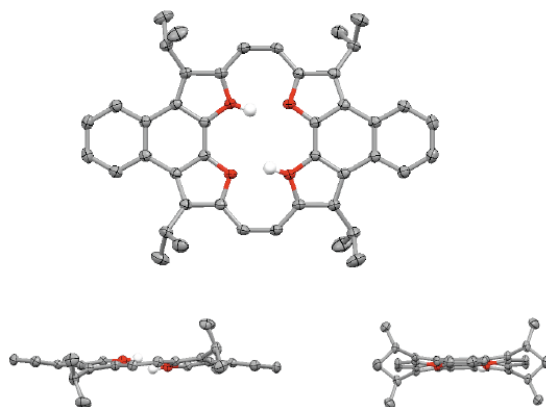


Figure 2.17. Three orthogonal views of the X-ray structure of **2.56b**. All hydrogen atoms bound to carbon atoms are omitted for clarity. Thermal ellipsoids were scaled to the 50% probability level.

A facile route to disubstituted naphthobipyrroles **2.50a,b**, **2.54a,b** and **2.55a,b** developed by the candidate is described in this chapter and provides an incentive to further explore the applicability of this π -extended bipyrrole in areas including, but not limited to, porphyrin analogues and expanded porphyrins. Porphycenes **2.56** are the early examples of what are thought would be a large body of work furthering an understanding of π -extended systems and developing practical applications thereof.

Experimental section.

General procedure for the synthesis of ethyl α -oxocarboxylates 2.51a and 2.51b:

The appropriate alkyl magnesium bromide (1.1 equiv., etheral solution) was added under a nitrogen atmosphere to a solution (0.9 M) of diethyl oxalate (1.0 equiv.) cooled to -78°C in dry diethyl ether over the course of ca. 40 min. The reaction was then kept stirring at -78°C for an additional hour before being quenched with 1 M HCl_{aq} at -78°C . The reaction mixture was allowed to warm to r.t. The aqueous phase was separated off and extracted with ether. The combined organic layers were then dried over Na_2SO_4 . After evaporative removal of the solvent, the product obtained was dried and used without further purification.

Ethyl 2-oxo-4-ethyl-octanoate 2.51a.

After evaporation of the solvent as per the above general procedure, this compound (a colorless liquid) was used without further purification. ¹H NMR (400 MHz, CDCl₃) δ 4.25 (q, J = 7.1, 2H), 2.69 (d, J = 6.7, 2H), 1.91 – 1.81 (m, 1H), 1.49 – 0.99 (m, 11H), 0.89 – 0.72 (m, 6H). ¹³C NMR (101 MHz, CDCl₃) δ 195.5, 162.0, 62.8, 44.1, 35.5, 33.7, 29.4, 26.9, 23.4, 14.6, 14.5, 11.3. GC-MS (m/z = 215, [M+H]⁺)

Ethyl 2-oxo-4-methyl-pentanoate 2.51b.

After evaporation of the solvent as per the above general procedure, this compound (a colorless liquid) was used without further purification. ¹H NMR (400 MHz, CDCl₃) δ 4.22 (q, J = 7.1, 2H), 2.62 (d, J = 6.8, 2H), 2.09 (m, 1H), 1.27 (t, J = 7.1, 2H), 0.87 (d, J = 6.7, 6H). ¹³C NMR (101 MHz, CDCl₃) δ 194.84, 161.87, 62.79, 48.33, 24.64, 22.89, 14.45. GC-MS (m/z = 159, [M+H]⁺)

General procedure for the synthesis 2,3-(Ethyl alkynoate-2)-naphthelenehydrazone 2.53a-c.

A solution of **2.51** (2.5 equiv.) in ethanol (10 M) was added to a suspension of 2,3-naphthalene dihydrazine **2.52** (1.0 equiv.) in ethanol (0.4 M). The reaction mixture turned into a clear solution upon stirring overnight at r.t. At this point, the solvent was removed under reduced pressure and the crude product was purified via flash chromatography on silica gel with mixture of hexane-dichloromethane being used as the eluent. Both major yellow bands were collected together and carried into next step. These two fractions/isomers were in some cases separated individually on small scale for the purpose of characterization.

2,3-(Ethyl 4-ethyl-octanoate-2)-naphthelenehydrazone 2.53a.

This product was purified by column chromatography over silica gel using 20% hexanes-DCM as the eluent. The product was isolated as a sticky mass in a yield of 83%. For the faster-eluting, less polar and lower symmetry isomer: ¹H NMR (400 MHz,

CDCl₃) δ 12.52 (s, 1H), 9.62 (d, J = 4.2, 1H), 8.02 (s, 1H), 7.76 (d, J = 9.0, 1H), 7.66 (d, J = 9.0, 1H), 7.46 (s, 1H), 7.35 – 7.26 (m, 2H), 4.38 (q, J = 7.1, 2H), 4.31 (q, J = 7.1, 2H), 2.70 – 2.44 (m, 4H), 1.97 – 1.62 (m, 2H), 1.44 (t, J = 7.1, 3H), 1.38 (t, J = 7.1, 3H), 1.41 – 1.22 (m, 16H), 0.94 (t, J = 7.1, 6H), 0.91 (t, J = 7.1, 6H). ¹³C NMR (101 MHz, CDCl₃) δ 166.0, 164.4, 139.3, 133.5, 131.3, 131.1, 130.8, 130.8, 130.4, 127.5, 127.0, 125.2, 124.9, 111.0, 112.7, 61.9, 61.4, 37.0, 38.5, 38.1, 33.7, 33.4, 30.9, 29.5, 29.4, 27.0, 26.6, 23.6, 23.5, 14.9, 14.67, 14.7, 14.6, 11.6, 11.6. Second, more polar and higher symmetry isomer: ¹H NMR (400 MHz, CDCl₃) δ 9.41 (s, 2H), 7.65 (s, 2H), 7.62 (dd, J = 6.2, 3.3, 2H), 7.24 (dd, J = 6.2, 3.2, 2H), 4.32 (q, J = 7.1, 4H), 2.67 (d, J = 7.3, 4H), 1.76 (s, 2H), 1.36 (t, J = 7.1, 6H), 1.34 – 1.20 (m, 16H), 0.94 – 0.86 (m, 12H). ¹³C NMR (101 MHz, CDCl₃) δ 166.0, 164.4, 139.3, 133.5, 131.3, 131.1, 130.8, 130.8, 130.4, 127.5, 127.0, 125.2, 124.9, 113.0, 112.7, 61.7, 61.4, 38.9, 38.5, 38.1, 38.0, 33.7, 33.4, 30.9, 29.5, 29.5, 29.4, 27.0, 26.6, 23.6, 23.5, 14.9, 14.7, 14.7, 14.60, 11.6, 11.6. Both the ESI MS (+) (581, [M+H]⁺) and hi-res ESI MS (+) (found 581.4058, calc. for C₃₄H₅₃N₄O₄⁺ 581.4061) data proved identical for both isomers.

2,3-(Ethyl 4-methylpentanoate-2)-naphthelenehydrazone 2.53b.

This product was purified over silica gel using 10% hexanes-DCM as eluent. The product was obtained as yellow sticky mass in 92% yield. ESI MS (+) spectra proved identical for both presumed isomers (469, [M+H]⁺) and therefore, the ¹H NMR spectrum was recorded only for the high symmetry isomer. ¹H NMR (400 MHz, CDCl₃) δ 9.21 (s, 2H), 7.68 (dd, J = 6.2, 3.3, 2H), 7.65 (s, 2H), 7.30 (dd, J = 6.2, 3.2, 2H), 4.34 (q, J = 7.1, 4H), 2.65 (d, J = 7.5, 4H), 2.10 (dp, J = 13.7, 7.0, 2H), 1.38 (t, J = 7.1, 6H), 0.99 (d, J = 6.6, 12H).

2,3-(Ethyl propanoate-2)-naphthelenehydrazone 2.53c.

This bishydrazone has been reported earlier, but without spectral data.⁴³ In our hands, the mixture of isomers could be separated on a silica gel column using

dichloromethane as the eluent. The first fraction proved to be the unsymmetric and less polar isomer: ^1H NMR (400 MHz, CDCl_3) δ 12.58 (s, 1H), 10.56 (s, 1H), 8.15 (s, 1H), 7.83 (d, $J = 7.4$, 1H), 7.68 (d, $J = 7.7$, 1H), 7.45 – 7.31 (m, 2H), 4.47 (q, $J = 7.1$, 2H), 4.36 (q, $J = 7.1$, 2H), 2.21 (s, 3H), 2.18 (s, 3H), 1.54 (t, $J = 7.1$, 3H), 1.47 (t, $J = 7.1$, 3H). The second fraction was the symmetric and more polar isomer: ^1H NMR (400 MHz, CDCl_3) δ 9.18 (s, 2H), 7.65 (dd, $J = 6.2, 3.3$, 2H), 7.61 (s, 2H), 7.29 (dd, $J = 6.2, 3.2$, 2H), 4.33 (q, $J = 7.1$, 4H), 2.18 (s, 6H), 1.37 (t, $J = 7.1$, 6H). Both isomers showed identical molecular peaks in the ESI (+) mass spectrum (385, $[\text{M}+\text{H}]^+$).

General procedure for the synthesis of diethyl 3,8-dialkyl-1,10-dihydro-benzo[e]pyrrolo[3,2-g]indole-2,9-dicarboxylates 2.54a-c.

Dihydrazone **2.53** (1 equiv.) and tosic acid hydrate (10 equiv.) were heated at reflux in ethanol (0.1 M in **2.54**) for 24 hrs. Then solvent was removed under reduced pressure and the reaction mixture was mixed with an excess of water. The undissolved mass that resulted was either collected by filtration or via decantation of the aqueous phase. It was then redissolved in dichloromethane and subject to extensive washing with water. After drying the organic layer over Na_2SO_4 and removal of the volatiles under reduced pressure, the resulting crude products were purified via column chromatography over silica gel using a mixture of 0.5% methanol in dichloromethane as the mobile phase. For most of the diesters **2.54**, the ^1H NMR spectrum at r.t. revealed a significant broadening of the signals. However, heating the samples to 100°C generally increased the resolution of the spectra. ^{13}C NMR spectra were not recorded for the compounds **2.54a-c** due to the conformational complexity these diesters displayed at r.t.

Diethyl 3,8-di-1-ethylpentyl-1,10-dihydro-benzo[e]pyrrolo[3,2-g]indole-2,9-dicarboxylate 2.54a.

Yield 61% as a yellowish glassy solid product. ^1H NMR (600 MHz, $\text{DMSO}-d_6$, 100°C) δ 11.82 (s, 2H), 8.53 (s, 2H), 7.44 (dd, $J = 6.3, 3.4$, 2H), 4.43 (q, $J = 7.1$, 4H), 2.18 – 2.03 (m, 4H), 2.03 – 1.89 (m, 4H), 1.42 (t, $J = 7.1$, 6H), 1.40 – 1.05 (m, 10H), 0.85

(t, J = 7.4, 6H), 0.77 (t, J = 7.2, 6H). MS ESI(+): 547 [M+H]⁺. HiRes ESI MS (+): found 547.3523, calc. for C₃₄H₄₇N₂O₄⁺ 547.3530.

Diethyl 3,8-diisopropyl-1,10-dihydro-benzo[e]pyrrolo[3,2-g]indole-2,9-dicarboxylate 2.54b.

Yield 67% as a yellowish glassy solid product. ¹H NMR (400 MHz, CDCl₃) δ 10.85 (br. s, 2H), 8.44 (br. s, 2H), 7.50 (dd, J = 6.2, 3.4, 2H), 4.37 (br. m, 6H), 1.74 – 1.08 (br. m, 18H). MS ESI(+): 435 [M+H]⁺. HiRes ESI MS (+): found 435.2276, calc. for C₂₆H₃₁N₂O₄⁺ 435.2278.

Diethyl 1,10-dihydro-benzo[e]pyrrolo[3,2-g]indole-2,9-dicarboxylate 2.54c.

After the reflux step noted in the general procedure above was complete, the product precipitated from the reaction solution upon cooling to r.t. This compound is a known material and the characterization data was found to match that detailed in the literature.⁴³

General procedure for the synthesis of 3,8-dialkyl-1,10-dihydro-benzo[e]pyrrolo[3,2-g]indole 2.50a-c.

A mixture of diester **2.54** (1 equiv.) and sodium hydroxide (10 equiv.) was heated at reflux in ethylene glycol (0.1 M in **2.54**) under an argon atmosphere for 1.5 hrs. The reaction was then cooled to r.t. and diluted with cold water (10x the initial ethylene glycol volume). The resulting precipitate was collected by filtration and redissolved in dichloromethane. The resulting solution was dried over Na₂SO₄ and then filtered. The volatiles were removed using a rotary evaporator. To remove colored impurities, if any, after drying over Na₂SO₄, the resulting solution can be passed through a short silica gel column using dichloromethane as the eluent.

3,8-Di-1-ethylpentyl-1,10-dihydro-benzo[e]pyrrolo[3,2-g]indole 2.50a.

Using the above procedure, this product was obtained as an off-white solid product in 90% yield. ¹H NMR (400 MHz, CDCl₃) δ 8.56 (dd, J = 6.3, 3.5, 2H), 7.52 (dd,

J = 6.3, 3.3, 2H), 7.46 (s, 2H), 6.67 (s, 2H), 3.57 (br. s, 2H), 2.07 – 1.63 (m, 8H), 1.62 – 1.18 (m, 8H), 0.99 (t, J = 7.3, 6H), 0.92 (t, J = 6.8, 6H). ¹³C NMR (101 MHz, CDCl₃) δ 127.4, 125.1, 125.0, 123.6, 123.0, 118.1, 117.3, 38.9, 34.6, 30.1, 28.0, 23.8, 14.8, 12.0. ESI MS (+): 403 [M+H]⁺. HiRes ESI MS (+): found 403.3111, calc. for C₂₈H₃₉N₂⁺ 403.3109.

3,8-Diisopropyl-1,10-dihydro-benzo[e]pyrrolo[3,2-g]indole 2.50b.

This product was obtained as an off-white crystalline solid in 83% yield. ¹H NMR (400 MHz, CDCl₃) δ 8.51 (dd, J = 6.3, 3.5, 2H), 7.49 (dd, J = 6.3, 3.3, 2H), 7.25 (s, 2H), 6.67 (s, 2H), 3.88 – 3.70 (m, J = 13.4, 6.7, 2H), 1.49 (d, J = 6.7, 12H). ¹³C NMR (101 MHz, CDCl₃) δ 128.2, 127.1, 125.0, 123.8, 123.1, 117.0, 116.8, 27.4, 24.3. MS ESI(+): 291 [M+H]⁺. HiRes ESI MS (+): found 291.1856 calc. for C₂₀H₂₃N₂⁺ 291.1856. M.p. 240–243° C.

General procedure for the synthesis of 2,9-diformyl-3,8-dialkyl-1,10-dihydro-benzo[e]pyrrolo[3,2-g]indoles 2.55a,b

Phosphorus oxytrichloride (2.2 equiv.) was added dropwise to a clear solution of naphthobipyrrole **2.50** (1 equiv.) in dry DMF (0.1 M in **2.50**) under a nitrogen atmosphere at r.t. The reaction was then stirred for 2 hrs at 80° C. After cooling to r.t., 1 M aqueous NaOH (5x the volume of original quantity of DMF) was added to quench the reaction mixture. The yellow solid obtained as a result of the quenching step was collected by filtration.

2,9-diformyl-3,8-di-1-ethylpentyl-1,10-dihydro-benzo[e]pyrrolo[3,2-g]indole 2.55a.

After the basic work up noted in the general procedure above, the product was collected by filtration. It was then redissolved in dichloromethane and dried over Na₂SO₄. Removal of the solvent yielded **2.55a** in the form of yellow glassy solid (92%). ¹H NMR (600 MHz, DMSO-*d*₆, 100° C) δ 11.99 (s, 2H), 10.14 (s, 2H), 8.54 (s, 2H), 7.49 (dd, J = 6.3, 3.4, 2H), 3.84 (m, 2H), 2.25 – 1.84 (m, 8H), 1.49 – 1.03 (m, 8H), 0.91 (t, J = 7.3,

6H), 0.78 (t, J = 7.1, 6H). MS ESI(+): 459 [M+H]⁺. The ¹³C NMR spectrum was not recorded due to the conformational complexity of **2.55a** inferred to pertain at r.t. MS ESI(+): 459 [M+H]⁺. HiRes ESI MS (+): found 459.3009, calc. for C₃₀H₃₉N₂O₂⁺ 459.3006.

2,9-diformyl-3,8-diisopropyl-1,10-dihydro-benzo[e]pyrrolo[3,2-g]indole 2.55b.

The crude product obtained from the above general procedure was recrystallized from dichloroethane. Yield (81%). ¹H NMR (400 MHz, CDCl₃) δ 12.28 (s, 2H), 10.34 (s, 2H), 8.50 (dd, J = 6.1, 3.5, 2H), 7.55 (dd, J = 6.2, 3.3, 2H), 4.35 – 4.13 (m, 2H), 1.73 (d, J = 7.1, 12H). ¹³C NMR (101 MHz, DMSO-*d*₆) δ 181.7, 137.6, 131.9, 127.8, 125.5, 125.1, 125.0, 119.5, 26.9, 24.8. MS ESI(+): 347 [M+H]⁺. HiRes ESI MS (+): found 347.1749, calc. for C₂₂H₂₃N₂O₂⁺ 347.1754. M.p. 383-385°C.

General procedure for the synthesis of 2,7,12,17-tetraalkylporphycenes 2.56a,b.

Titanium tetrachloride was added dropwise to a mixture of Zn (50 equiv.) and copper (I) chloride (1.6 equiv.) in dry and oxygen-free tetrahydrofuran (ca. 0.3 M in zinc) under a nitrogen atmosphere at r.t. The mixture was then heated under reflux for 3 hrs. Subsequently, a solution of dialdehyde **2.55** in oxygen-free dry tetrahydrofuran (6 mM in **2.55**) was added over the course of 6 hrs by means of a syringe pump. The resulting reaction mixture was then stirred under reflux for an additional 10-12 hrs before being cooled to 0°C using an ice bath. Aqueous ammonia (6%) was added dropwise over the course of 1 hr. This caused the reaction solution to turn greenish-yellow. The resulting solution of what is presumed to be dihydroporphycene was filtered through celite and then subsequently treated with DDQ (1 equiv.). This caused an instantaneous change in the color from yellow-green to dark blue. After removal of the solvent under reduced pressure, the desired porphycene was purified over silica gel using with 10% ethyl acetate – hexanes as the eluent.

2,7,12,17-Tetra-1-ethylpentylporphycene 2.56a.

The product was obtained as a dark blue waxy-solid in 52% yield. ¹H NMR (500 MHz, toluene-*d*₈, 100° C) δ 9.66 (s, 2H), 9.35 (s, 4H), 8.79 (dd, J = 5.8, 3.5, 4H), 7.32 (dd, J = 6.0, 3.3, 4H), 4.43 (s, 4H), 2.66 (m, 8H), 2.43 (m, 8H), 1.71 – 1.18 (m, 16H), 1.17 – 1.10 (m, 12H), 0.80 – 0.72 (m, 12H). ¹³C NMR (126 MHz, toluene-*d*₈, 100° C) δ 148.5, 142.7, 135.3, 133.8, 133.0, 128.5, 127.7, 116.6, 38.4, 32.6, 30.1, 27.9, 23.3, 14.4, 14.0. ESI MS (+): 852 [M+H]⁺. HiRes MS ESI(+): found 851.5983, calc. for C₆₀H₇₅N₄O⁺ 851.5986.

2,7,12,17-Tetraisopropylporphycene 2.56b.

This product was obtained as a dark blue crystalline material (15% yield). ¹H NMR (400 MHz, CDCl₃) δ 9.45 (s, 4H), 9.27 (s, 2H), 8.59 (dd, J = 5.9, 3.5, 4H), 7.49 (dd, J = 5.9, 3.3, 4H), 4.86 – 4.68 (m, 4H), 2.09 (d, J = 7.2, 24H). ¹³C NMR (101 MHz, CDCl₃) δ 147.3, 144.5, 134.4, 132.2, 132.0, 129.0, 128.0, 117.0, 29.1, 25.7. MS ESI(+): 627 [M+H]⁺. HiRes ESI MS (+): found 627.3477, calc. for C₄₄H₄₃N₄⁺ 627.3482. Melting or decomposition point > 450° C.

Chapter Three. Polynaphthobipyrrole.*⁵⁹

A synthetic advancement in the area of porphyrin chemistry inspires work on polypyrrole and *vice versa*. For instance, the synthesis of hydroxy and alkoxy substituted pyrroles and subsequently of corresponding porphyrins⁶⁰ occurred concomitant with the development of the poly(3,4-dioxypyrrole)s.⁶¹ The latter display electrochromic properties such as changing their color depending on the applied potential, which is a typical feature of many conductive polymeric materials. Pyrrole annulated with bicyclo[2.2.2]octane, being a saturated congener of pyrrole **2.14**, has been used in the synthesis of the corresponding polypyrroles with annulated bicyclo[2.2.2]octane.⁶² Such a relationship in synthetic chemistry between porphyrin and polypyrroles is well recognized. New naphthobipyrroles developed by the candidate in the previous chapter showed high utility in the synthesis of novel π -extended porphycenes and pose great interest as monomers in the design and preparation of novel polycyclic conducting polymers.

In general, conjugated polymers obtained by polymerization of suitable redox active monomers, are attracting considerable attention at present, in particular as electrochromic materials. Much of this interest reflects their potential utility in a variety of industrial and military applications, that run the gamut from use in color-tuning windows, displays, smart windows, mirrors, and the like,^{63,64} to the creation of specialty security documents⁶⁵ and chameleon and adaptive camouflage materials.⁶⁶ This utility continues to drive new research in the area and is providing a specific incentive to create and test new electropolymerizable monomers.

It is now recognized that the defining features (and ultimate utility) of a given conjugated polymer material, including film-forming properties, color efficiency,

* Spectroelectrochemical study described in this chapter was conducted in Austin and in Pfinztal in collaboration with Dr. Roznyatovskaya (Fraunhofer Institute of Chemical Technology, Pfinztal 76327, Germany).

response time, low-power operation, stability, etc., often depend critically on the structure and properties of the precursor (monomer) from whence it is derived. Desirable features for these precursors are ones that give rise *inter alia* to polymers with broader absorptions and decreased band gaps. This, in turn, has led to design criteria for monomers that include 1) increased planarity for better π - π^* overlap, 2) chemical rigidification to ensure structural integrity and uniformity following polymerization, and 3) properly chosen substituents to control intramolecular charge transfer interactions.⁶⁷

To date, most common monomers for the preparation of electrochromic polymers have consisted of alternating or sandwich-structured donor and acceptor units, including arenes (benzene, alkyl- and alkoxybenzene, N-alkylcarbazole, 4,4'-biphenylene, and others) and electron rich heterocycles (thiophene and pyrrole, and their derivatives with open α -positions for polymerization).^{68,69} Within the latter subset, most attention has focused on thiophene derivatives; indeed, the literature on functionalized pyrroles as precursors for robust conjugated polymer materials is scarce, presumably reflecting the low chemical stability of pyrrole toward over-oxidation.⁷⁰ For instance, a highly stable electrochromic polymer based on 3,4-ethylenedioxyppyrrrole was reported by Reynolds in 2000.⁷¹ In this case, the poly(3,4-ethylenedioxyppyrrrole) solutions obtained up on electro-oxidation were found to pass from a bright red neutral state to light blue transmissive in its oxidized state. Upon increasing the ring of the alkyl bridge to propylen-, or butylen- another colored state is observed at low doping levels, thus producing materials characterized by multichromic changes.⁷¹

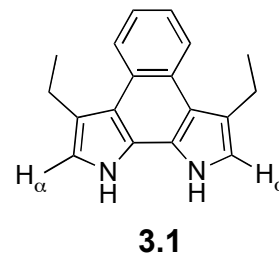
A series of 1,4-bis(pyrrol-2-yl)phenylene monomers, as well as other bis(pyrrol-2-yl)arylene derivatives were prepared by the groups of Reynolds and Katrizky in 1994 and 1996 following the concept of extending the conjugation in the monomer to reduce the oxidation potential.^{68,69} These monomers could be rapidly electropolymerized at ca. 0.15-0.4 V vs. Ag/Ag⁺ to form highly electroactive polymers with smaller electronic band

gaps than polypyrrole. This lowering of the band gap is attributed to an increased structural regularity arising from the use of a three-ring-containing monomer.

Generally, synthetic routes to structurally well defined oligomers of pyrrolic polymer involve polymerization of 2,5-disubstituted pyrrole monomers bearing protective group on the N center through the use of regioselective Stille or Ullman coupling strategies. An alternative approach to reducing unwanted 2,3'- and 2,4'-couplings is to employ a dimer, such as 2,2-bipyrrole, as the precursor in otherwise standard chemical polymerization protocols.⁶³

Building on the successful application of naphthobipyrroles to π -extend porphyrines⁴² diethylnaphthobipyrrole **3.1** was studied with a view to exploring its electrochemical behavior and possible application in the electrochromic material.

3,8-Diethyl-1,10-dihydro-benzo[e]pyrrolo[3,2-g]indole (**3.1**) (referred to as β,β' -diethylnaphthobipyrrole) offers several advantages, such as unequivocal reactivity at the pyrrole α -positions due to the β -positions being blocked by alkyl substituents, a higher level of rigidity as compared to simple



pyrrole or bipyrrole precursors, an expanded system of conjugated bonds and a correspondingly lower oxidation potential due to the annulated phenyl ring. It also benefits from a synthesis that appears cleaner and easier than those used to prepare various previously reported linked pyrrolic precursors.⁷² As a consequence, monomer **3.1** appears attractive for the development of multi-color electrochromic materials.

Several polycyclic benzodipyrroles were prepared by Berlin *et al.* in 1987 and studied as polymer precursors.⁷³ Unfortunately, chemical oxidative polymerization of these species resulted in the formation of black, insoluble powders that precipitated from the reaction medium. On the other hand, it has been reported that the use of a polycyclic aromatic core, such as that present in various poly(naphthodithiophene)s, serves to

enforce planarity between the adjacent heterocycles in the monomeric precursor, resulting in a robust conjugated polymer.⁷⁴

Evidence that this postulate extends to pyrroles (as opposed to thiophenes) comes from a report by Nadeau and Swager that appeared in 2004.⁷² These researchers proposed that the naphthobipyrrole intermediate **3.2** is formed via intramolecular oxidative cyclization during the electrochemical oxidation of a β -linked pyrrole monomer **3.3** (Figure 3.1A). This putative naphthobipyrrole intermediate undergoes polymerization concurrent with its presumed formation. Therefore, it could not be isolated or characterized after its proposed electro-synthesis. Thus, the actual species involved in this particular polymerization remains indeterminate. Further complicating the chemistry is that fact that under the conditions of electro-oxidation, reaction at both β - and α -pyrrolic positions could have occurred in either an intramolecular or intermolecular fashion (Figure 3.1 B).

The placement of the substituents, such as alkyl groups, at the β -positions limits the number of reactive sites during the polymerization. Therefore, 3,8-diethyl-1,10-dihydro-benzo[e]pyrrolo[3,2-g]indole (**3.1**) (referred to as β,β' -diethylnaphthobipyrrole) was synthesized to study its electropolymerization in accord with the conditions proposed by Nadeau and Swager.⁷² It was found that the use of **3.1** produces, after electropolymerization, a stable multi-electrochromic material (Figure 3.1C).

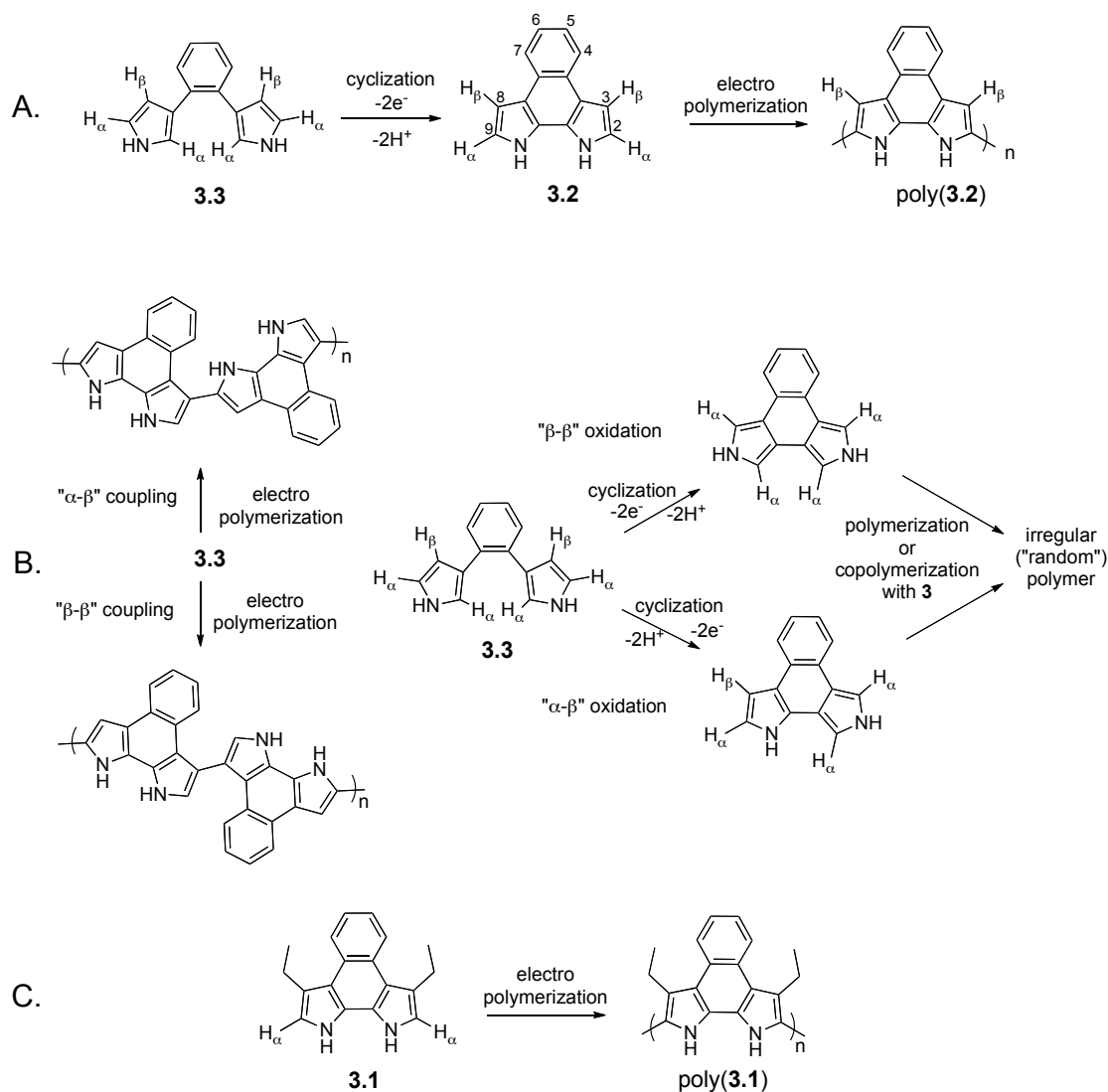


Figure 3.1. Formation of polynaphthobipyrroles. A. Coupling reactions proposed by Nadeau and Swager; B. Alternative structures that could arise from reaction of **3.2** or **3.3**; C. Regiocontrolled electropolymerization.

The key monomer was prepared in accordance with the protocol described in the previous chapter. The choice of substituents was based on the desired solubility of both monomer and resulting polymeric material, namely sufficient solubility of the monomer to allow its dissolution in a solvent suitable for electrodeposition but low solubility for the resulting electrochromic material that could be isolated easily. In order to impart alkyl substituents in the β positions (carbons 3 and 8) and to direct the polymer chain growth

towards the α -pyrrolic positions (carbons 2 and 9) ethyl 2-oxopentanoate **3.4** was synthesized from diethyl oxalate and propylmagnesium bromide.⁵¹

Similarly to dialkyl naphthobipyrroles described in the previous chapter a condensation reaction of naphthalene dihydrazine **2.52** with **3.4** was used to produce dihydrazone **3.5** under acidic conditions, which was subsequently converted into diester **3.6**. Saponification of **3.6** and subsequent decarboxylation quantitatively yielded desired monomer **3.1**.

Previously, the unsubstituted naphthobipyrrole **3.2** was shown to react predominantly at carbons 3 and 8 (i.e., the β -pyrrolic carbons; cf. Figure 3.1 for atom labeling). For instance, Vilsmeier formylation, aminomethylation, and reactions with aryldiazonium salts were found to result in electrophilic substitution at the β -pyrrolic positions.^{44,75} Therefore, it is quite likely that under the conditions of electrochemical

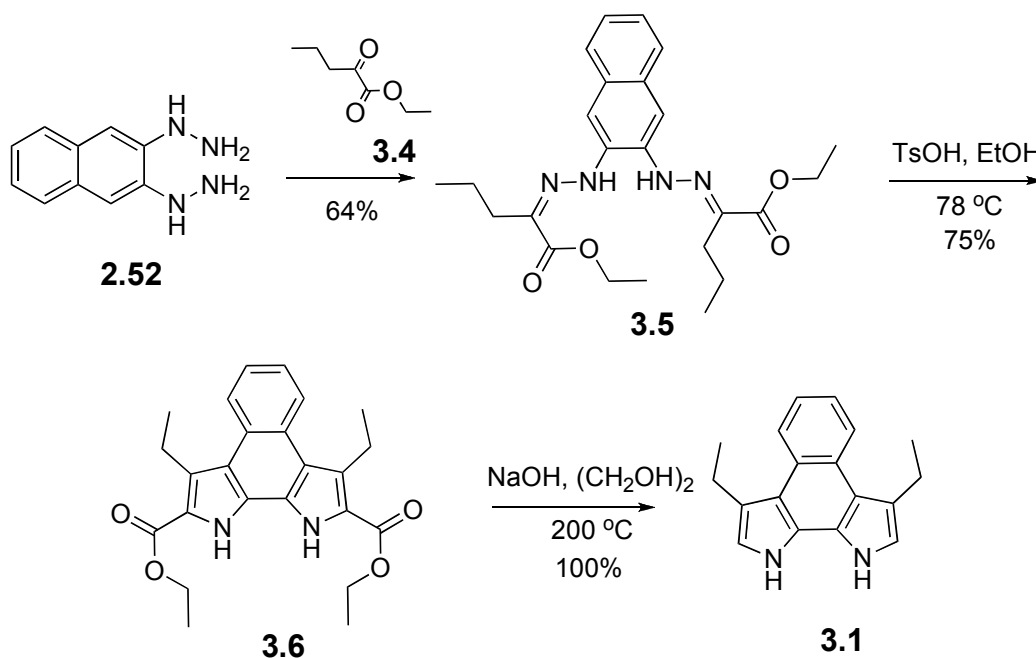


Figure 3.2 Synthesis of the 3,8-diethyl-1,10-dihydro-benzo[e]pyrrolo[3,2-g]indole

oxidation leading to polymerization, the putative bipyrrolic intermediate produced by Nadeau and Swager⁷² undergoes reaction at the β -pyrrolic carbons in addition to, or

instead of, coupling at the α -pyrrolic positions (Figure 3.1B). Therefore, to enforce reaction at just the α -pyrrolic positions, monomer **3.1** was designed to incorporate ethyl groups at carbons 3 and 8. A further potential advantage of the present approach is that it entails a simpler synthesis than used by Nadeau and Swager.⁷² In particular it avoids the need for metalation with butyl lithium and the use of a Suzuki coupling. Instead as noted above, it creates the key bipyrrolic core under simple acid-promoted conditions.

Electrochemistry.

The cyclic voltammogram recorded using an ITO electrode and an electrolyte solution of monomer **3.1** is shown in Figure 3.3. The first feature is an irreversible oxidation starting at a potential of ca. 0.15 V (this and other potentials are vs. Ag/Ag⁺ unless otherwise noted). The same irreversible oxidation peak has been observed previously for a fused-pyrrole 1,4-dihydropyrrolo[3,2- β]pyrrole⁷⁶ and for an α -linked bipyrrole that was studied at moderate scan rates (100 mV/s) and which was assigned to a one-electron process.⁷⁷ By inference, a similar assignment is made here. This prior work also revealed that, similar to what is seen with pyrrole, repetitive cycling of the potential does not produce polymer unless water, typically 1%, is deliberately added. Water is thought to act as a proton scavenger, and in its presence normal nucleation and growth of polymer is observed.⁷⁷

In the case of **3.1**, cycling several times over the potential range from -0.4 V to 0.4 V gives rise to two redox peaks with anodic potentials at 0.1 and 0.25 V, respectively (shown with a thick line in Figure 3.3). The currents of these peak decrease slightly with consecutive cycling. The solution of **3.1** after initial cycles quickly becomes red near the surface of the working electrode and a more intensive red coloration is observed after completing 40-60 cycles. The UV-vis spectrum of the red-colored product displays an absorption maximum at 320 nm, with a shoulder at 360 nm; a distinct spectral feature is also seen at 530 nm, which is ascribed to radical cation intermediates. In contrast to what

is seen after electrochemical cycling, monomer **3.1** is characterized by a strong absorption in the UV region and a very weak absorption peak at 700 nm (Figure 3.4). The red coloration observed after the solution-phase electrooxidation of **3.1** was retained without any visible changes being seen over the course of a couple of days at ambient conditions; subsequently, a black solid begins to precipitate out from solution.

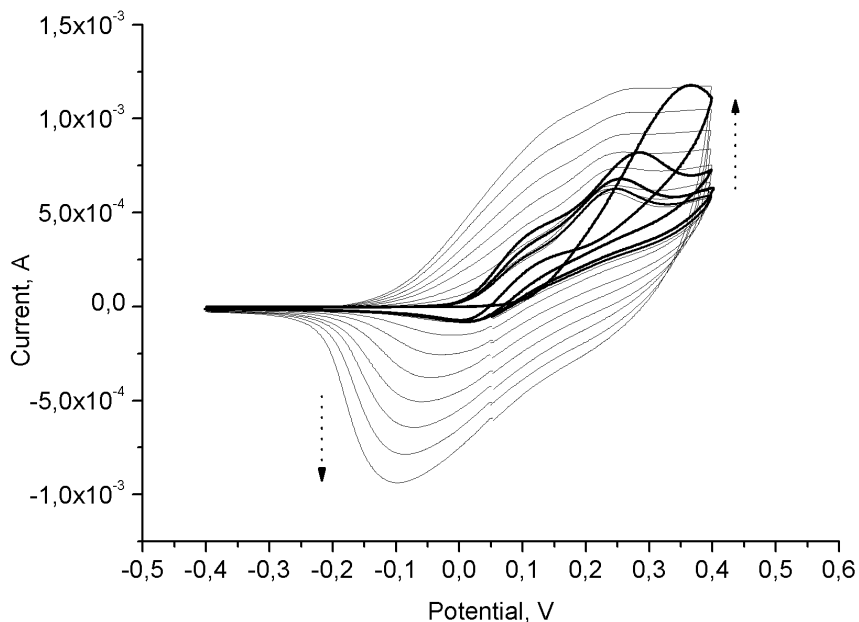


Figure 3.3. Cyclic voltammograms of **3.1** oxidation (1st cycle) and polymer growth observed during repeated oxidation cycles (1-4th cycles – thick line; after this, every 5th cycle up to the 40th cycle is shown) vs. Ag/Ag⁺. The scan rate is 50 mV/s. Arrows denote the evolution of voltammograms as the cycle number increases

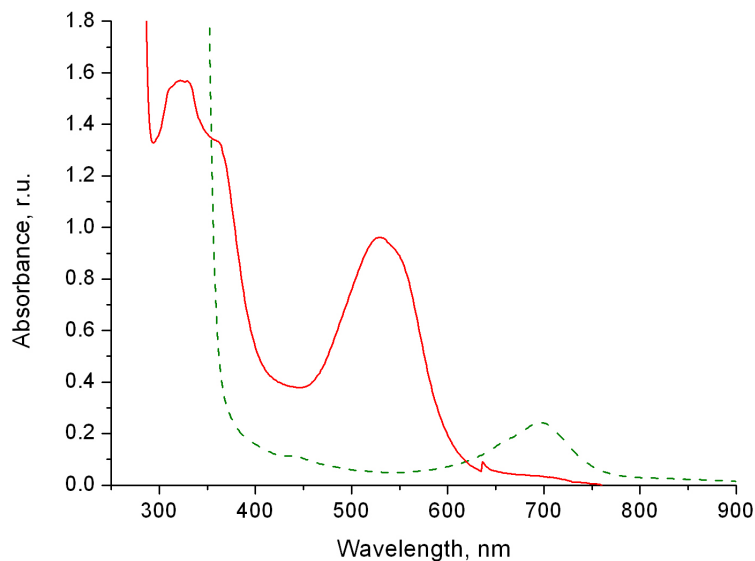


Figure 3.4. Absorption spectra of 5 mM solutions **3.1** in 0.1 M LiClO₄ recorded in MeCN before electrooxidation (dashed line) and after electropolymerization under conditions of cyclic voltammetry (solid line). Because of its high optical density, the sample obtained via electropolymerization was subject to a 20-fold dilution with background electrolyte solution prior to recording the spectrum.

Further potential cycling (cycles 10-40) revealed a continued growth in the anodic and cathodic currents and resulted in formation of a conducting polymer film, deposited on the ITO electrode. Two oxidation peaks observed during the course of the initial cycling are no longer seen distinctly; they are either combined or, more likely, become unresolved, presumably because of the resistance of the polymer film or ohmic contribution of the ITO electrode. It is interesting to note, that a less reversible voltammetric response at a similar range of potentials was observed during the electropolymerization of the fused-pyrrole 1,4-dihydropyrrolo[3,2-β]pyrrole;⁷⁶ this latter precursor also forms ultimately a black thin film on the electrode surface after being subject to electropolymerization.

In analogy to what has been proposed in the case of α -linked bipyrrroles,^{77,78} we assume that the observation of two redox peaks during the course of the initial electrochemical cycling shown in Figure 3.3 is consistent with the fact that the short chain oligomers of **3.1** are oxidized further in MeCN to give in sequence the corresponding radical cation and dication. However, it is to be noted that no modification of voltammetric behavior was observed upon repetitive cycling in solution of a quaterpyrrole monomer.⁷⁹ Further, the electropolymerization of pentapyrrole occurs only at more positive potentials, higher than those of the first and second oxidation processes, i.e., only after generation of the cation radical and dication, respectively.⁷⁷ Thus, it is inferred that higher order oligopyrrolic species play a key role as intermediates in the electropolymerization of **3.1**.

Since the β -pyrrolic positions are blocked, oxidation-induced coupling is expected to take place exclusively at the α -positions. Reactions at the naphthalene ring are ruled out on the basis of the relatively low potentials used for electrooxidation. In general, polycyclic aromatic derivatives, such as acenaphthofluoranthene, undergo oxidative polymerization only at high potentials ($E_{pa} +1.6$ vs SCE).⁸⁰ While it is likely that the naphthalene subunit in **3.1** should have a lower oxidation potential than in the parent hydrocarbon, reactions at the naphthalene subunit are nevertheless considered unlikely to proceed at the applied potentials of between -0.4 to +0.4 V vs. Ag/Ag⁺.

Cyclic voltammograms of **poly3.1** in monomer-free electrolyte solution (Figure 3.5) are characterized by two redox waves with half wave potentials at 0.215 and 0.675 V (at 5 mV/s), respectively. With scan rates higher than 20 mV/s, these waves become poorly resolved and the voltammograms are characterized by broad oxidation and reduction peaks at E_{pa} 0.4 and E_{pc} 0.23 V. Thus, monomer **3.1** oxidizes more readily than polypyrrole, however the observed E_{pa} values are higher, at least in MeCN.⁸¹

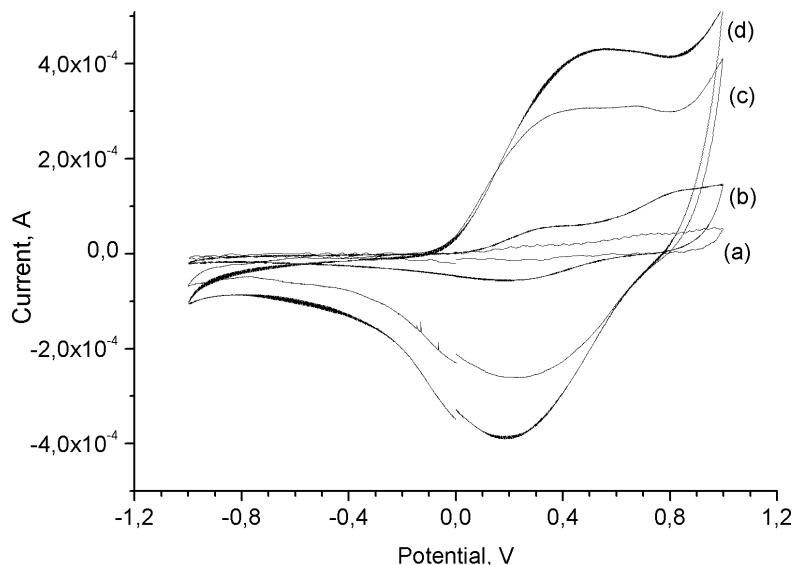


Figure 3.5. Typical cyclic voltammograms recorded for films of **poly3.1** deposited on an ITO substrate (0.1 M LiClO₄, MeCN) vs. Ag/Ag⁺ at (a) 5, (b) 20, (c) 50, (d) 100 mV/s.

The dependence of current values on scan rate, as seen even for the first redox peak of **poly3.1** (Figure 3.5), deviates from linearity at scan rates higher than 50 mV/s. A linear dependence would be consistent with an absence of any kinetic or diffusion limitations for the redox transformations of the species adsorbed at the electrode surface (i.e. polymer film). However, this is not true for **poly3.1** or for polypyrrole. In fact, both the oxidation and reduction electrochemistry of polypyrrole is accompanied by doping and dedoping processes involving counter anions; it is thus proposed that the inferred barrier to reversibility seen for **poly3.1** derives in part from a slow dopant exchange process. This, in turn, could reflect the relatively thick nature of the film.

Morphology of the polymer film

The surface morphology of the **poly3.1** film was investigated by scanning electron microscopy. The film prepared on an ITO electrode was cycled several times in

background electrolyte between -0.7 and +1.0 V, before being left in its partially oxidized state (potential +0.3 V). The green film obtained in this way was dried at ambient conditions before imaging.

The SEM image presented in Figure 3.6a shows that the film is likely to be homogeneous and compact. The image taken with 2000x magnification (Figure 3.6b) reveals finer small features of the **poly3.1** film. It is particularly noteworthy that the surface consists of close-packed nodular grains of ca. 1 μm diameter and spherical, almost uniform, globules of ca. 2 μm diameter. Close-packed grain morphology, a so called “cauliflower surface”, is typical for polypyrroles grown in acetonitrile and doped with perchlorate ions.⁷⁹ The presence of bigger spherical globules has, however, been reported for, e.g., polypyrrole grown from ionic liquids by electropolymerization.⁷⁹

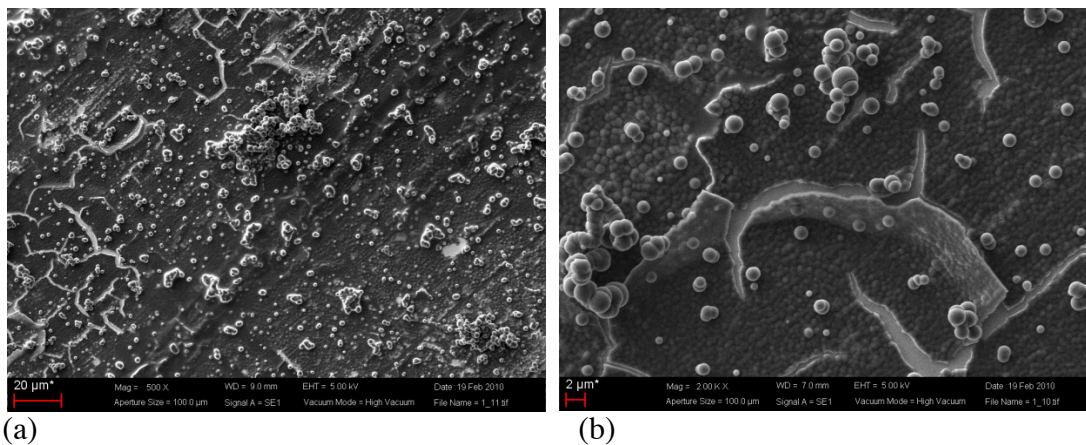


Figure 3.6. Scanning electron microscopy images of **poly3.1** film deposited on an ITO electrode taken after equilibration of the film in a background electrolyte solution (0.1 M LiClO_4 , MeCN). Enlargement is (a) 500x, (b) 2000x.

It was found that a film suitable for use in spectroelectrochemical studies could be deposited via 15-20 rounds of potential cycling. Further cycling to 40 or 60 cycles results in the formation of very thick films, which easily detach from the electrode surface and which have a lot of cracks. The adhesion of the **poly3.1** film to the ITO electrode can be

improved by hydrophobization of the ITO surface by treatment with siloxanes before electropolymerization. On the other hand, this weak adhesion of the polymer on the electrode support might be useful for the preparation of free-standing films.

Spectroelectrochemistry.

The **poly3.1** film was cycled potentiodynamically at least 3-5 times between -0.7 and +1.0V at 50 mV/s after deposition onto an ITO electrode so as to equilibrate the polymer before the spectroelectrochemical measurements. Changes in the absorption spectral features of **poly3.1** as a function of the applied potential are presented in Figure 3.7. The evolution of the absorption spectra of **poly3.1** with applied potential is similar to that of thin films of polypyrrole (less than ca. 0.5 micrometer) as observed in acetonitrile media.^{82,83} However, there are important differences in the spectral features of **poly3.1** relative to those of polypyrrole.

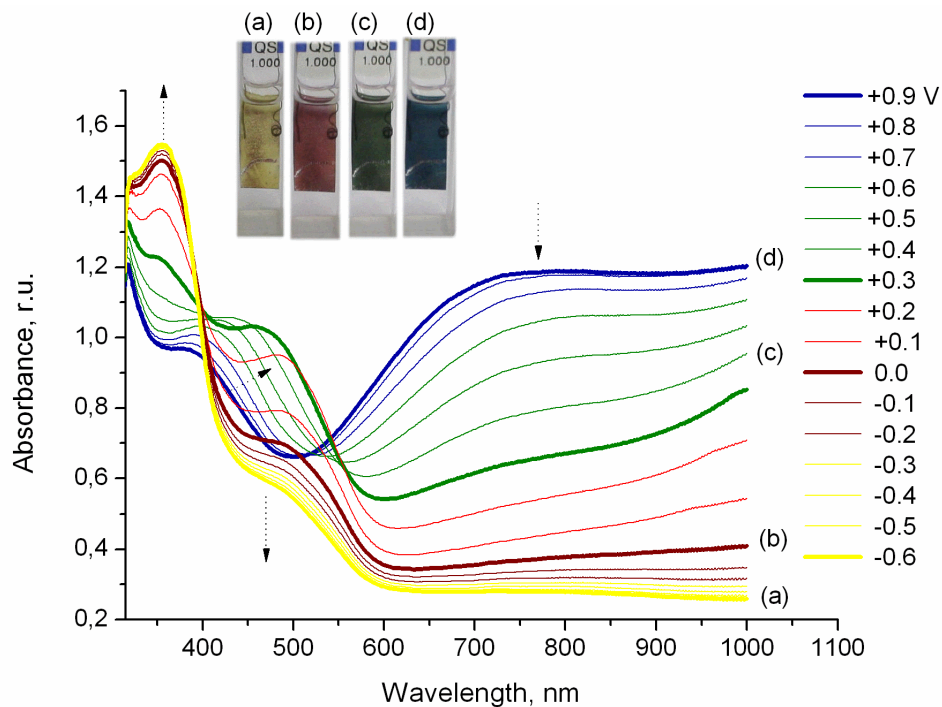


Figure 3.7. Results of spectroelectrochemical studies of **poly3.1** film deposited on an ITO electrode. The measurements were conducted in MeCN, 0.1 M LiClO₄ with 100 mV steps between +0.9 V and -0.6 V vs. a Ag pseudo reference electrode (each step is 60 s long). Inserts show photographs of the polymer films as obtained at potentials of (a) -0.6 V, (b) 0.0, (c) +0.3 and (d) +0.9 V. Arrows denote changes in the spectra associated with a decrease in the applied potential.

Fully oxidized **poly3.1** is blue in color (insert (d) in Figure 3.7). It exhibits a broad absorption band that extends into the near-IR region with a λ_{max} of ca. 750 nm (1.7 eV), as well as a band at 390 nm (3.2 eV) in the visible region. Fully oxidized polypyrrole highly doped with perchlorate ions is characterized by two bipolaron bands at 1240 nm and 450-475 nm, as well as a π - π^* band,^{82,83} and is gray-black or brownish-black in color. General features, notably, the deep blue color observed for oxidized **poly3.1** differ from the black color (broad band in the visible region) reported for oxidized poly(bipyrrolonaphthalene).⁷² We ascribe this difference to the presence of the β -alkylsubstituents and the cleaner nature of the polymerization expected in the case of **3.1** as compared to the system of Nadeau and Swager.

When the applied potential is decreased, the peak in the spectrum of **poly3.1** at 390 nm shifts to 420 nm and the absorbance in the near-IR region decreases. At +0.3 V (insert (c) in Figure 3.7), a potential that corresponds to the partially oxidized **poly3.1**, the absorption spectrum shows two peaks at 355 nm (4.5 eV) and 467 nm (2.6 eV) in the visible region, while the film itself is green. Further cathodic shifts in the applied potential result in a decrease in the absorption intensity at 470 nm with a slight bathochromic shift to 490 nm and an increase in the absorbance at 355 nm. At 0 applied voltage, the film appears red or red-brown (insert (b) in Figure 3.7). Corresponding partially oxidized forms of polypyrrole as reviewed by Murray in 1995⁸³ showed three absorptions, at 1770, 885 and 590 nm. The band at 885 nm, was argued to be caused by the preparation conditions and was not considered to be an intrinsic feature of polypyrrole.

Reduction of the **poly3.1** to the neutral state causes the peak at 490 nm to diminish in intensity and, ultimately it becomes a shoulder of the peak at 355 nm. When the potential reaches -0.6 V the **poly3.1** film becomes pale-yellow (insert (a) in Figure 3.7). The spectrum of the neutral **poly3.1** can be assigned to the π - π^* transition, which occurs at 344-390 nm in case of polypyrrole.^{82,83}

Poly3.1 undergoes two oxidations in the range of -1.0 to +1.0 V (Figure 3.5), which are accompanied by a reversible color change from pale-yellow (neutral form), red to green (partially oxidized and mixture of redox forms) and blue (fully oxidized). These chromatic changes are easily described in terms of the formation of four co-existing or dominating forms (states) of the polymer, namely the neutral form, as well as polaronic, bipolaronic, and so-called transverse bipolaronic states, with the latter state being caused by efficient interchain coupling of polarons on adjacent polymer chains.⁸³ The terms “polaron” and “bipolaron” were introduced to identify the charge carriers in polypyrrole, which were not unpaired electrons, and to explain the nature of its conductivity and optical features.⁸³ An overview of the optical absorption bands of polypyrrole was

published by Potje-Kamloth in 2000,⁸² who ascribed the absorption below 1.4 eV and the band at 1.8 eV to the sum of the polarons and transverse bipolarons, the band at 2.44-2.5 eV to the sum of polarons, bipolarons and transverse bipolarons, and the band around 3.2-3.6 eV to the band gap transition of polypyrrole.

This ability to span multiple colors, including those needed for color mixing does not appear to depend strongly on electropolymerization conditions or level of defects, as it is for regular polypyrrole. It is interesting to note, that color changes similar to those seen for **poly3.1** are reported for a hybrid polypyrrole material incorporating (octa(thiophenophenyl)silsesquioxane) subunits within the polymer chains.⁸⁴ However, the properties of **poly3.1** differ from those of polypyrrole and the previous system of Nadeau and Swager. These differences, noted in the discussion above, are specifically summarized in Table 3.1.

Table 3.1. UV-Vis spectral features of selected polypyrrole polymers.

Polymer/ redox state	Optical absorption bands			Color	Reference
Poly3.1 / neutral partially-oxidized fully-oxidized	355 nm	shoulder 490 nm 470-490 nm shoulder 400 nm	broad 750 nm	yellow red blue	59
poly(bipyrrolonaphthalene) / neutral partially-oxidized fully-oxidized	390 nm **	540 nm **	broad 780 nm	yellow black	72
Polypyrrole / neutral partially-oxidized fully-oxidized	344-390 nm 387 nm	430, 490-508, 590 475 nm	885* 690, 885*-900 nm	yellow black (blue)	70,82,83,85

* the existence of this band is still subject to discussion. ** Broad absorption across the whole visible region

Figure 3.8 presents the results of chronovoltabsorptometry experiments, namely subjecting the film to switching with an applied square wave potential between extreme electrochromic states (neutral and fully oxidized **poly3.1**). To estimate the switching time and the coloration efficiency, these cycling experiments were carried out while recording the optical absorption at a particular wavelength (700 nm) as a function of time.

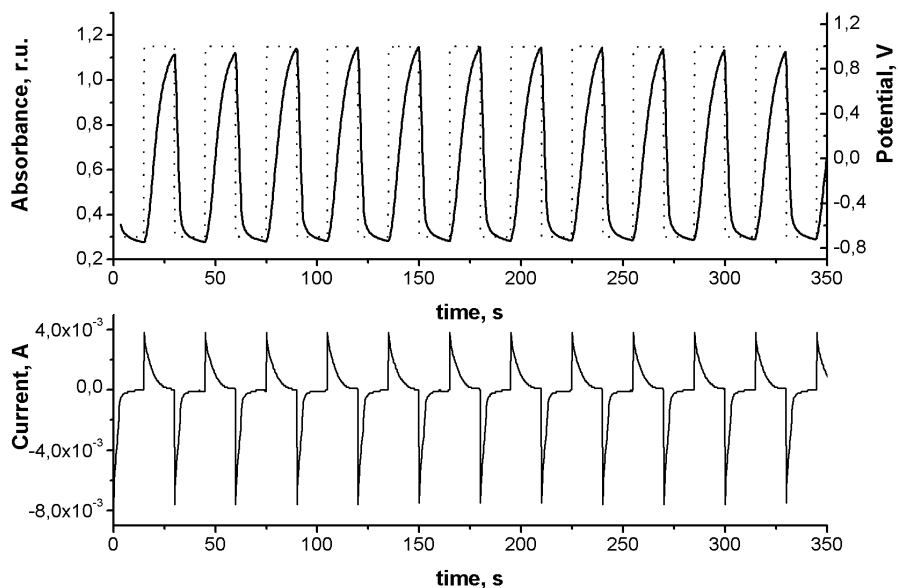


Figure 3.8. Current transients and changes in the absorbance features of **poly3.1** film supported on an ITO electrode (solid lines) at 700 nm observed upon repetitive switching of the applied potential between -0.7 and +1.0 V (dotted line) in 0.1 M LiClO₄, MeCN.

Using the literature definition of the switching time (i.e. the time between 10% and 90% of steady state absorbance at the electrochromic extremes), we found a switching rate of 6-7 s.⁸⁶ This time is longer than typical switching times seen for thiophene derivatives, but is comparable to the switching times seen for pyrrole derivatives, such as dipyrromethane (ca. 5 s).⁸⁷

Coloration efficiency, defined as the ratio between the change in optical density units and the injected/ejected charge as a function of electrode area, was estimated from the data shown in Figures 3.7 and 3.8, and was found to be 98 cm²/C at 700 nm and 74 cm²/C at 355 nm. These values are lower than what can be attained in the case of the widely used electrochromic material, poly(3,4-ethylenedioxythiophene)(183 cm²/C).⁸⁸ On the other hand, the first maximal coloration efficiency approaches the 100 cm²/C value considered acceptable for a working electrochromic device.⁸⁶

A new annulated bipyrrrole **3.1** was prepared and its electrochemical properties analyzed. It was found that **3.1**, a fully characterized monomeric species, can be electropolymerized under oxidizing conditions to form an electrochromic polymer, **poly3.1**. **Poly3.1** undergoes two redox transitions in the range of -0.6 to +1 V vs. Ag/Ag+. These redox changes are accompanied by variations in color that range from pale-yellow, through red, green to blue. The corresponding UV-vis spectra are characterized by considerable bathochromic shifts with an increase in the applied voltage. Nevertheless, compared to a previously reported polymer based on the *in situ* creation of **3.2**, **poly3.1** offers a number of advantages, including a structure that is necessarily better defined, and a monomer that is easier to prepare. It is thus proposed that **poly3.1** and its congeners could find use as electrochromic materials.

Experimental section.

2,3-(Ethyl pentanoate-2)-naphthalenehydrazone 3.5.

A solution of **3.4** (6.70 g, 37.2 mmole, 80% mixture with diethyloxalate) in 2.5 ml ethanol was added to a suspension of 2,3-naphthalene dihydrazine **2.52** (2.00 g, 10.64 mmol) in 25 ml of ethanol. The reaction mixture became a clear solution during the course of stirring for 3 hours at r.t. At this point, the solvent was removed under reduced pressure and the crude product was purified via flash chromatography on silica gel with a

mixture of hexane (10 to 0%)-dichloromethane being used as the eluent. The major, yellowish band was collected yielding **3.5** as an orange goo after removal of the solvent (2.99 g, 64%). ¹H NMR (400 MHz, CDCl₃): δ 9.34 (s, 2H), 7.65 (m, 4H), 7.42 – 7.05 (m, 2H), 4.33 (q, J = 7.1, 4H), 2.75 – 2.70 (m, 4H), 1.61 (m, 4H), 1.37 (t, J = 7.1, 6H), 0.99 (t, J = 7.4, 6H). ¹³C NMR (101 MHz, CDCl₃) δ 165.8, 138.9, 132.9, 131.0, 127.5, 125.6, 113.7, 62.1, 27.1, 19.7, 15.3, 14.9. ESI MS (+): 903 [2M+Na]⁺. HiRes MS ESI(+): found 903.4740, calc. for C₄₈H₆₄N₈O₈Na⁺ 903.4739.

3,8-Diethyl-1,10-dihydro-benzo[e]pyrrolo[3,2-g]indole-2,9-dicarboxylic acid, 2,9-diethyl ester 3.6.

Dihydrazone **3.5** (1.54 g, 3.51 mmol) and tosic acid hydrate (6.75 g, 35.53 mmol, 10 equiv.) were heated at reflux in ethanol (150 ml) for 48 hrs. Then solvent was removed under reduced pressure and the product was purified on silica gel using dichloromethane as the mobile phase; this yielded **3.6** as an off-white solid (1.07 g, 75%). M.p. 267-270° C. ¹H NMR (400 MHz, CDCl₃) δ 10.92 (s, 2H), 8.12 (br. s, 2H), 7.45 (br. s, 2H), 4.24 (br. d, J = 6.9, 4H), 3.02 (br. s, 4H), 1.23 (br. s, 6H), 1.11 (t, J = 7.0, 6H). ¹H NMR (500 MHz, DMSO-*d*₆) δ 11.68 (s, 2H), 8.41 (m, 2H), 7.50 (m, 2H), 4.42 (q, J = 7.1, 4H), 3.50 (q, J = 7.4, 4H), 1.42 (t, J = 7.1, 6H), 1.35 (t, J = 7.4, 6H). ¹³C NMR (101 MHz, CDCl₃) δ 164.6, 132.2, 128.5, 125.1, 124.8, 120.9, 120.9, 61.9, 20.2, 15.1, 14.7. MS ESI(+): 407 [M+H]⁺. HiRes ESI MS (+): found 407.1967, calc. for C₂₄H₂₇N₂O₄⁺ 407.1965. Note: most of the signals in the ¹H NMR spectrum of **3.6** were broadened at room temperature; however, the peaks narrowed upon heating the sample to 100° C in DMSO-*d*₆.

3,8-Diethyl-1,10-dihydro-benzo[e]pyrrolo[3,2-g]indole 3.1.

A mixture of **3.6** (220 mg, 0.54 mmol) and sodium hydroxide (216 mg, 5.4 mmol, 10 equiv.) was heated at reflux in ethylene glycol (5 ml) under an argon atmosphere for 1.5 hrs. Then reaction was cooled to r.t. and diluted with cold water (70 ml). The

resulting off-white precipitate was collected and redissolved in dichloromethane. The solution was dried over Na_2SO_4 and then filtered. The volatiles were removed using a rotary evaporator and the sample was further dried under high vacuum at 50°C . Yield 140 mg (100%). M.p. $209\text{-}211^\circ\text{C}$. ^1H NMR (400 MHz, CDCl_3) δ 8.49 (dd, $J = 6.2, 3.4$, 2H), 7.48 (dd, $J = 6.3, 3.3$, 2H), 7.36 (s, 2H), 6.69 (s, 2H), 3.21 (q, $J = 7.3$, 4H), 1.49 (t, $J = 7.4$, 6H). ^{13}C NMR (101 MHz, CDCl_3) δ 127.6, 125.0, 124.0, 123.4, 122.8, 118.6, 117.7, 22.6, 15.2. ESI MS (+): 263 $[\text{M}+\text{H}]^+$. HiRes MS ESI(+): found 262.1467 $[\text{M}]^+$, calc. for $\text{C}_{18}\text{H}_{18}\text{N}_2^+$ 262.1465. Elemental analysis calculated for $\text{C}_{18}\text{H}_{18}\text{N}_2$: C 82.41, H 6.92, N 10.68. Found: C 82.51, H 6.82, N 10.61.

Chapter Four. A Method for Rapid Screening of Photosensitizers by Scanning Electrochemical Microscopy (SECM) and the Synthesis and Testing of a Porphyrin Sensitizer^{89*}

Laborious synthetic work is commonly concomitant, if not inevitable, while designing new classes of compounds. As evident from chapters one and two, significant synthetic efforts have been made in preparation of the π -extended porphyrinoids, luckily with auspicious outcome. However, a quick access to porphyrin derivatives is often desired to test one supposition or another before investing more efforts into advancing and optimizing procedures. In this chapter a part of larger methodological work, developed by the candidate but not included in this manuscript, is used in the form of a short synthetic protocol to obtain porphyrin with electron rich substituents. The objective of this strategy, thus, is to prepare and use an easily accessible derivative to test whether the derivatization in question produces positive results and to confirm if the original hypothesis is accurate, specifically if an addition of the electron rich substituents increases sensitizing ability of the studied chromophores.

Dye-sensitized solar cells (DSSCs) (also known as Grätzel cells) based on mesoporous TiO₂ electrodes have attracted extensive attention in recent years due to their expected low fabrication costs and relatively high efficiencies, η .^{90,91} Although ruthenium polypyridyl complexes have proven to be excellent TiO₂ sensitizers and have achieved the η values, up to 11.5%, difficulties in large-scale manufacturing have been encountered. Ongoing efforts have been devoted to finding metal-free organic chromophores or inexpensive metal complexes that are suitable for use in DSSCs. In this context, porphyrins have proved particularly attractive. These venerable chromophores bear analogy to pigments found in natural photosynthetic systems and are characterized

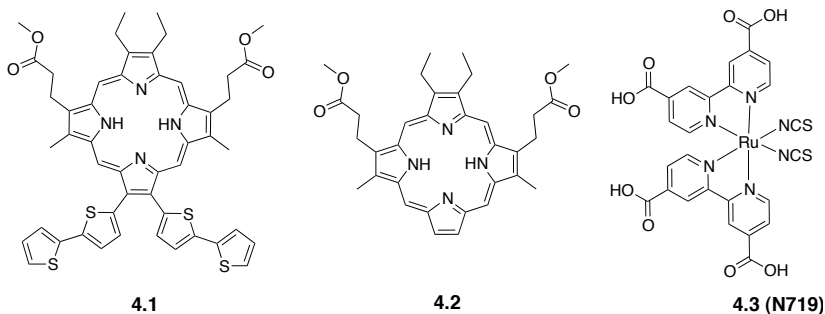
* Photoelectrochemical study described in this chapter was done jointly with Dr. Bard's group in UT Austin. Specifically, SECM measurements were conducted by the visiting researcher, Fen Zhang.

by a Soret band in the 400-450 nm spectral region, as well as weaker Q bands centered around 550-600 nm but often extending over a greater spectral frequency.^{92,93}

To date, scanning electrochemical microscopy (SECM) techniques have been applied in a number of areas,⁹⁴ including electrocatalyst and photocatalyst selection and proved to be very helpful in a number of research tasks. For example, SECM-based approaches were used to screen bimetallic and trimetallic complexes as potential electrocatalysts for use in the oxygen reduction reaction (ORR). In fact, using SECM several useful Pd-Co based electrocatalysts have been identified⁹⁵⁻⁹⁸ that displayed activities in strong acid comparable to that of Pt. SECM methods have also been used to study oxygen evolution reactions.⁹⁹ Furthermore, by replacing the usual SECM ultramicroelectrode (UME) tip with an optical fiber, Bard group has proved possible to test rapidly potential semiconductor photocatalysts for use in photoelectrochemical (PEC) cells. In these latter screening studies, one end of the optical fiber was connected to a 150 W Xe lamp, and the other end was placed in the SECM tip holder over the spot array at a distance of about 100 μm . The photoactivity was determined from the photocurrent generated. This method was used previously by the Bard group to identify several good photocatalysts, including tungsten-doped bismuth vanadate, tin-doped iron oxide and a number of others.^{100,101}

Given the successful employment of the SECM method, this technique was tested to screen arrays of DSSC porphyrin photosensitizers prepared via a rapid deposition method on a TiO_2

nanotube substrate (anodized Ti). To facilitate these efforts, the candidate designed



and synthesized a new functionalized bis-bithiophene porphyrin derivative **4.1**. In

conjunction with the Bard group it was used to prepare arrays consisting of a photosensitizer on an anodized TiO₂ nanotube substrate. These were then tested using the modified SECM method. Photosensitizer arrays (consisting of spots on the TiO₂ nanotube substrate) were prepared from solutions of porphyrin **4.1**, as well from those of the control porphyrin system **4.2** and the known ruthenium-based sensitizer **4.3**, commonly referred as N719. The sensitized photocurrents of the constituent dyes (contained within the spots) were then measured by scanning an optical fiber over each spot on the array and reflected sensitizing ability of the dye in question.

SENSITIZER DESIGN CONSIDERATIONS

Although porphyrins have not shown the desired efficiency for use in practical devices, the large number of previous studies of porphyrins led us to consider that elaboration of a porphyrin with electron rich substituents, in particular bithiophenes, might improve its behavior as a sensitizer. To test this hypothesis, we set out to create porphyrins bearing this functionality. However, in considering the placement of these electron rich groups, we wanted to avoid substitution at the meso or bridging carbon, positions. In porphyrins, the electron density in the highest occupied molecular orbitals (HOMOs) is generally higher on the meso positions compared to the rest of the macrocycle. This makes these sites the more reactive ones in electrophilic substitution reactions (halogenation, nitration, etc.).¹⁰² However, substitution at the meso substituents, *e.g.*, with phenyl groups, generally places the substituents in a geometry that is orthogonal or at least tilted away from the plane of the porphyrin (*i.e.*, a high dihedral angle). This tends to reduce the extent of coupling with the porphyrin conjugation pathway.¹⁰³ Therefore, a general and easy way to functionalize porphyrins at the so-called β -pyrrolic positions was sought. Dihalogenated meso-free porphyrins seem especially

appealing precursors for accomplishing this goal. Halogen atoms in the porphyrin periphery have been shown to act as effective coupling partners in Suzuki-Miyaura reactions,¹⁰⁴ making β -dihalogenated porphyrins attractive intermediates for the preparation of the targeted bis-bithiophene functionalized porphyrins sought in the context of this study.

Although halogenated *meso*-free porphyrins have been reported, their synthesis is tedious and utilizes sensitive material (dibromopyrroles or dibromotripyrranes).¹⁰⁵ Therefore, we developed an alternative approach based on a so-called “3 + 1” condensation; this chemistry is discussed further below.

SYNTHESIS OF THE PORPHYRIN-BASED SENSITIZERS

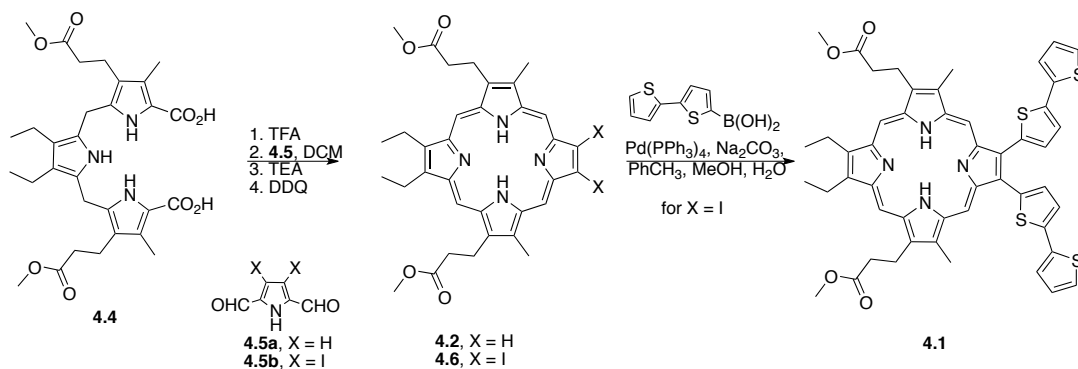


Figure 4.1. Synthesis of the porphyrin-based sensitizers.

Porphyrin **4.1** was synthesized from porphyrin **4.6** as shown in Figure 4.1. Porphyrin **4.6**, in turn, was prepared from the known diiodopyrrole **4.5b** and diacid **4.4** via a “3 + 1” procedure analogous to that described in the literature.^{106,107} Specifically, decarboxylation of the diacid **4.4** in neat TFA and followed by the condensation with **4.5b** produced the reduced, porphyrinogen form of **4.6**. Treatment with DDQ then gave diiodoporphyrin **4.6**. Suzuki coupling between **4.6** and bithiophene boronic acid then produced porphyrin **4.1** in 74% yield.

We also prepared the unsubstituted porphyrin **4.2** as a control compound. While similar porphyrins are known,¹⁰⁶ this specific compound does not appear to have been reported previously.

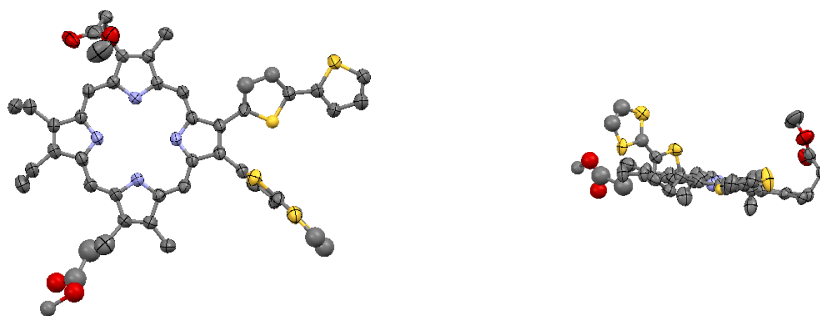


Figure 4.2. Top and side views of a single crystal X-ray diffraction structure of porphyrin **4.1** showing two orientations of the bithiophene substituents. All hydrogen atoms are omitted for clarity. Thermal ellipsoids are scaled to the 50% probability level.

A single crystal of **4.1** suitable for X-ray diffraction analysis was obtained by recrystallizing from a DCM/MeOH mixture. Although disorder in the crystal packing was observed in the resulting structure, it was found that, at least in the solid state, one bithiophene moiety is orthogonal to the porphyrin, whereas the other is fairly coplanar with this latter macrocyclic ring (Figure 4.2).

PHOTOELECTROCHEMISTRY

As mentioned before the SEM technique is attractive for studying and

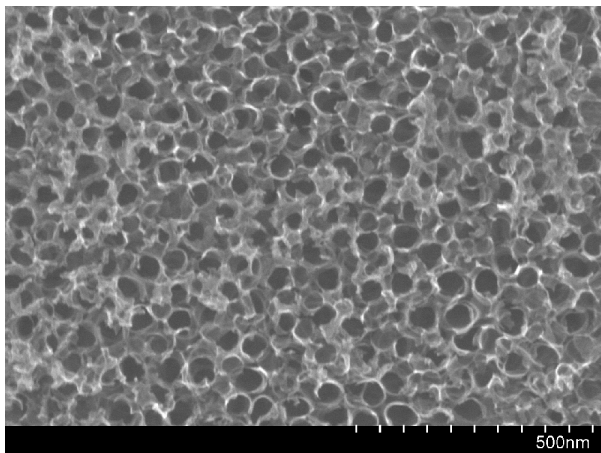


Figure 4.3. SEM image of TiO₂ nanotubes anodized at 20 V in ethylene glycol/water (99:1, volume ratio) with the addition of 0.5 wt.% NH₄F.

comparing various chromophores in DSSC assemblies. Bipyridine-based ruthenium complexes, such as the N3, N719, and C101 dyes are among the most efficient photosensitizers to date.^{91,108-110} Therefore, as a control, **N719** was also measured under the conditions applied to compounds **4.1** and **4.2**.

TiO₂ was chosen as the target material because it has been used in nanoparticle (NP) form in

most DSSCs and has a large band gap that gives rise to little visible response. We thus considered it likely that vertically oriented anodic TiO₂ films might be appropriate for enhancing electron transport in TiO₂ films.¹¹¹ TiO₂ nanotube electrodes possess a relatively large surface area and the quantity of dye molecules absorbed onto the nanostructures is considerably increased relative to what is true for NP TiO₂ films. As a result, the efficiency of charge collection is generally much better than that of NP films. There are several studies using TiO₂ nanotubes as the electrode in DSSCs.^{112,113} The hollow nature of these tubes makes both inner and outer surface areas accessible for modification with sensitizing dyes. The titanium base that supports the nanotube arrays facilitates electrical contact to collect the photogenerated charge carriers. The 10 μm thick nanostructured TiO₂ film is now being used as the electron transporting layer which consists typically of interconnected nanometer-sized TiO₂ particles.¹¹¹ Figure 4.3 shows a scanning electron microscopy (SEM) image of a typical substrate of TiO₂ nanotubes (thickness ~5 μm) with a ~60 nm inner diameter and a ~80 nm outer diameter. It would

probably also be possible to use nanoporous TiO₂ or ZnO as conventionally used in DSSCs as a substrate for these arrays.

Photosensitizers then were arrayed and screened. Figure 4.4a shows the array pattern created by a different number of drops of dispensed solution. The numbers inside the circles represent the number of drops dispensed for that spot. For example, the spot at the upper left corner has no dye while the spot at the bottom right corner contains 30 drops of the same dye. Figures 4.4b and 4.4c show the SECM images obtained for a sensitizer array consisting of dye **N719** and exposed to UV-Vis and visible light irradiation ($\lambda > 420$ nm) respectively. The applied potential was 0.2 V vs AgQRE (silver quasi reference electrode), when the solution contained 0.1 M TBAI in MeCN. As shown in this figure, the anodic photocurrent increased with the number of **N719** dye drops. The same trend was seen at higher bias potentials (not shown). The maximum photocurrent of the spot showed a 30 times larger current compared to the pure TiO₂ nanotubes (substrate), 2240 nA versus 81.8 nA, under UV-visible irradiation. It is worth noting that under visible light irradiation ($\lambda > 420$ nm), the background current changed to a positive (reduction) current, due to the reduction of photogenerated iodine on the TiO₂ substrate. Another contribution to this change in background current is the reduction of O₂ dissolved in the electrolytes under the conditions used to screen the arrays. Under both UV-visible light and visible light irradiation, the spots with larger amounts of dye displayed larger photocurrents in the range of dye deposited. However it should be noted that there is an adsorption limit for the TiO₂ nanotube substrate. When the amount of dye reached the limit or exceeded the limit, the dye tended to desorb from the TiO₂ surface. Such tendencies were noted in the experiments.

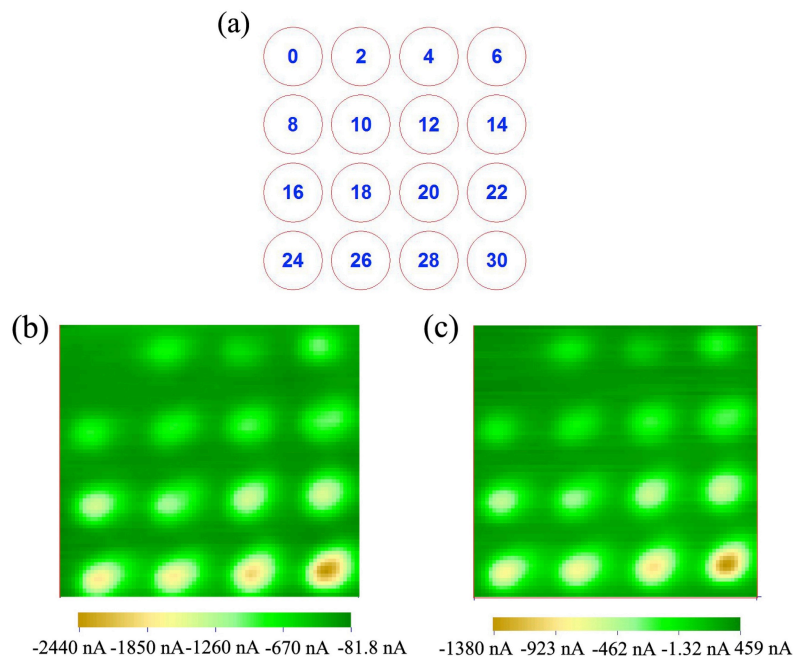


Figure 4.4. (a) Dispensed pattern of a **N719** sensitizer array. Shown are number of drops dispensed at a given location. SECM images of **N719** sensitizer on TiO_2 nanotubes/Ti foil at an applied potential of 0.2 V vs AgQRE (quasi reference electrode) under (b) UV-visible and (c) visible light ($\lambda > 420$ nm). Scan rate: 500 $\mu\text{m/s}$ (SECM setting 50 $\mu\text{m}/0.1$ s); solution, 0.1 M TBAI in MeCN.

Numerous papers have discussed the **N719** dye and its use in DSSC assemblies. In fact, a number of substrate materials have been sensitized by this ruthenium complex, including TiO_2 nanotubes,¹¹² as well as SrTiO_3 ¹¹⁴ and Zn_2SnO_4 ¹¹⁵ substrates. The purpose of our initial experiments using TiO_2 nanotubes and **N719** was to test whether a modified SECM technique could be used to effect the rapid screening of sensitizers; **N719** was thus chosen as a positive control in these studies because it is a widely known, efficient sensitizer.

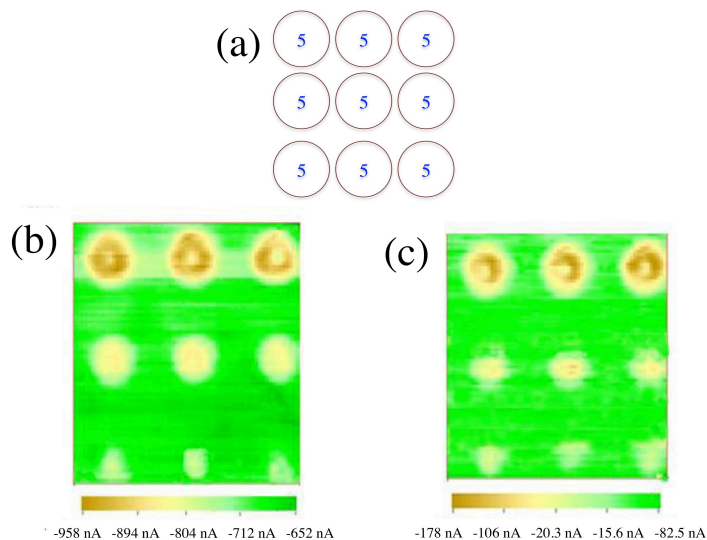


Figure 4.5. (a) Dispensed pattern of three different kinds of dye arrays. SECM images of three different kinds of dyes on TiO_2 nanotubes/Ti foil at applied potential of 0.5 V vs an AgQRE under (b) UV-visible and (c) visible light. Scan rate: 500 $\mu\text{m/s}$ (SECM setting 50 $\mu\text{m}/0.1$ s); solution, 0.1 M TBAI in MeCN.

After proving that the SECM technique can be used to monitor this particular photosensitizer, new porphyrin dyes were tested. Toward this end, the bisbithiophene-substituted porphyrin **4.1** was prepared, as noted above. SECM was then used to compare its efficiency and that of a porphyrin-based, negative control system, **4.2**, with that of **N719**. Figure 4.5a shows three different kinds of dye array patterns. The numbers inside the circles represent the number of drops dispensed for that spot. The first row is pure **N719**, the second row is pure porphyrin **4.1**, and the last row is pure control porphyrin **4.2**. Figures 4.5b and 4.5c show the images obtained for the sensitizer arrays consisting of **N719**, porphyrin **4.1** and control porphyrin **4.2**. The applied potential was 0.5 V vs. AgQRE and the solution was 0.1 M TBAI in MeCN.

As seen in Figures 4.5b and 4.5c, the modified SECM method makes it easy to compare the relative photocurrents of the dyes. As noted above, the iodine

photogenerated by irradiation of dyes is reduced on TiO₂ at a sufficiently small bias that only a low background reduction current is obtained. To avoid or decrease this small reduction current further, we applied a more positive potential (0.5 V vs AgQRE) when screening the arrays. The ruthenium-based sensitizer **N719** displayed average anodic photocurrents of 945 nA and 170 nA under UV-visible and visible illumination, respectively, compared to porphyrin **4.1**, with average photocurrents of 850 nA and 74 nA and the control porphyrin **4.2** with average photocurrents of 791 nA and 13 nA, respectively, upon irradiation with UV-visible and visible light. The TiO₂ nanotubes have a high response in the UV region ($\lambda < 420$ nm) so the response indicated under UV-visible light illumination is high because of the direct TiO₂ response.¹¹⁶ Thus the sensitized photooxidation current under visible light illumination is more diagnostic of the relative efficiency. By comparing the photocurrent values of the three different dyes under visible light irradiation, it becomes possible to rank order the relative efficiencies of the three photosensitizers studied here (**N719**, porphyrin **4.1** and porphyrin **4.2**). Clearly **N719** was the most effective sensitizer, but the ruthenium-free porphyrin **4.1** produced a reasonable response, while the negative control, **4.2**, produced a photocurrent only 25-35% of that of porphyrin **4.1**. Note that for these studies, the concentration of porphyrin **4.1** and control porphyrin **4.2** were 5 times larger than that of **N719**; the results have been normalized to take this into account. Based on the above analysis, we thus conclude that the SECM technique is a fast and convenient way to compare the relative sensitization efficiencies of different dyes.

Previously, the SECM technique was used to investigate the effect of metal or nonmetal element dopants on known photocatalysts^{100,116} as well as for binary metallic electrocatalysts.⁹⁵⁻⁹⁸ This leads to the suggestion that this method could be used to test whether there is a synergistic benefit when two kinds of dyes are used together. Both **N719** and porphyrins represent established dyes for spectral sensitization, as noted in this work. Therefore, we chose **N719** and porphyrin **4.1** as test systems with which to probe

whether the SECM technique could be used to observe an improved effect with mixtures of the dyes, assuming that this synergetic behavior exists. Figure 4.6a displays the dispensed pattern. The first spot in row 1 consists of 100% **N719**. The first number in the circles is the number of drops of an ethanol solution containing 0.2 mM **N719** used to make the spot in question, whereas the second number is the number of drops of a 0.2 mM solution of porphyrin **4.1** in DCE used on the same spot. Figure 4.6b displays the photocurrent obtained at a 0.2 V applied potential in the presence of I⁻ as the electron donor. However in this case the highest photocurrent was found with a molar ratio of **N719**:porphyrin **4.1** of 10:0, i.e. spots containing pure (100%) **N719** displayed superior photocatalysis. As the amount of porphyrin **4.1** increased and the **N719** decreased, the photocurrent of the spots decreased. This decrease is in accord with the relative photosensitization ability of these two dyes, as illustrated in Figure 4.5. While no particular synergy between the two dyes was found, SECM can be used to monitor mixtures of two or more dyes, particularly where one can absorb light over a larger portion of the spectrum.

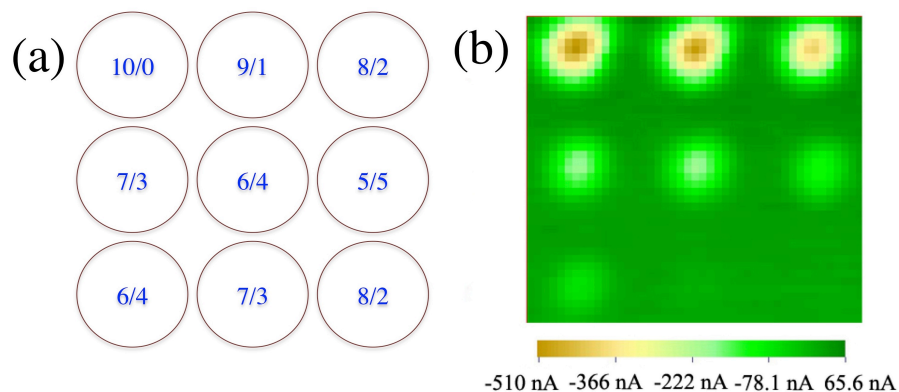


Figure 4.6. (a) Dispensed pattern of dye arrays. The first spot in the first row is 100% **N719**. The first and second numbers inside each circle represent the number of drops of **N719** and porphyrin **4.1**, respectively. (b) SECM image of dyes on TiO₂ nanotubes/Ti foil at an applied potential of 0.2 V vs an AgQRE under visible light. Scan rate: 500 $\mu\text{m/s}$ (SECM setting 50 $\mu\text{m}/0.1$ s); solution, 0.1 M TBAI in MeCN.

To complement the utility of the SECM technique for preliminary screens of dye efficacy and further characterize new compounds **4.1** and **4.2**, PEC measurements were carried out with bulk films. Dye bulk films were prepared using the immersion method as detailed in the experimental section. PEC measurements were then carried out with these films in a three-electrode cell containing 0.1 M TBAI in MeCN under UV-visible and visible light illumination. Figure 4.7 shows the linear sweep voltammograms (LSVs) of control porphyrin **4.2**, porphyrin **4.1** and **N719** bulk films in 0.1 M TBAI in MeCN under conditions of UV-visible and visible light irradiation and in the dark, with the potential being swept from 0.15 to 0.7 V vs an AgQRE for both the control porphyrin **4.2** and porphyrin **4.1** bulk films. For the bulk film produced from dye **N719**, the potential was swept from -0.15 to 0.7 V vs the AgQRE.

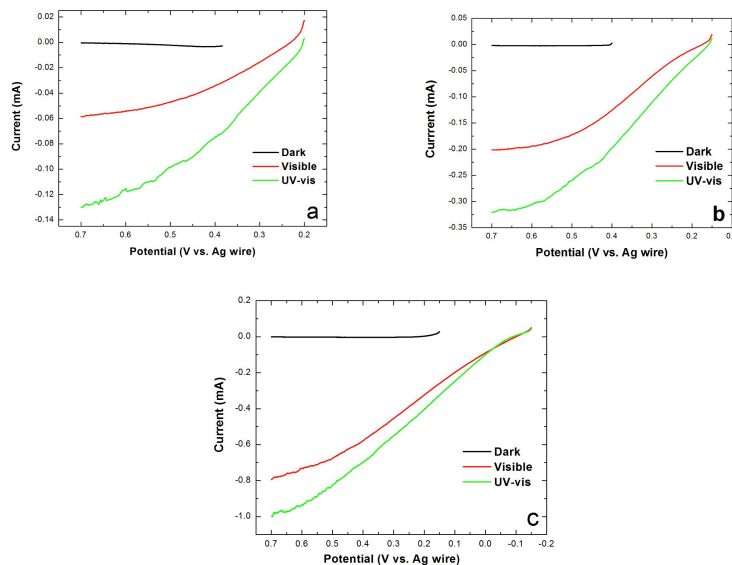


Figure 4.7. Linear sweep voltammograms (LSVs) of (a) control porphyrin **4.2** and (b) porphyrin **4.1** and (c) **N719** bulk films in MECN with 0.1 M TBAI as the sacrificial reagent under dark, visible, and UV-visible light irradiation. Scan rate: 20 mV/s. Exposed electrode area, $\sim 0.2 \text{ cm}^2$.

As shown in Figure 4.7, the onset photocurrent potential was about 0.20 V, 0.15 V and -0.10 V for control porphyrin **4.2**, porphyrin **4.1** and dye **N719**, respectively. The open circuit photopotential under visible light irradiation was about 0.25 V, 0.20 V and -0.10 V *vs* an AgQRE for control porphyrin **4.2**, porphyrin **4.1** and dye **N719**, respectively, indicating that among those three dyes tested, dye **N719** had the highest open circuit photovoltage with respect to I^-/I_3^- redox potential on a Pt counter electrode for a two-terminal PEC device. It is worth noting that the first and second peak potentials for the oxidation of I^- on Pt in MeCN occur at 0.047 and 0.363 V *vs* Ag/Ag $^+$ (0.01 M).¹¹⁷ The bulk film produced from dye **N719** showed the highest photocurrents under both UV-visible and visible irradiation. The bulk film prepared from porphyrin **4.1** displayed a higher photocurrent than that of the control porphyrin bulk film made from **4.2**. The enhancements in the sensitized photocurrent seen for films made with the **N719** dye or

porphyrin **4.2** relative to this latter control system (i.e., **4.2**) were comparable to what was seen in the case of the SECM measurements.

The UV-visible absorption spectra of porphyrin **4.1**, control porphyrin **4.2**, and **N719** were measured in DCE (Figure 4.8). The peak positions and molar absorption coefficients (ϵ) of the Soret and Q bands are listed in Table 4.1. As shown in Figure 4.8,

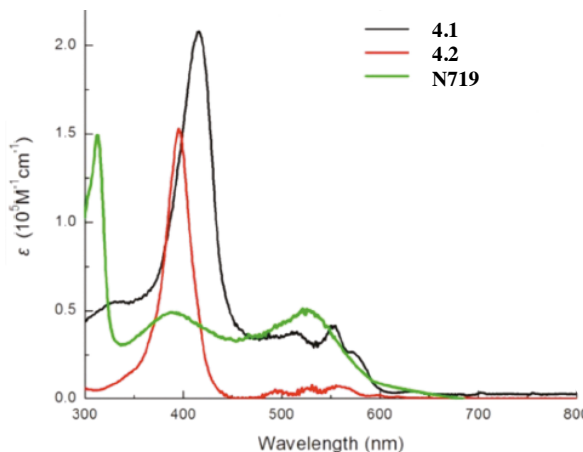


Figure 4.8. UV-visible absorption spectra of porphyrin **4.1**, control porphyrin **4.2**, and dye **N719** measured in dichloroethane.

the UV-visible absorption spectra of porphyrin **4.1** and control porphyrin **4.2** exhibit typical strong Soret bands near 400 nm and weaker Q bands in the region of 500-650 nm. The Soret band of porphyrin **4.1** is red-shifted and broadened relative to that of control porphyrin **4.2**, a finding that is likely due to the presence of the bithiophene substituents. Although the Q band of the control porphyrin is slightly red-shifted in comparison with

that of porphyrin **4.1**, the molar absorption coefficient (ϵ) of the Q band of control porphyrin **4.2** is much lower. The molar absorption coefficients at the Soret bands of the control porphyrin are $\sim 70\%$ of that for porphyrin **4.1**. More importantly, the integrated values of the molar absorption coefficients for the Q bands (500-700 nm) of porphyrin **4.1** are nearly seven times larger than those for the control porphyrin **4.2**. This means that, compared to **4.2**, the bisbithiophene-substituted porphyrin **4.1** is more attractive for the purpose of harvesting solar energy. Specifically, porphyrin **4.1** can absorb much more incident light in the visible region than can control porphyrin **4.2**. However, porphyrin **4.1** is still not as effective as dye **N719**; this latter system is characterized by three typical absorption peaks, as shown in Figure 4.8. The maxima of these peaks appear at ca. 387

nm, 313 nm, and 529 nm, respectively. The integrated value of their molar absorption coefficients over the 500-700 nm spectral regions is 1.3 times larger than what is found in the case of porphyrin **4.1**.

Table 4.1. Spectroscopic data for porphyrin **4.1**, control porphyrin **4.2**, and **N719** recorded in DCE.

	$\lambda_{\text{abs}}/\text{nm}$ ($\epsilon/10^3 \text{ M}^{-1}\text{cm}^{-1}$)
Porphyrin 4.1	416 (207.7)
	494 (35.8)
	510 (38.2)
	553 (41.6)
	396 (152.8)
Control porphyrin 4.2	493 (5.3)
	535 (6.7)
	555 (7.4)
N719	313 (149.3)
	387 (49.2)
	529 (50.2)

Described in this chapter is a new synthetic route to *meso*-unsubstituted porphyrins bearing β -substituents. This method, which relies on the construction of a bis-iodo β -functionalized porphyrin precursor and its subsequent elaboration, was used to prepare the bis-bithiophene substituted porphyrin **4.1**. This new porphyrin was shown to act as an efficient sensitizer for use in DSSCs. The present work also serves to highlight

the utility of a modified SECM-based technique, which permits a rapid, initial evaluation of photosensitizers for use in DSSC applications. This SECM technique is attractive in that it should not only permit the facile identification of individual new dyes, but also permit the potential synergetic effects of multiple dyes to be easily tested. In addition to the latter benefits, the present study serves to underscore the combination of a piezodispenser and SECM as a means of fabricating quickly, easily, and in reproducible fashion ca. 400 μm spot-size sensitizer arrays and evaluating their sensitization effects.

EXPERIMENTAL SECTION

Materials. 2,5-Diformylpyrrole, 3,4-diiodo-2,5-diformylpyrrole and 2,2'-bithiophene-5-boronic acid were prepared according to published procedures.¹¹⁸⁻¹²⁰ *Cis-bis*-(isothiocyanato)*bis*(2,2'-bipyridy-4,4'-dicarboxylato)-ruthenium(II)-*bis*-tetrabutyl ammonium (**N719**), was obtained from Aldrich. 21H,23H-Porphine-2,13-dipropanoic acid, 7,8-diethyl-3,12-dimethyl-17,18-di-(5-(2,2'-bithiophene))-, dimethyl ester (**4.1**), 21H,23H-porphine-2,13-dipropanoic acid, 7,8-diethyl-3,12-dimethyl-, dimethyl ester (**4.2**) and 21H,23H-porphine-2,13-dipropanoic acid, 7,8-diethyl-3,12-dimethyl-17,18-diiodo-, dimethyl ester (**4.6**) were prepared as described below. Solutions of the dye **N719** were prepared in ethanol at a concentration of 2×10^{-4} M. Solutions of porphyrins **4.1** and **4.2**, also studied as dyes (*vide infra*), were prepared in dichloroethane (DCE) at concentrations of 1×10^{-3} M.

Porphyrim 4.2.

Control porphyrim **4.2** was synthesized via a “3 + 1” condensation procedure (Figure 4.1) as follows. First, tripyrrane **4.4** (231 mg, 492.5 μmol) was stirred in neat trifluoroacetic acid (2 mL) at r.t. under a nitrogen atmosphere for 10 min. The reaction was then diluted with 150 mL of dried, deaerated dichloromethane (DCM), and then treated with 2,5-diformylpyrrole **4.5a** (55 mg, 447.2 μmol). After stirring for 2 h at r.t., dichlorodicyanoquinone (DDQ) (152 mg, 669.6 μmol) was added. The reaction was

stirred for an additional 30 min before 3.7 mL of triethylamine was added. The volatiles were then removed using a rotary evaporator. The desired porphyrin was purified over silica gel using dichloromethane as the eluent. After removal of the solvent, the first, major red fraction was obtained as a red solid. Recrystallization from a mixture of dichloromethane/methanol (DCM/MeOH) then yielded porphyrin **4.2** (36.5 mg, 14%) as a crystalline product. ^1H NMR (400 MHz, CDCl_3) δ 10.18 (s, 2H), 10.12 (s, 2H), 9.41 (s, 2H), 4.45 (t, $J = 7.8$, 4H), 4.12 (q, $J = 7.6$, 4H), 3.67 (s, 6H), 3.66 (s, 6H), 3.29 (t, $J = 7.8$, 4H), 1.93 (t, $J = 7.6$, 6H), -3.77 (s, 2H). ^{13}C NMR (101 MHz, CDCl_3) δ 174.2, 119.8, 101.4, 96.6, 52.4, 37.6, 22.5, 20.4, 19.2, 12.2. ESI MS (+): 567 $[\text{M}+\text{H}]^+$. HiRes MS ESI(+): found 567.2965, calc. for $\text{C}_{34}\text{H}_{39}\text{N}_4\text{O}_4^+$ 567.2971. HPLC analysis confirmed the bulk purity of the product (99%).

Diiodoporphyrin 4.6.

In a vessel protected from ambient light, tripyrrane **4.4** (44 mg, 77.2 μmol) was stirred in neat trifluoroacetic acid (1 mL) at r.t. under a nitrogen atmosphere for 10 min. The reaction was then diluted with 8 mL of dry, deaerated DCM followed by treatment with 3,4-diiodo-2,5-diformylpyrrole **4.5b** (29 mg, 77.2 μmol). After stirring for 2 h at r.t., DDQ (18 mg, 79.3 μmol) was added. Then the reaction was stirred for an additional 30 min before 1.8 mL of triethylamine was added. The volatiles were removed using a rotary evaporator. The desired porphyrin was purified over silica gel using dichloromethane as the eluent. After evaporative removal of the solvent, the first, major red fraction was obtained as a red solid, which was recrystallized from a mixture of DCM and MeOH; this yielded **4.6** (34.2 mg, 54%) in the form of a red crystalline product. ^1H NMR (400 MHz, CDCl_3) δ 10.02 (s, 2H), 9.88 (s, 2H), 4.40 (t, $J = 7.7$, 4H), 3.98 (q, $J = 7.6$, 4H), 3.64 (s, 6H), 3.61 (s, 6H), 3.21 (t, $J = 7.8$, 4H), 1.87 (t, $J = 7.6$, 6H), -4.41 (s, 2H). ^{13}C NMR (101 MHz, CDCl_3) δ 173.9, 154.9, 151.6, 145.6, 137.1, 136.2, 136.1,

135.9, 108.3, 102.1, 97.1, 37.4, 30.39, 22.3, 20.5, 19.2, 12.2. MS ESI (+) 819 [M+H]⁺. HiRes MS ESI(+): found 819.0894, calc. for C₃₄H₃₇N₄O₄I₂⁺ 819.0899.

Porphyrin 4.1.

Deaerated toluene (10 mL), deaerated methanol (3 mL), and deaerated water (1 mL) were added to a mixture of diiodoporphyrin **4.6** (28.5 mg, 34.8 μmol), 2-bithiophene boronic acid (29.3 mg, 139.5 μmol), Pd(PPh₃)₄ (4.0 mg, 3.5 μmol), and Na₂CO₃ (29.3 mg, 273 μmol) under a nitrogen atmosphere. The resulting reaction mixture was stirred at 80° C for 10 h. The reaction mixture was then cooled to r.t. The aqueous layer was separated off and extracted with dichloromethane (2 x 50 mL). The combined organic phases were dried over Na₂SO₄ and then filtered. The volatiles were removed using a rotary evaporator. The desired porphyrin was purified over silica gel using dichloromethane as the eluent. The first, major red fraction was obtained in the form of a red solid product after evaporative removal of the solvent. After recrystallization from a mixture of DCM/MeOH, product **4.1** was obtained as crystalline product (23.2 mg, 74%). ¹H NMR (400 MHz, CDCl₃) δ 10.31 (s, 2H), 10.01 (s, 2H), 7.62 (dd, J = 32.8, 3.2, 4H), 7.37 (dd, J = 31.4, 4.0, 4H), 7.14 (d, J = 3.9, 2H), 4.41 (t, J = 7.5, 4H), 4.04 (q, J = 7.6, 4H), 3.68 (s, 6H), 3.59 (s, 6H), 3.27 (t, J = 7.6, 4H), 1.93 (t, J = 7.5, 6H), -3.71 (s, 2H). ¹³C NMR (101 MHz, CDCl₃) δ 174.0, 145.3, 140.5, 138.4, 137.0, 136.6, 136.6, 136.5, 136.1, 131.7, 128.7, 125.3, 125.2, 125.1, 124.6, 100.7, 96.9, 52.5, 37.4, 22.4, 20.5, 19.2, 12.3. ESI MS (+): 896 [M+H]⁺. HiRes MS ESI(+): found 895.2477, calc. for C₅₀H₄₇N₄O₄S₄⁺ 895.2475. Elemental analysis calculated for C₅₀H₄₈N₄O₄S₄: C 67.09, H 5.18, N 6.26; found: C 67.12, H 5.47, N 5.97.

Preparation of TiO₂ nanotubes/Ti foil substrate.

The TiO₂ nanotubes were prepared using a previously reported procedure.¹¹⁶ Briefly, anodic titania templates with a pore size of about 80 to 100 nm were grown on high purity titanium plates (0.25 mm thick, 99.5% purity) by constant voltage anodization

at 20 V in ethylene glycol/water (99:1, volume ratio) with addition of 0.5 wt.% NH_4F at 20° C for about 20 h. The resulting samples were then annealed at 450° C in air for 3 h.

Preparation of photosensitizer arrays.

A CH Instruments dispenser (model 1550, Austin, TX) was used to fabricate the photosensitizer arrays. It consisted of a computer-controlled stepper-motor-operated XYZ stage with a piezoelectric dispensing tip (MicroJet AB-01-60, MicroFab, Plano, TX) attached to the head and a sample platform. The arrays were prepared in accordance with a previously reported procedure.⁹⁸ Namely, the TiO_2 nanotubes/Ti foil substrate was placed on the sample platform of the dispenser and the XYZ stage moved the tip in preprogrammed pattern, while programmed voltage pulses were applied to the dispenser to eject the requested number of drops (~100 pL each) of the precursor solution (dye solution) onto the TiO_2 nanotubes/Ti foil. The first dye (dye solution) was loaded and dispensed in a preprogrammed pattern onto the TiO_2 nanotubes/Ti foil substrate. After flushing and washing the piezodispenser several times, a second dye was loaded into the dispenser and dispensed into different positions than the first dye spots. The dye arrays were kept in the air under ambient conditions to allow the solvent to evaporate.

Screening of the array.

The screening of the sensitizer arrays was performed by an optical fiber-modified SECM setup described previously.¹⁰⁰ Briefly, a 400 μm optical fiber (FT-400-URT, 3M, St. Paul, MN) coupled to a 150 W xenon lamp was fixed in the tip holder of a CHI model 900B SECM instrument. The prepared sensitizer arrays were placed in a Teflon cell with the sensitizer/ TiO_2 nanotubes/Ti foil working electrode exposed at the bottom through a hole sealed with an O-ring (exposed area 1.0 cm^2). To test the effect of the dye sensitizer, a Pt wire counter electrode and an Ag wire quasi-reference electrode (AgQRE) were used to complete the three-electrode configuration. A 0.1 M solution of tetrabutylammonium iodide (TBAI) in acetonitrile (MeCN) was used as the electrolyte and as an electron

donor. The optical fiber was positioned perpendicular to the array at a distance of about 100 μm and scanned across the surface at a speed of 500 $\mu\text{m/s}$ (SECM setting 50 $\mu\text{m}/0.1$ s). A 420 nm long-pass wavelength filter was used to block the UV light in visible light illumination experiments. During the scan, a given potential was applied to the working electrode array using the SECM. The measured photocurrent during the scan produced a color-coded, two-dimensional image.

Preparation and photoelectrochemical measurements of bulk samples.

The annealed TiO_2 nanotubes/Ti foil electrodes were immersed in an ethanol solution containing 2×10^{-4} M **N719**, a DCE solution containing 2×10^{-4} M porphyrin **4.1** or a DCE solution of control porphyrin **4.2** for a 24 h period, in all three cases. The resulting thin films were used as a photo-working electrode with 0.2 cm^2 geometrical area exposure to the electrolyte solution and the light source. Light irradiation was performed through the electrolyte solution using a Xe lamp (Oriel, 150 W) with an incident light intensity of about 100 mW/cm^2 . A UV cutoff filter (> 420 nm) was used for visible light irradiation. The PEC measurements were carried out in a 0.1 M TBAI in MeCN.

Chapter Five. Electrochemical Synthesis of a Thiophene-containing Cyclo[9]pyrrole*

Cyclo[n]pyrroles, [5.1H₆]²⁺, [5.2H₇]²⁺, and [5.3H₈]²⁺ with n = 6, 7 and 8, respectively (Figure 5.1), have emerged in recent years as an attractive class of expanded porphyrins.¹²¹⁻¹²⁴ They have attracted attention *inter alia* for their potential utility in anion binding,^{125,126} nonlinear optics,¹²⁷ liquid crystals¹²⁸ and molecular electronics.^{129,130} Their chemical reactivity¹³¹⁻¹³³ along with their physical properties has been investigated in depth.¹³⁴⁻¹³⁶ Until recently, the only available chemical strategy to prepare these highly symmetric macrocycles involved subjecting β-substituted bipyrroles to an iron-mediated coupling process carried out in the presence of various mineral acids.^{137,138} Although not yet not fully understood, the proposed mechanism of cyclo[n]pyrrole formation under these oxidative conditions involves, as a primary step, the generation of a bipyrrole radical cation. It is thought that this radical evolves through a series of dimerization, deprotonation, and, possibly, bipyrrole-bipyrrole cleavage steps to produce the final cyclo[n]pyrroles. The exact number of redox and chemical steps required to convert bipyrrole into various cyclo[n]pyrroles is still under debate. However, the dependence of the product distribution (n = 6, 7 or 8) on the nature of the mineral acid employed is consistent with the suggestion that self-condensation of the bipyrrole radical cation formed after initial oxidation involves an anion-templated process.

The need for more selective oxidation procedures, involving less-forcing conditions, as well as less expensive and toxic reagents, has recently led a few research groups to begin exploring alternative electrochemical oxidative coupling methods. This approach is attractive since it permits, as a major benefit, an opportunity to exert a subtle tuning of the reactivity of the “reagent” *via* the choice of anodic voltage. This prospect is particularly appealing in the area of oligopyrrole chemistry where various coupling

* This work has been conducted together with Dr. Christophe Bucher, Université Joseph Fourier, Grenoble, France. Manuscript based on the work described in this chapter has been submitted for publication.

reactions and final aromatization processes, require the application of precise oxidation potentials. Recently, Sessler, Bucher and co-workers pioneered the use of such methods in the synthesis of expanded porphyrins.¹³⁹⁻¹⁴¹ Specifically, the efficient preparation of the known cyclo[n]pyrroles, $[5.2H_7]^{2+}$ and $[5.3H_8]^{2+}$, from bipyrrrolic precursors was been

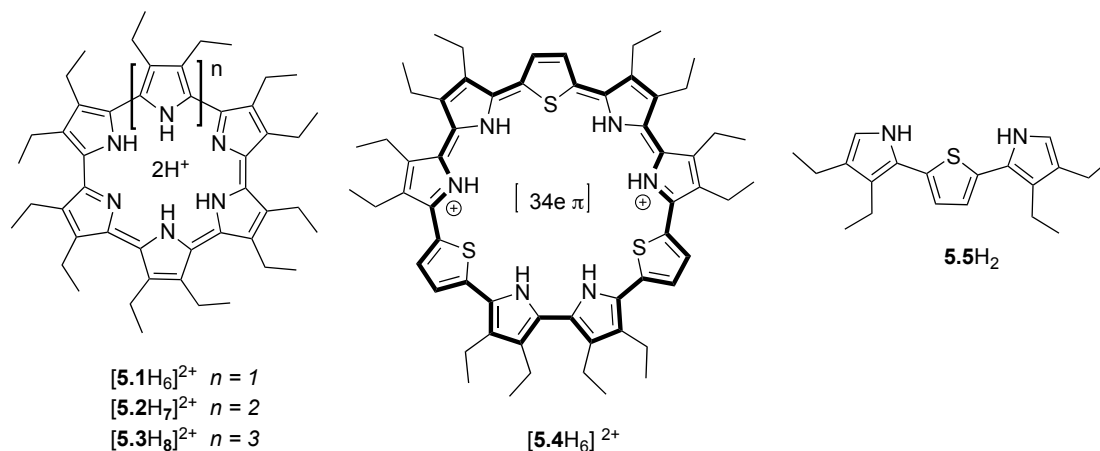


Figure 5.1. Representation of the previously reported cyclo[n]pyrroles $[5.1H_6]^{2+}$, $[5.2H_7]^{2+}$, $[5.3H_8]^{2+}$ and of the novel thiophene-containing cyclo[9]pyrrole $[5.4H_6]^{2+}$ as well as its bispyrrolylthiophene precursor $5.5H_2$.

reported. These products were obtained in yields equivalent to those obtained following the classical chemical oxidative routes.^{139,141} It was also found that these two cyclo[n]pyrroles could be obtained directly from 3,4-disubstituted pyrroles, albeit in low yield.¹³⁹ Separate from this, a straightforward electrochemical synthesis of [24]hexaphyrin(1.0.1.0.0.0) was developed.¹⁴⁰ Taken in concert these syntheses highlight the use of electrochemical oxidation methods as a “green” alternative to the classic chemical synthesis¹⁴² of at least certain expanded porphyrins. The success of these preliminary results led the Sessler-Bucher joint project team to propose that analogous electrochemical oxidation processes could be used to generate new expanded porphyrin products, including those containing heterocycles other than pyrrole. In particular, it was thought that an electrochemical synthesis could be used to prepare a new member of the

class of cyclo[n]pyrroles, namely the tris-thiophene nonaphyrin [**5.4H₆**]²⁺ (Figure. 5.1). This system, which bears formal analogy to the still-unknown cyclo[9]pyrrole, contains 6 pyrrole and 3 thiophene subunits directly connected through their respective α -positions in a fully symmetric arrangement. Experimental tests of this hypothesis, to which the author contributed, are described below.

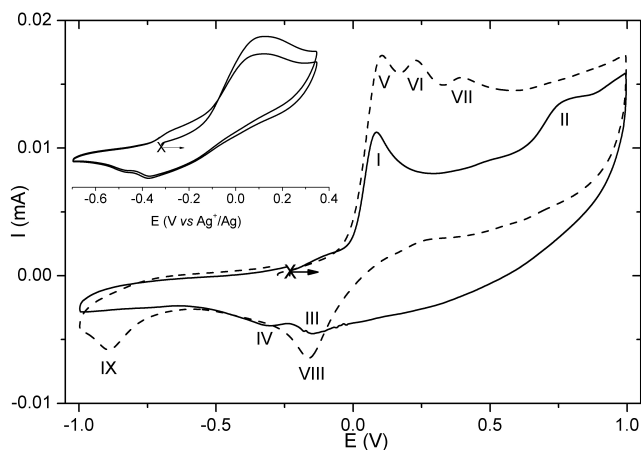


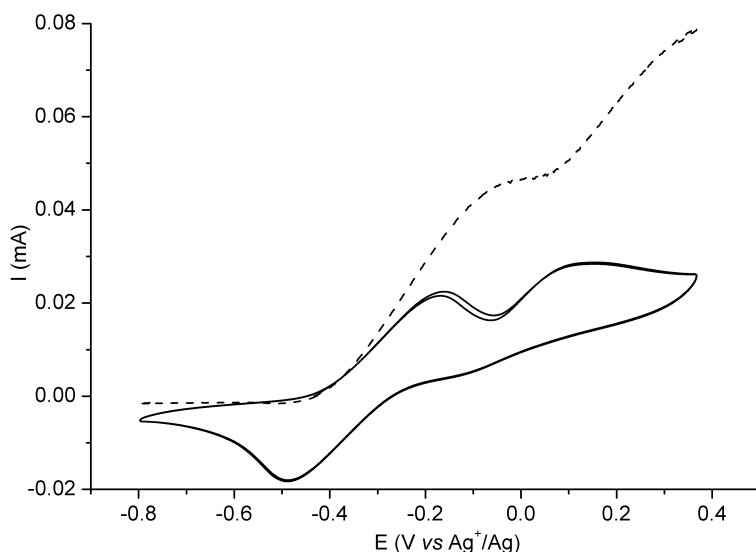
Figure 5.2. Cyclic voltammograms of 1 mM solution of **5.5H₂** in 0.1 M TBAP/CH₂Cl₂ recorded at r.t. using a glassy carbon working electrode ($\varnothing = 3$ mm, Ag/AgNO₃ reference electrode, scan rate 100 mV/s). Full line: **5.5H₂**; dashed line: **5.5H₂** after adding 1 molar equivalence of symcollidine; inset: First oxidation wave of **5.5H₂**

Based on previous work, it was considered likely that hitherto unknown cyclo[9]pyrroles could be formed in one-pot via the electrochemical oxidation of terpyrrole building blocks, or possibly even from β -disubstituted monomeric pyrroles. As in the case of the electrochemical oxidations leading to the smaller cyclo[n]pyrroles [**5.2H₇**]²⁺ and [**5.3H₈**]²⁺, success would require that competing polymerization

processes be avoided and that intermediates are not drawn off through, e.g., precipitation into either the bulk solution or onto the electrode. As reported earlier, cyclo[9]pyrrole could not be detected in the crude material obtained after electrochemical oxidation of 3,4-diethylpyrrole, even when a range of different anion salts were employed as the electrolyte.¹³⁹ Terpyrrole, therefore, was used as a potential precursor. In initial tests involving electrochemical oxidation, terpyrrole failed to produce any detectable amount of cyclo[9]pyrrole. A corresponding lack of success was found when various chemical

oxidants, notably Fe(III) and Cr(VI), were tested. This unfortunate result is thought to reflect the low stability and concomitant air sensitivity of the requisite terpyrrole precursor. Nevertheless, as will be discussed further in this chapter, an analog of the originally targeted macrocycle could be obtained by subjecting a thiophene containing terpyrrole, namely **5.5H₂** (Figure. 5.1), to electrochemical oxidation.

The 2,5-bis(3,4-diethyl-2-pyrrolyl)thiophene **5.5H₂** features a central thiophene ring that serves to bridge two β -alkylated pyrroles. This species was synthesized by the candidate by subjecting the α, α' -diester protected



intermediate formed by a Pd-catalyzed Suzuki-Miyaura cross coupling between 2-

Figure. 5.3. Cyclic voltammogram (solid line) and voltammogram at a rotating disk (dashed line) of **5.5H₂** and 1 molar equivalence of decamethylferrocene recorded in 0.1 M TBAP/CH₂Cl₂

borylpyrrole and 2,5-diiodothiophene¹⁴³ to ester hydrolysis followed by decarboxylation.

Once in hand, the electrochemical properties of **5.5H₂** were investigated by cyclic voltammetry (CV) in dichloromethane containing tetra-*n*-butylammonium bisulfate (TBAHSO₄) or tetra-*n*-butylammonium perchlorate (TBAP) as the supporting electrolytes (Figure 5.2). A first irreversible oxidation wave (process I) is observed at $E_p = 80$ mV (unless otherwise noted, all potentials are referenced vs Ag/AgNO₃ 0.01 M in 0.1 M TBAP/CH₃CN).

The irreversible nature of the first oxidation process, observed at all investigated scan rates from 50 mV/s to 1 V/s, provides support for the notion that the resulting cation radical $[5.5H_2]^+$ presumably undergoes self condensation reactions that give rise to linear

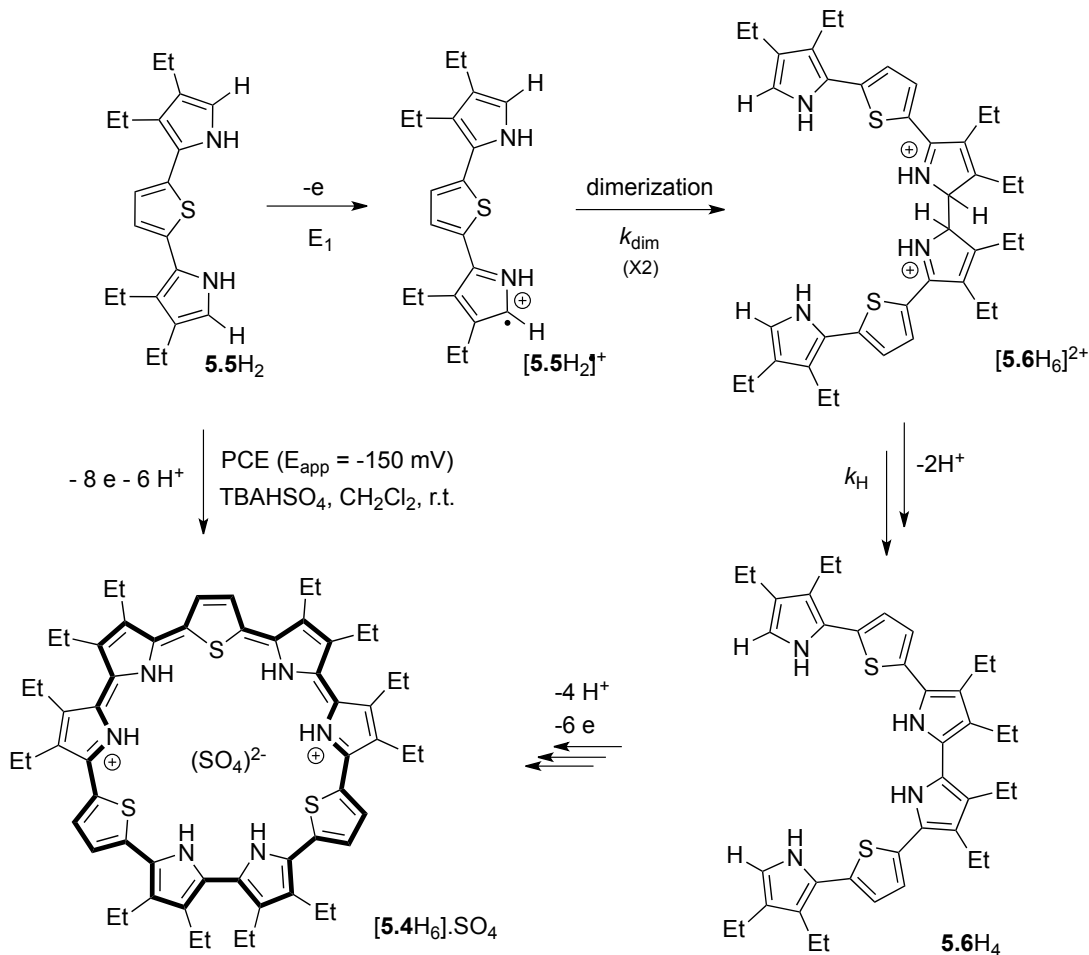


Figure 5.4. Schematic representation of the coupled electrochemical-chemical coupled processes leading to the formation of $[5.4H_6] \cdot SO_4$ from three molecules of $5.5H_2$.

and/or cyclic products. This preliminary investigation also revealed that repeated cycling does not lead to the physisorption of oligomeric or polymeric materials onto the electrode surface as commonly observed with pyrrole derivatives. The number of electrons involved in the first irreversible oxidation wave was estimated using decamethylferrocene (DMFc) as an internal reference (Figure 5.3). The reversible oxidation wave observed

around -0.5 V and the molecular weight of this reference matching that of **5.5H₂** are particularly suited to this first approximation knowing that the diffusion coefficient scales roughly with the inverse of the cube root of the molecular weight.

As calibrated against this standard and using an equimolar mixture of **5.5H₂** and DMFc, it was inferred that the first irreversible oxidation (process I) wave seen in Figure 5.2 involves more than one electron/mole. The observation of two reduction waves on the backward scan processes (III and IV) is likewise taken as a clear indication that coupling products are forming at the electrode interface.¹⁴⁴ The supposition that a chemical reaction follows the electron transfer event is further supported by the progressive decrease in the $I_p/(v)^{1/2}$ ratio, which is a measure of the apparent number of electrons transferred. Finally, consistent with this postulate is the finding that the peak potential E_p shifts towards more positive values, with increasing scan rate.

It can be assumed that the kinetics of the follow-up coupling reaction (k_{dim} on Figure 5.4) leading to the diprotonated σ -dimer [**5.6H₆**]²⁺ is very fast, probably in the range of 10^7 - 10^8 M⁻¹.s⁻¹, but that the rates of the subsequent deprotonation processes (k_{H} on Figure 5.4) leading to **5.6H₄** are relatively slow, at least on the CV time scale. Experimental findings consistent with the accumulation of a long-lived σ -dimer intermediate such as [**5.6H₆**]²⁺ at the electrode interface came from the study reproduced in Figure 5.2. Here, a weak, intense irreversible wave at $E_p = +650$ mV (process II) is seen. It is attributed to the oxidation of [**5.6H₆**]²⁺, which logically should be harder to oxidize than its neutral precursor **5.5H₂**. In agreement with this postulated sequence of events, the addition of *sym*-collidine (up to two molar equivalents) leads to a large enhancement in the peak current measured for the first oxidation wave. This is consistent with the organic base promoting the formation of the neutral hexapyrrole **5.6H₄**, a species that is instantaneously oxidized at this potential. This hypothesis is further supported by the observation of wave IX at $E_{\text{pc}} = -0.9$ V on the backward scan of Figure 5.2, which is attributed to the reduction of protonated collidine.

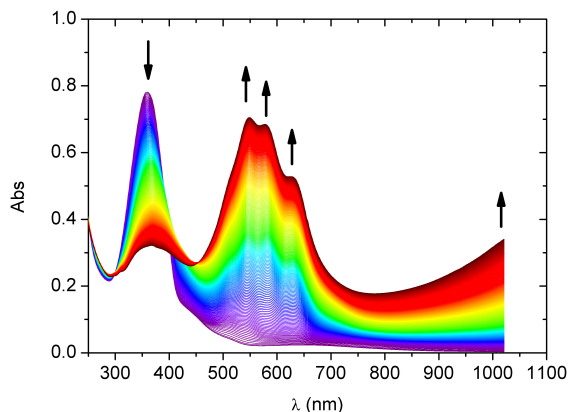


Figure 5.5. Time-dependent evolution of the UV/Vis spectra observed during an analytical scale electrolysis of **5.5H₂**.

55 cm² cylinder-shaped platinum gauze working electrode and an all quartz 1 mm optical path length UV/Vis immersion probe. Setting the potential of the working electrode at $E_{\text{app}} = -50$ mV caused a progressive decrease in the absorbance at 360 nm, a spectral feature attributed to the main π - π^* transition in **5.5H₂**, as well as a concomitant growth of new bands centered at 550, 580 and 630 nm and a band in the NIR domain.

The color of the electrolyzed solution underwent a progressive change from green to dark purple. A thin layer chromatography analysis of the resulting crude mixture revealed the presence of one well-defined purple spot, as well as a few blue colored products that tended to smear on the silica gel plate. On the other hand, mass spectrometric analysis of the crude mixture revealed the presence of signals at high m/z values, leading us to conclude that a wide range of self-condensation products may be formed from **5.5H₂** under the conditions of electrochemical oxidation.

Precursor **5.5H₂** was subjected to several preparative-scale bulk electrolysis experiments ($C = 2$ mM, $V = 60$ mL) in an effort to obtain sufficient material to permit a more detailed analysis of the anodic coupling products. These electrolyses were conducted at low potential values ($E_{\text{app}} \sim -150$ mV) and were generally kept running until the current had decayed to about 5% of its initial value. At this point, the consumed

In order to obtain further insights into the intermediate and final species produced following electrochemical oxidation, UV/Vis spectroelectrochemical analyses of **5.5H₂** were carried out. These experiments involved the controlled potential electrolysis of 0.5 mM solutions of **5.5H₂** in 0.25 M TBAHSO₄/CH₂Cl₂ (30 mL) using a

charge was equivalent to approximately 2 molar equivalents of electrons per terpyrrole. The electrolyzed solutions were then washed twice with water and the organic solvent was evaporated off under reduced pressure to afford a dark-purple solid. Separation of the purple and blue fractions of the crude material was best achieved via silica gel column chromatography under slightly acidic conditions. The chemical identity of the blue smearing fraction could not be established unequivocally since the ^1H NMR spectra of the species in question proved very complex and many peaks were seen in the mass spectra. These fractions were thus tentatively assigned to oligomeric products. On the contrary, the purple product isolated after purification yielded well defined spectra, which were readily assigned to the TFA salt of the target cyclo[9] derivative ($[\mathbf{5.4H}_6] \cdot 2\text{TFA}$). This product was obtained in 6% yield and is thought to involve a reaction pathway that relies on the self-condensation of three terpyrrole units.

The structural assignment for $[\mathbf{5.4H}_6] \cdot 2\text{TFA}$ was made on the basis of NMR, UV/Vis/NIR spectroscopic analyses, high resolution mass spectrometry, and electrochemical data. The ESI-MS spectrum exhibits two major peaks at $m/z = 485.7$ (100%) and 971.5 (36%) corresponding to the diprotonated $[\mathbf{5.4H}_6]^{2+}$ and monoprotonated $[\mathbf{5.4H}_5]^+$ species. A detailed 1D and 2D-NMR investigation conducted in deuterated benzene provided further support for the proposed cyclic structure. As expected for a highly symmetric species, the ^1H -NMR spectrum revealed only a few signals, which were readily assigned to the ethyl substituents, the β -hydrogen atoms on the thiophene rings, and the internal NH protons. The number of signals and their relative intensities are in perfect agreement with the D_{3h} symmetry expected for $[\mathbf{5.4H}_6]^{2+}$; furthermore, no signals attributed to the hydrogen atoms located on the α -positions of the two terminal pyrroles present in the starting terpyrrole-like material were seen in the ^1H -NMR spectrum of this electrochemically generated product. The presence of a strong ring current effect was revealed in the spectrum by the upfield shift of the internal NH protons, which were observed as a broad singlet at $\delta = -1.5$ ppm (6H), as well as by the

downfield shift of the singlet attributed to the outer β protons on the thiophene moieties, which were seen to resonate at an unusually high value of 11.5 ppm (6H). Finally, a broad multiplet at $\delta = 4.7$ ppm (24H) and two triplets at 2.5 (18H) and 2.1 ppm (18H), ascribed to the ethyl substituents on the periphery of the macrocycle, were seen. These chemical shifts are in agreement with what has been reported for other ethyl-substituted cyclo[n]pyrroles.^{137,138} Thus, taken in concert, these ^1H NMR spectroscopic observations are fully consistent with proposed structure for $[\mathbf{5.4H}_6]^{2+}$ and support the conclusion that it is a 34 π -electron aromatic macrocycle.

Absorbance measurements were conducted in the 250-1500 nm UV/Vis/NIR spectral range on $[\mathbf{5.4H}_6] \cdot 2\text{TFA}$ in dichloromethane (Figure 5.6). It shows a Soret-like signal centered at 550 nm ($\epsilon = 91500 \text{ M}^{-1}\text{cm}^{-1}$), which is slightly blue-shifted in CH_3CN ($\lambda_{\text{max}} = 530 \text{ nm}$) as well as a weaker and much broader band centered at 1194 nm ($\epsilon = 75500 \text{ M}^{-1}\text{cm}^{-1}$).

These UV/Vis spectroscopic data are summarized in Table 5.1, as are those for previously reported cyclo[n]pyrroles. A quick overview of these data reveals that the

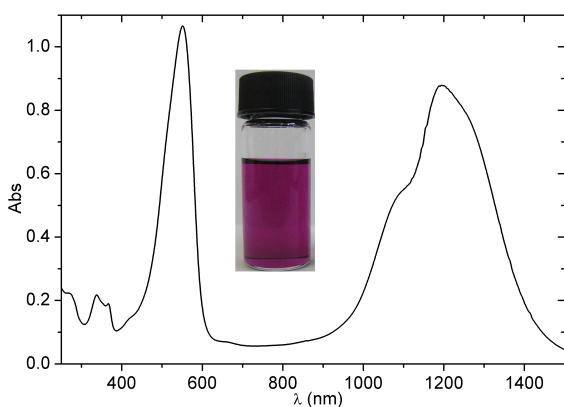


Figure 5.6. UV/Vis/NIR absorption spectrum of $[\mathbf{5.4H}_6] \cdot 2\text{TFA}$ in CH_2Cl_2 (11 μM , $l = 1 \text{ cm}$).

absorption bands become increasingly red-shifted as the size of the macrocycle increases. The red shift seen for the Soret-like band, upon transitioning from $[\mathbf{5.3H}_8] \cdot 2\text{Cl}$ to $[\mathbf{5.4H}_6] \cdot 2\text{TFA}$ turns out to be much larger than that observed

within cyclo[n]pyrrole series on going from $[\mathbf{5.1H}_6] \cdot 2\text{Cl}$ to $[\mathbf{5.3H}_8] \cdot 2\text{Cl}$. On the other hand, the characteristic broad absorption in the NIR region shifts almost linearly with the number of delocalized π -electrons (i.e., on going from

[**5.1H₆**]•2Cl to [**5.4H₆**]•2TFA; Table 5.1). A common feature found for the previously reported cyclo[n]pyrroles is that the intensity of the Soret band is always weaker than that of the near IR band. This is not the case for [**5.4H₆**]•2TFA; this new compound is characterized by Soret-like and near-IR bands that are of almost the same intensity. Nevertheless, in terms of general features, the UV/Vis/NIR spectrum of [**5.4H₆**]•2TFA is in good agreement with what can be expected for a cyclo[n]-type of macrocycle containing a larger number of delocalized π -electrons. The differences found relative to the previously reported cyclo[n]pyrroles presumably reflect the presence of three thiophene rings within the conjugated system.

Table 5.1. Optical and electrochemical properties of [**5.1H₆**]•2Cl, [**5.2H₇**]•2Cl, [**5.3H₈**]•2Cl, and [**5.4H₆**]•2TFA.

Compound	$\sum\pi e$	Electrochemical properties ^a				Optical properties (λ_{\max}/ϵ) ^c		Refs
		$E_{1/2}^{\text{Red}}$	$E_{1/2}^{\text{Ox1}}$	$E_{1/2}^{\text{Ox2}}$	$\Delta_{\text{HOMO-LUMO}}^c$	Soret band	Q band	
[5.1H₆]•2Cl	22	-0.66 ^b	0.64 ^b	1.25 ^b	1.30	397/122600	792/206400	¹³⁸
[5.2H₇]•2Cl	26	-0.49 ^b	0.36 ^b	0.79 ^b	0.85	429/44300	936/66700	¹³⁸
[5.3H₈]•2Cl	30	-0.39 ^b	0.21 ^b	0.46 ^b	0.60	431/79800	1112/132200	¹³⁷
[5.4H₆]•2TFA	34	-0.13 ^d	0.20 ^d	0.44 ^d	0.33	550/91500	1194/75500	This work

^aAll half-wave redox potentials ($E_{1/2}/V$) were reported with respect to Ag/AgNO₃ (0.01 M in 0.1 M TBAP/CH₃CN). ^bOriginal values, recorded with an SCE reference electrode in 0.1 M TBAP/CH₂Cl₂, have been converted using the following equation $E(\text{SCE}) = 0.31 + E(\text{Ag}/\text{AgNO}_3)$.¹⁴⁵ ^c $\Delta_{\text{HOMO-LUMO}}$ (eV) = $E_{1/2}^{\text{Ox1}} - E_{1/2}^{\text{Red}}$. ^dData recorded in 0.1 M TBAP/CH₃CN. ^eData recorded in CH₂Cl₂, values of ϵ are expressed in M⁻¹cm⁻¹.

The addition of triethylamine (from 0.5 to 25 molar equivalents) to the original solution of [**5.4H₆**]•2TFA produces drastic changes in the UV/Vis range with a progressive decrease in the absorbance at 550 nm being observed, along with the concurrent growing in of two other signals at 425 and 800 nm, respectively. Similar results were obtained upon washing CH₂Cl₂ samples of [**5.4H₆**]•2TFA with a 10% aqueous NaOH solution. Two successive isosbestic points, at 500 nm and 450 nm, respectively, were observed in the series of spectra recorded as the titration with

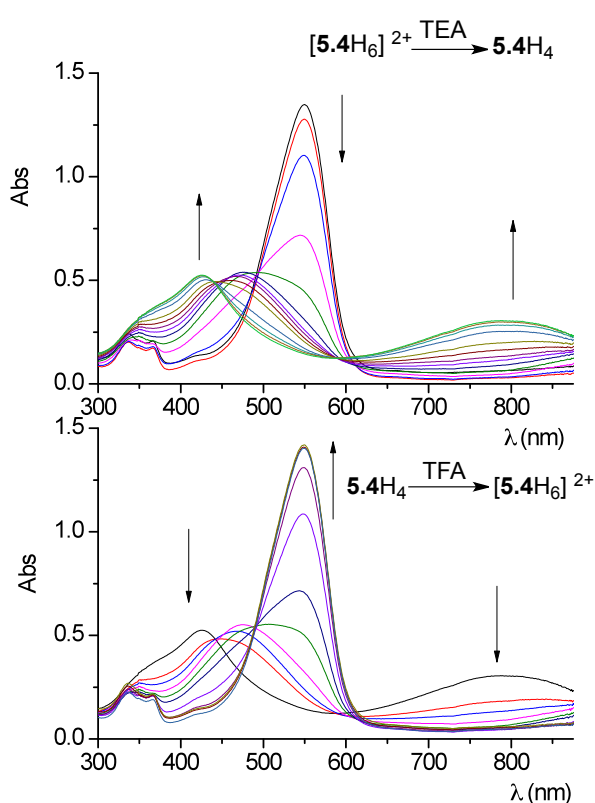


Figure 5.7. Spectral changes corresponding to the equilibrium between the protonated and free base states of **5.4H₄** in CH₂Cl₂ solution.

initial spectrum of **[5.4H₆]²⁺·2TFA**. Furthermore, the same isosbestic points were observed at 450 nm and 500 nm during the spectral evolution associated with this reprotonation process.

The diprotonated form, **[5.4H₆]²⁺·2TFA**, proved easier to isolate than the neutral species

triethylamine proceeds (Figure 5.7). The optical signature of the free base form, **5.4H₄**, was inferred from this experiment since no further spectral changes were observed once ≥ 20 molar equivalents of triethylamine were added. From these observations, we propose that the two successive isosbestic points correspond to the two deprotonation processes required to convert **[5.4H₆]²⁺·2TFA** to **5.4H₄**. In the event, this conversion process proved to be fully reversible. Specifically, addition of trifluoroacetic acid to the free base **5.4H₄** leads to a regeneration of the

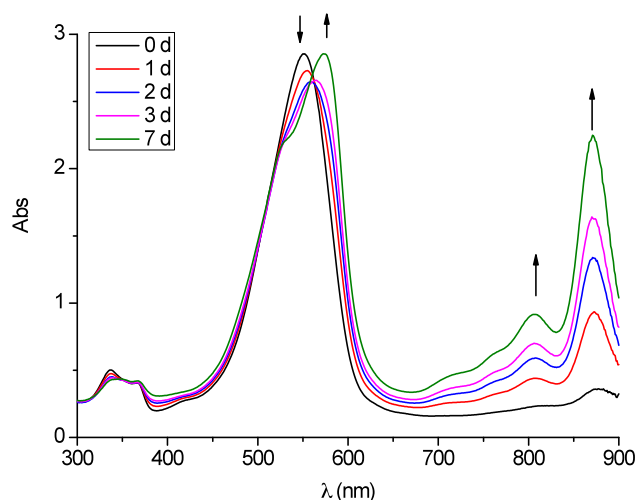


Figure 5.8. Time dependent evolution of the UV/Vis spectra of **[5.4H₆]²⁺·2TFA** recorded in CF₃COOH/CH₂Cl₂ (1:99 v/v).

5.4H₄, since the original workup and purification was carried out under acidic conditions. Nevertheless, the stability of **5.4H₄** as well as [**5.4H₆**]•2TFA in dichloromethane solution was assessed by UV/Vis spectroscopic means; this was done by checking for spectral changes that might be occurring as a function of time. No significant changes were noticed for the spectrum of **5.4H₄** (produced *in situ* by adding more than 1000 molar equivalents of triethylamine to [**5.4H₆**]•2TFA) over the course of 7 days. The diprotonated form [**5.4H₆**]•2TFA also proved to be stable in CH₂Cl₂ solution, at least for a couple of days. Interestingly, however, instability was noted in the presence of an excess of trifluoroacetic acid in dichloromethane (more than 1000 molar equivalents). As detailed below, the evolution of the UV/Vis spectra recorded when [**5.4H₆**]•2TFA in dichloromethane was treated with excess acid turned out to be quite similar to what was observed by UV/Vis spectroelectrochemistry when [**5.4H₆**]•2TFA was subject to further oxidation. In fact, mixtures of CF₃COOH and CH₂Cl₂ have been used to form π -dimers of end-capped oligopyrrole cation radicals (Figure 5.8).¹⁴⁶

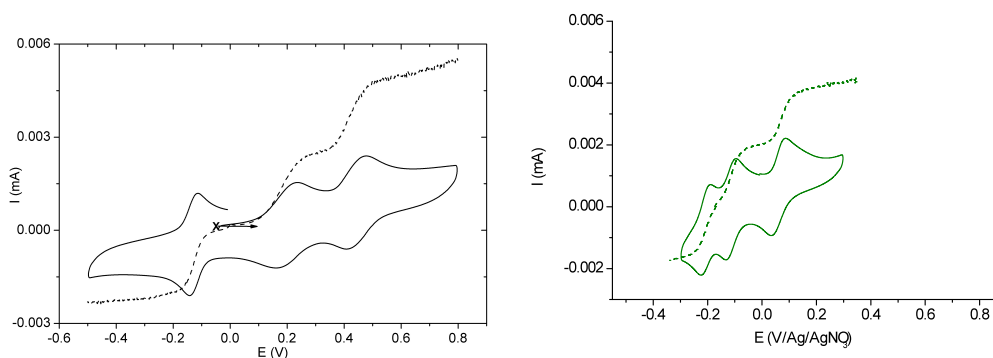


Figure 5.9. Cyclic voltammogram (continued line) and voltammogram at a rotating disk (dashed line) recorded at r.t. of 0.135 mM solution of [**5.4H₆**]•2TFA (left) and [**5.4H₆**]•2TFA neutralized by 1200 molar equivalents of *sym*-collidine (right) in 0.1 M TBAP/CH₃CN, Pt metal wire counter and Ag/AgNO₃ 0.01 M in 0.1 M TBAP/CH₃CN reference electrodes. CV: 2-mm Pt disk working electrode, 100 mV/s. RDE: 3-mm glassy disk carbon tip working electrode, 10 mV/s, 500 rd/min.

The electrochemical properties of **[5.4H₆]**•2TFA were investigated by CV and by rotating disk voltammetry (RDE) in 0.1 M TBAP/CH₃CN and the corresponding $I = f(E)$ curves are shown in Figure 5.9. These data reveal three reversible single electron processes between -1 and +1 V. Specifically, two successive oxidations and a single reduction are observed at $E_{1/2} = 0.20, 0.44$ V and -0.13 V, respectively. The addition of a large excess of *sym*-collidine (up to 1200 molar equivalents) to a solution of **[5.4H₆]**•2TFA in acetonitrile shifted both oxidation waves towards less positive potential values as a result of the progressive accumulation of the neutral form **[5.4H₄]** in solution (Figure 5.9). The electrochemical data found for **[5.4H₆]**•2TFA and those corresponding to the parent cyclo[n]pyrroles are summarized in Table 5.1.

For well-behaved systems, the difference between the first reduction and the first oxidation potentials provides a direct measurement of the energy gap between the HOMO and LUMO levels ($\Delta_{\text{HOMO-LUMO}}$). The values reported in Table 5.1, measured for macrocycles of various sizes, are in agreement with the decrease in $\Delta_{\text{HOMO-LUMO}}$ expected with increasing conjugation. The small $\Delta_{\text{HOMO-LUMO}}$ gap of 0.33 eV found for **[5.4H₆]**•2TFA contrasts, for instance, with the relatively large gap of 2.27 eV typically found for porphyrins.¹⁴⁷ In the cyclo[n]- series, the $\Delta_{\text{HOMO-LUMO}}$ energetic gap gradually decreases as the size of the ring increases. For instance, a $\Delta = 1.30$ eV is found for cyclo[6]pyrrole **[5.1H₆]**•2Cl (22 π -electrons),¹³⁸ whereas for the new cyclo[9]derivative **[5.4H₆]**•2TFA (34 π -electrons, $\Delta = 0.33$ eV) this gap is almost 1 eV smaller, as would be expected from its greater sized and larger number of delocalized electrons. Within the all-pyrrole cyclo[n]pyrrole series, the first oxidation and first reduction potentials shift towards less positive and less negative values, respectively, as the number of delocalized π -electrons increases (Table 5.1). The data for the present cyclo[9]pyrrole derivative **[5.4H₆]**•2TFA is consistent with this trend. However, the presence of three thiophene heterocyclic subunits, which are characterized by a higher ionization potential (IP) than pyrrole ($\text{IP}_{\text{pyrrole}} = 8.2$ eV; $\text{IP}_{\text{thiophene}} = 8.86$ eV), within **[5.4H₆]**•2TFA makes any direct

comparison difficult. It is known, for instance, that replacing pyrrole with thiophene in open chain oligopyrroles shifts the oxidation potential towards more positive values.¹⁴⁸

Macrocycle $[\mathbf{5.4H}_6]^{2+}$ was further characterized by UV/Vis spectroelectrochemical methods. For these analyses, the absorption spectra were recorded periodically as CV scans were conducted in 0.1 M TBAP/ CH_3CN using a platinum gauze inserted in a 1 mm slit inside a quartz electrochemical cell. The UV/Vis spectra recorded during a cathodic scan, from 0 to -400 mV (50 mV/s), with a micro electrolysis of about 45 seconds at -140 mV, are shown on Figure 5.10a. The intensity of both signals above 400 nm decreases, while the absorbance at 350 nm increases progressively as the potential at the working electrode decreases. The final spectrum, recorded at the end of this scanning experiment, is attributed to the radical monocation $[\mathbf{5.4H}_6]^+$. This species was stable on the CV time scale as inferred from the fact that the spectral signature of the starting dication ($[\mathbf{5.4H}_6]^{2+}$) could be recovered after scanning back to 0V.

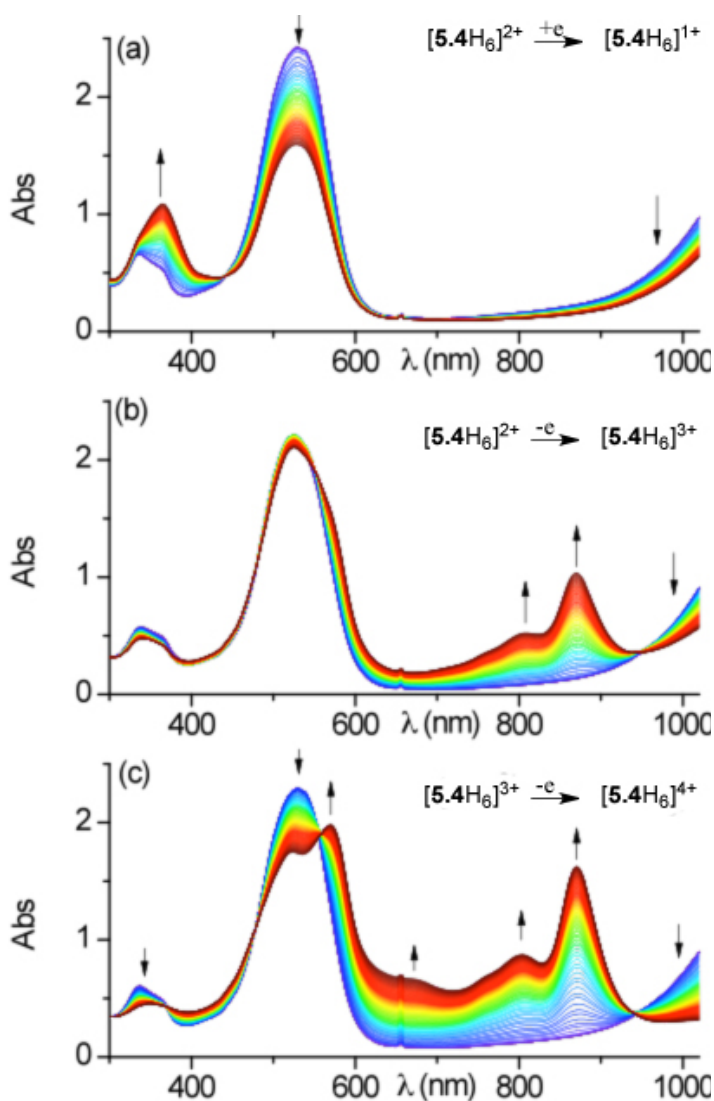


Figure 5.10. UV-Vis-NIR spectroelectrochemical signatures for $[5.4H_6]^{2+}$ recorded periodically during CV scans conducted in 0.1 M TBAP/ CH_3CN in the presence of TFA (> 20 molar equivalents) on a platinum gauze (WE) inserted in a 1 mm slit inside a quartz electrochemical cell. Scan rate: 100 mV/s. (a) monoreduced form, $[5.4H_6]^{1+}$, recorded upon scanning the WE potential from 0 to -140 mV and electrolysis at -140 mV for 45 s, (b) monooxidized form, $[5.4H_6]^{3+}$, recorded upon scanning from 0 to +230 mV followed by an electrolysis at +230 mV for 45 s, (c) doubly oxidized form, $[5.4H_6]^{4+}$, recorded upon scanning from 0 to +475 mV followed by an electrolysis at 475 mV for 45 s.

In a second experiment, designed to generate $[5.4H_6]^{3+}$ selectively as well as characterize the intermediate one-electron oxidation product, the working electrode potential was swept from 0 V up to 230 mV and then kept at this value for 45 seconds (Figure 5.10b). The presumed accumulation of $[5.4H_6]^{3+}$ at the electrode interface was correlated with the appearance of two signals at 807 and 871 nm, along with a progressive drop in the intensity of the absorption above 1000 nm. Under these conditions, little variation in the nature or intensity of the Soret-like band at 530 nm was seen.

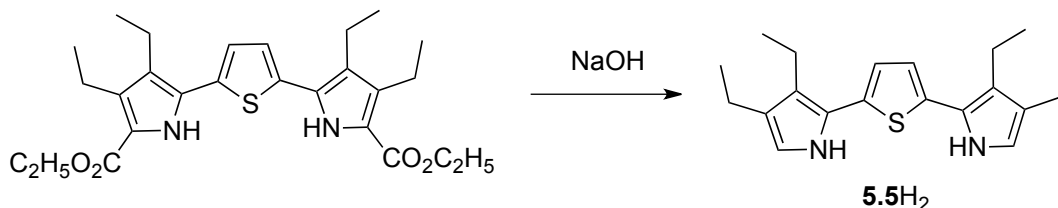
Finally, when the potential was scanned up to 800 mV, the features attributed to the production of $[5.4H_6]^{3+}$ as described above

were found to be amplified (Figure 5.10c). Specifically, a larger decrease in the absorbance band above 1000 nm was seen, along with the concomitant development of signals at both 807 and 871 nm. In addition, changes were observed between 500 and 600 nm; here, a clear splitting of the Soret-like transition was seen, resulting from the growth of an intense signal at 570 nm. These new features are ascribed to the formation of the doubly oxidized species $[\mathbf{5.4H}_6]^{4+}$ under these highly oxidizing conditions. Scanning the potential back to 0 V from either 300 or 800 mV led to an almost quantitative recovery of the spectrum assigned to $[\mathbf{5.4H}_6]^{2+}$. This reversibility and that seen upon initial reduction and reoxidation provides support for the contention that the spectroelectrochemical assignments are correct and that the oxidized and reduced forms of $[\mathbf{5.4H}_6]^{2+}$ are stable on the CV time scale.

It is worth noting that although now produced as a new member of the generalizable class of cyclo[n]pyrroles, $\mathbf{5.4H}_6$ ·2TFA failed to form using standard chemical oxidative coupling procedures. However, it was obtained from a thiophene-containing terpyrrole analogue using a mild electrochemical oxidative procedure. The isolated macrocycle, featuring nine heterocyclic subunits directly connected through their α, α' -positions, is the largest cyclo[n]pyrrole derivative reported to date. This system was assigned as being a 34 π -electron aromatic system on the basis of ^1H NMR spectroscopic measurements. Support for this assignment and confirmation of the structure came from photochemical, electrochemical and spectroelectrochemical analyses. These studies also allowed for the identification of reduced and oxidized forms of this novel expanded porphyrin. These latter species proved stable on the electrochemical time scale.

EXPERIMENTAL SECTION

Synthesis of 2,5-bis(3,4-diethyl-2-pyrrolyl)thiophene (**5.5H₂**)



The 5,5'-diester form of compound **5.5H₂** was synthesized according to a literature procedure.¹⁴³ Once in hand, this compound (3.660 g, 7.8 mmol) and sodium hydroxide (3.110 g, 77.8 mmol) were stirred in boiling ethylene glycol (30 ml) under a nitrogen atmosphere for 1 hr. The reaction mixture was then cooled to room temperature and subsequently was sparged into ice water (400 ml). The light green precipitate obtained in this way was collected by filtration, washed thoroughly with water and dried under vacuum. Yield 2.336 g (92%). ¹H NMR (400 MHz, CDCl₃) δ_{ppm} = 7.90 (s, 2H), 6.91 (s, 2H), 6.57 (d, *J* = 2.6, 2H), 2.66 (q, *J* = 7.5, 4H), 2.51 (dt, *J* = 7.5, 3.8, 4H), 1.25 (m, 6H), 1.20 (t, *J* = 7.5, 6H). ¹³C NMR (101 MHz, CDCl₃) δ_{ppm} = 134.2, 127.3, 123.1, 123.1, 123.0, 115.3, 19.0, 18.7, 16.3, 15.2. MS (ESI+): 327.2 [M+H]⁺, HRMS (ESI+): 327.1889 - C₂₀H₂₇N₂S¹⁺.

Electrosynthesis of the bis protonated dodecaethyl-substituted thiophene-containing cyclo[9]pyrrole [**5.4H₆**]•2TFA

The requisite electrolyses were conducted at room temperature using a cylinder-shaped platinum gauze working electrode (*S* ≈ 55 cm²) and a large piece of carbon felt, isolated from the electrolytic solution through an ionic bridge, as the counter-electrode. A homemade AgNO₃ (0.01 M) + TBAP (0.1 M) in CH₃CN / Ag electrode was used as the reference electrode. In a three-compartment electrolysis cell equipped with a magnetic stirrer, were placed 60 mL of a 0.25 M TBAHSO₄ solution in CH₂Cl₂. The solution was stirred well and degassed by bubbling with argon for approximately 30 minutes before 2,5-bis(3,4-diethyl-2-pyrrolyl)thiophene **5.5H₂** (38.8 mg) was added. The green reaction

mixture was further degassed for 5 minutes and then kept under a slight argon stream, which was maintained during the whole experiment. The potential of the working electrode was set to -150 mV. The experiment was stopped when the current was seen to decay to about 5% of its initial value. Under these conditions, the charge passed reached *ca.* 21 C (approximative 1.9 electrons per molecule). The contents of both the anodic and middle compartments were collected, washed twice with water, dried over anhydride MgSO₄, and concentrated under reduced pressure with the aid of a rotary evaporator. The dark purple crude product was then purified by column chromatography (silica gel; CH₂Cl₂/CH₃OH/CF₃COOH: 98.5/1.5/0.1, eluent). The fractions containing the desired product were collected and concentrated to afford a violet solid. The final purification was achieved by precipitation this violet solid from a CH₂Cl₂ solution by the addition of *n*-heptane containing a trace quantity of CF₃COOH. The product obtained in this way proved to be the desired thiophene-containing cyclo[9]pyrrole, which was isolated in its bis-protonated state ([**5.4H₆**]•2TFA). The yield was 6.5% as determined from UV-Vis absorption spectroscopy. ¹H NMR (400 MHz, C₆D₆, r.t.) δ_{ppm} = 11.52 (s, 6 H, H_{Thiophene}), 4.71 (m, 24 H, -CH₂-CH₃), 2.52 (t, *J* = 7.2 Hz, 18 H, -CH₂-CH₃), 2.10 (t, *J* = 7.2 Hz, 18 H, -CH₂-CH₃), -1.47 (br, 6 H, NH). MS (ESI +): *m/z* = 485.7 ([M+2]²⁺, 100%), 971.5 ([M+1]⁺, 36%); MS (MALDI-TOF): 971.5 ([M+1]⁺); HRMS (ESI+): found 971.4909, calculated 971.4897 for [M+1]. Washing a CH₂Cl₂ solution of [**5.4H₆**]•2TFA with distilled water provided the follow characterization data: MS (ESI +): *m/z* for pH_{water} = 2: 486.3 ([M+2]²⁺, 100%), 971.5 ([M+1]⁺, 91%); for pH_{water} = 5: 971.5 ([M+1]⁺, 100%), 486.3 ([M+2]²⁺, 6%). UV-Vis-NIR (r.t.): λ_{max} in CH₂Cl₂ (nm) / ε (L•mol⁻¹•cm⁻¹): 550 / 91500, 1194 / 75500. λ_{max} in CH₃CN (nm): 530 nm.

References

- (1) Vogel, E. *Pure Appl. Chem.* **1993**, *65*, 143.
- (2) Vogel, E. *Pure Appl. Chem.* **1996**, *68*, 1355.
- (3) Sessler, J.; Weghorn, S. *Expanded, Contracted & Isomeric Porphyrins*; Pergamon, 1997.
- (4) Tanaka, Y.; Shin, J.-Y.; Osuka, A. *Eur. J. Org. Chem.* **2008**, *2008*, 1341.
- (5) Cheprakov, A. V. *The Synthesis of π -Extended Porphyrins*, In *Handbook of Porphyrin Science*; Guillard, R., Kadish, K. M., Smith, K. M., Eds. 2011; Vol. 13.
- (6) Cheprakov, A. V.; Filatov, M. A. *J. Porphyr. Phthalocyan.* **2009**, *13*, 291.
- (7) Ono, N.; Yamada, H.; Okujima, T. *Synthesis of Porphyrins Fused with Aromatic Rings*, In *Handbook of Porphyrin Science*; Guillard, R., Kadish, K. M., Smith, K. M., Eds. 2010; Vol. 2.
- (8) Apreleva, S. V.; Wilson, D. F.; Vinogradov, S. A. *Appl. Opt.* **2006**, *45*, 8547.
- (9) Finikova, O. S.; Troxler, T.; Senes, A.; DeGrado, W. F.; Hochstrasser, R. M.; Vinogradov, S. A. *The J. Phys. Chem. A* **2007**, *111*, 6977.
- (10) Lash, T. D. *Energy & Fuels* **1993**, *7*, 166.
- (11) Finikova, O.; Cheprakov, A.; Beletskaya, I.; Vinogradov, S. *Chem. Commun.* **2001**, 261.
- (12) Fuhrhop, J.-H.; Hosseinpour, D. *Leibigs Ann. Chem.* **1985**, 689.
- (13) Zhao, L.; Han, B.; Huang, Z.; Miller, M.; Huang, H.; Malashock, D. S.; Zhu, Z.; Milan, A.; Robertson, D. E.; Weiner, D. P.; Burk, M. J. *J. Am. Chem. Soc.* **2004**, *126*, 11156.
- (14) Belokon, Y. N.; Chusov, D.; Peregudov, A. S.; Yashkina, L. V.; Timofeeva, G. I.; Maleev, V. I.; North, M.; Kagan, H. B. *Adv. Synth. & Catal.* **2009**, *351*, 3157.
- (15) Barton, D. H. R.; Zard, S. Z. *JCS Chem. Commun.* **1985**, 1098.

- (16) Inomata, K.; Hirata, T.; Suhara, H.; Kinoshita, H.; Kotake, H.; Senda, H. *Chem. Lett.* **1988**, *17*, 2009.
- (17) Hirata, T.; Sasada, Y.; Ohtani, T.; Asada, T.; Kinoshita, H.; Senda, H.; Inomata, K. *Bull. Chem. Soc. Jpn.* **1992**, *65*, 75.
- (18) Filatov, M. A.; Cheprakov, A. V.; Beletskaya, I. P. *Eur. J. Org. Chem.* **2007**, *2007*, 3468.
- (19) Sessler, J.; Roznyatovskiy, V.; Lynch, V. *J. Porphyr. Phthalocyan.* **2009**, *13*, 322.
- (20) Johnstone, K. D.; Pearce, W. A.; Pyke, S. M. *J. Porphyr. Phthalocyan.* **2002**, *6*, 661.
- (21) Filatov, M. A.; Lebedev, A. Y.; Vinogradov, S. A.; Cheprakov, A. V. *The J. Org. Chem.* **2008**, *73*, 4175.
- (22) Choudary, B. M.; Chowdari, N. S.; Jyothi, K.; Kantam, M. L. *J. Am. Chem. Soc.* **2002**, *124*, 5341.
- (23) Becker, H.; King, S. B.; Taniguchi, M.; Vanhessche, K. P. M.; Sharpless, K. B. *J. Org. Chem.* **1995**, *60*, 3940.
- (24) Tsuda, A.; Osuka, A. *Science* **2001**, *293*, 79.
- (25) Arroyo, I. J.; Hu, R.; Merino, G.; Tang, B. Z.; Pena-Cabrera, E. *The J. Org. Chem.* **2009**, *74*, 5719.
- (26) Loudet, A.; Burgess, K. *Chem. Rev.* **2007**, *107*, 4891.
- (27) Wada, M.; Ito, S.; Uno, H.; Murashima, T.; Ono, N.; Urano, T.; Urano, Y. *Tetrahedron Lett.* **2001**, *42*, 6711.
- (28) Okujima, T.; Tomimori, Y.; Nakamura, J.; Yamada, H.; Uno, H.; Ono, N. *Tetrahedron* **2010**, *66*, 6895.
- (29) Gresser, R.; Hummert, M.; Hartmann, H.; Leo, K.; Riede, M. *Chem. A Eur. J.* **2011**, *17*, 2939.
- (30) Naumovski, L.; Ramos, J.; Sirisawad, M.; Chen, J.; Thiemann, P.; Lecane, P.; Magda, D.; Wang, Z.; Cortez, C.; Boswell, G.; Gyu Cho, D.; Sessler, J.; Miller, R. *Mol. Cancer Ther.* **2005**, *4*, 968.
- (31) Ono, N.; Kuroki, K.; Watanabe, E.; Ochi, N.; Uno, H. *Heterocycles* **2004**, *62*, 365.

- (32) Okujima, T.; Kikkawa, T.; Kawakami, S.; Shimizu, Y.; Yamada, H.; Ono, N.; Uno, H. *Tetrahedron* **2010**, *66*, 7213.
- (33) Panda, P. K.; Kang, Y.-J.; Lee, C.-H. *Angew. Chem. Int. Ed.* **2005**, *44*, 4053.
- (34) Vogel, E.; Kocher, M.; Schmickler, H.; Lex, J. *Angew. Chem. Int. Ed.* **1986**, *25*, 257.
- (35) Kuzuhara, D.; Mack, J.; Yamada, H.; Okujima, T.; Ono, N.; Kobayashi, N. *Chem. A Eur. J.* **2009**, *15*, 10060.
- (36) Kuzuhara, D.; Yamada, H.; Yano, K.; Okujima, T.; Mori, S.; Uno, H. *Chem. A Eur. J.* **2011**, *17*, 3376.
- (37) Vogel, E.; Koecher, M.; Lex, J.; Ermer, O. *Isr. J. Chem.* **1989**, *29*, 257.
- (38) Vogel, E.; Koch, P.; Hou, X.-L.; Lex, J.; Lausmann, M.; Kisters, M.; Aukauloo, M. A.; Richard, P.; Guilard, R. *Angew. Chem. Int. Ed.* **1993**, *32*, 1600.
- (39) Dobkowski, J.; Galievsky, V.; Starukhin, A.; Vogel, E.; Waluk, J. *J. Phys. Chem. A* **1998**, *102*, 4966.
- (40) Dobkowski, J.; Galievsky, V.; Starukhin, A.; Waluk, J. *Chem. Phys. Lett.* **2000**, *318*, 79.
- (41) Dobkowski, J.; Lobko, Y.; Gawinkowski, S.; Waluk, J. *Chem. Phys. Lett.* **2005**, *416*, 128.
- (42) Roznyatovskiy, V.; Lynch, V.; Sessler, J. L. *Org. Lett.* **2011**, *12*, 4424.
- (43) Samsoniya, S. A.; Trapaidze, M. V.; Kuprashvili, N. A.; Kolesnikov, A. M.; Suvorov, N. N. *Khim. Geterotsikl. Soedin.* **1985**, 1222.
- (44) Trapaidze, M. V.; Samsoniya, S. A.; Kuprashvili, N. A.; Mamaladze, L. M.; Suvorov, N. N. *Khim. Geterotsikl. Soedin.* **1988**, 603.
- (45) Samsoniya, S. A.; Trapaidze, M. V.; Kuprashvili, N. A.; Samsoniya, N. S.; Suvorov, N. N. *Khim. Geterotsikl. Soedin.* **1994**, 1048.
- (46) Samsoniya, S. A.; Trapaidze, M. V.; Kuprashvili, N. A.; al., e. *Khim. Geterotsikl. Soedin.* **1998**, 942.
- (47) Li, X.; Xiao, Y.; Qian, X. *Org. Lett.* **2008**, *10*, 2885.
- (48) Surin, M.; Hennebicq, E.; Ego, C.; Marsitzky, D.; Grimsdale, A. C.; Mullen, K.; Bredas, J.-L.; Lazzaroni, R.; Leclere, P. *Chem. Mat.* **2004**, *16*, 994.

- (49) Rambaud, M.; Bakasse, M.; Duguay, G.; Villieras, J. *Synthesis* **1988**, 564.
- (50) Rozen, S.; Ben-David, I. *J. Org. Chem.* **2000**, *66*, 496.
- (51) Singh, J.; Kissick, T. P.; Mueller, R. H. *Org. Prep. Proced. Int.* **1989**, *21*, 501.
- (52) Franzen, H. *Berichte der Deutschen Chemischen Gesellschaft* **1905**, *38*, 266.
- (53) Franzen, H. *J. Praktische Chemie* **1908**, *76*, 205.
- (54) Wagaw, S.; Yang, B. H.; Buchwald, S. L. *J. Am. Chem. Soc.* **1998**, *26*, 6621.
- (55) Stepien, M.; Donnio, B.; Sessler, J., L. *Chem. A Eur. J.* **2007**, *13*, 6853.
- (56) Pietrzak, M.; Shibl, M. F.; Broring, M.; Kuhn, O.; Limbach, H.-H. *J. Am. Chem. Soc.* **2006**, *129*, 296.
- (57) Bernard, C.; Gisselbrecht, J. P.; Gross, M.; Jux, N.; Vogel, E. *J. Electroanal. Chem.* **1995**, *381*, 159.
- (58) Gisselbrecht, J. P.; Gross, M.; Koecher, M.; Lausmann, M.; Vogel, E. *J. Am. Chem. Soc.* **1990**, *112*, 8618.
- (59) Roznyatovskiy, V. V.; Roznyatovskaya, N. V.; Weyrauch, H.; Pinkwart, K.; Tubke, J.; Sessler, J. L. *J. Org. Chem.* **2010**, *75*, 8355.
- (60) Merz, A.; Schroppe, R.; Doetterl, E. *Synthesis* **1995**, 795.
- (61) Walczak, R. M.; Reynolds, J. R. *Adv. Mat.* **2006**, *18*, 1121.
- (62) Ito, S.; Watanabe, H.; Uno, H.; Murashima, T.; Ono, N.; Tsai, Y. C.; Compton, R. G. *Tetrahedron Lett.* **2001**, *42*, 707.
- (63) Baetens, R.; Jelle, B. P.; Gustavsen, A. *Sol. Energy Mater. Sol. Cells*, **2010**, *94*, 87.
- (64) Carpi, F.; De, R. D. *Opt. Laser Technol.* **2006**, *38*, 292.
- (65) Georg, A.; Brucker, F. Patent EP1936603A1, **2008**, 17.
- (66) Beaupre, S.; Breton, A.-C.; Dumas, J.; Leclerc, M. *Chem. Mater.* **2009**, *21*, 1504.
- (67) Cheng, Y.-J.; Yang, S.-H.; Hsu, C.-S., 109, 5868. *Chem. Rev.* **2010**, *109*, 5868.

- (68) Reynolds, J. R.; Katritzky, A. R.; Soloducho, J.; Belyakov, S.; Sotzing, G. A.; Pyo, M. *Macromol.* **1994**, *27*, 7225.
- (69) Sotzing, G. A.; Reynolds, J. R.; Katritzky, A. R.; Soloducho, J.; Belyakov, S.; Musgrave, R. *Macromol.* **1996**, *29*, 1679.
- (70) *Conductive electroactive polymers: Intelligent materials, systems*; Wallace, G. G.; Spinks, G. M.; Kane-Maguire, L. A. P.; Teasdale, P. R., Eds.; CRC Press Inc.: Boca Raton, FL, 2003.
- (71) Schottland, P.; Zong, K.; Gaupp, C. L.; Thompson, B. C.; Thomas, C. A.; Giurgiu, I.; Hickman, R.; Abboud, K. A.; Reynolds, J. R. *Macromol.* **2000**, *33*, 7051.
- (72) Nadeau, J. M.; Swager, T. M. *Tetrahedron* **2004**, *60*, 7141.
- (73) Berlin, A.; Ferraccioli, R.; Pagani, G. A.; Sannicolo, F. *Synth. Met.* **1987**, *22*, 89.
- (74) Tovar, J. D.; Rose, A.; Swager, T. M. *J. Am. Chem. Soc.* **2002**, *124*, 7762.
- (75) Samsoniya, S. A.; Trapaidze, M. V.; Kuprashvili, N. A. *Pharm. Chem. J.* **2009**, *43*, 92.
- (76) Oyama, N.; Ohsaka, T.; Chiba, K.; Miyamoto, H.; Mukai, T.; Tanaka, S.; Kumagai, T. *Synth. Met.* **1987**, *20*, 245.
- (77) Zotti, G.; Martina, S.; Wegner, G.; Schlueter, A. D. *Adv. Mater. (Weinheim, Fed. Repub. Ger.)* **1992**, *4*, 798.
- (78) Andrieux, C. P.; Hapiot, P.; Audebert, P.; Guyard, L.; An, M. N. D.; Groenendaal, L.; Meijer, E. W. *Chem. Mater.* **1997**, *9*, 723.
- (79) Deepa, M.; Ahmad, S. *Eur. Polym. J.* **2008**, *44*, 3288.
- (80) Debad, J. D.; Bard, A. J. *J. Am. Chem. Soc.* **1998**, *120*, 2476.
- (81) Zotti, G.; Cattarin, S.; Comisso, N. *J. Electroanal. Chem. Interfacial Electrochem.* **1987**, *235*, 259.
- (82) Cabala, R.; Skarda, J.; Potje-Kamloth, K. *Phys. Chem. Chem. Phys.* **2000**, *2*, 3283.
- (83) Saunders, B. R.; Fleming, R. J.; Murray, K. S. *Chem. Mater.* **1995**, *7*, 1082.
- (84) Ak, M.; Gacal, B.; Kiskan, B.; Yagci, Y.; Toppare, L. *Polymer* **2008**, *49*, 2202.

- (85) Arjomani, J.; Holze, R. *J. Solid State Electrochem.* **2007**, *11*, 1093.
- (86) Chandrasekhar, P. In *Conducting Polymers, Fundamentals and Applications: A Practical Approach*, Kluwer: Dordrecht, The Netherlands, 1999, p 65.
- (87) Ak, M.; Gancheva, V.; Terlemezyan, L.; Tanyeli, C.; Toppare, L. *Eur. Polym. J.* **2008**, *44*, 2567.
- (88) Gaupp, C. L.; Welsh, D. M.; Rauh, R. D.; Reynolds, J. R. *Chem. Mater.* **2002**, *14*, 3964.
- (89) Zhang, F.; Roznyatovskiy, V.; Fan, F.-R. F.; Lynch, V.; Sessler, J. L.; Bard, A. J. *J. Phys. Chem. C* **2011**, *115*, 2592.
- (90) Gao, F.; Wang, Y.; Shi, D.; Zhang, J.; Wang, M.; Jing, X.; Humphry-Baker, R.; Wang, P.; Zakeeruddin, S. M.; Gratzel, M. *J. Am. Chem. Soc.* **2008**, *130*, 10720.
- (91) Nazeeruddin, M. K.; De, A. F.; Fantacci, S.; Selloni, A.; Viscardi, G.; Liska, P.; Ito, S.; Takeru, B.; Graetzel, M. *J. Am. Chem. Soc.* **2005**, *127*, 16835.
- (92) Mozer, A. J.; Griffith, M. J.; Tsekouras, G.; Wagner, P.; Wallace, G. G.; Mori, S.; Sunahara, K.; Miyashita, M.; Earles, J. C.; Gordon, K. C.; Du, L.; Katoh, R.; Furube, A.; Officer, D. L. *J. Am. Chem. Soc.* **2009**, *131*, 15621.
- (93) Jasieniak, J.; Johnston, M.; Waclawik, E. R. *J. Phys. Chem. B* **2004**, *108*, 12962.
- (94) Bard, A. J.; Mirkin, M. V. *Scanning Electrochemical Microscopy*; 1st. ed.; Marcel Dekker: New York, 2001.
- (95) Fernandez, J. L.; Raghuveer, V.; Manthiram, A.; Bard, A. J. *J. Am. Chem. Soc.* **2005**, *127*, 13100.
- (96) Fernandez, J. L.; White, J. M.; Sun, Y.; Tang, W.; Henkelman, G.; Bard, A. J. *Langmuir* **2006**, *22*, 10426.
- (97) Walsh, D. A.; Fernandez, J. L.; Bard, A. J. *J. Electrochem. Soc.* **2006**, *153*, E99.
- (98) Fernandez, J. L.; Walsh, D. A.; Bard, A. J. *J. Am. Chem. Soc.* **2005**, *127*, 357.
- (99) Minguzzi, A.; Alpuche-Aviles, M. A.; Lopez, J. R.; Rondinini, S.; Bard, A. J. *Anal. Chem. (Washington, DC, U. S.)* **2008**, *80*, 4055.

- (100) Lee, J.; Ye, H.; Pan, S.; Bard, A. J. *Anal. Chem. (Washington, DC, U. S.)* **2008**, *80*, 7445.
- (101) Liu, W.; Ye, H.; Bard, A. J. *J. Phys. Chem. C*, *114*, 1201.
- (102) Ghosh, A. In *The Porphyrin Handbook*; Kadish, K. S., Smith, K. M., Guillard, R., Eds.; Academic Press: 2000; Vol. 7, p 1.
- (103) Medforth, C. J.; Berber, M. D.; Smith, K. M.; Shelnutt, J. A. *Tetrahedron Lett.* **1990**, *31*, 3719.
- (104) Zhou, X.; Tse, M. K.; Wan, T. S. M.; Chan, K. S. *J. Org. Chem.* **1996**, *61*, 3590.
- (105) Siri, O.; Smith, K. M. *Tetrahedron Lett.* **2003**, *44*, 6103.
- (106) Sessler, J. L.; Genge, J. W.; Urbach, A.; Sanson, P. *Synlett* **1996**, 187.
- (107) Lin, V.; Lash, T. D. *Tetrahedron Lett.* **1995**, *36*, 9441.
- (108) Campbell, W. M.; Burrell, A. K.; Officer, D. L.; Jolley, K. W. *Coord. Chem. Rev.* **2004**, *248*, 1363.
- (109) Gratzel, M. *Nature* **2001**, *414*, 338.
- (110) Wang, Q.; Ito, S.; Graetzel, M.; Fabregat-Santiago, F.; Mora-Sero, I.; Bisquert, J.; Bessho, T.; Imai, H. *J. Phys. Chem. B* **2006**, *110*, 25210.
- (111) Adachi, M.; Murata, Y.; Okada, I.; Yoshikawa, S. *J. Electrochem. Soc.* **2004**, *150*, G488.
- (112) Chen, C.-C.; Chung, H.-W.; Chen, C.-H.; Lu, H.-P.; Lan, C.-M.; Chen, S.-F.; Luo, L.; Hung, C.-S.; Diau, E. W.-G. *J. Phys. Chem. C* **2008**, *112*, 19151.
- (113) Kang, S. H.; Kim, J.-Y.; Kim, Y.; Kim, H. S.; Sung, Y.-E. *J. Phys. Chem. C* **2007**, *111*, 9614.
- (114) Yang, S.; Kou, H.; Wang, J.; Xue, H.; Han, H. *J. Phys. Chem. C* **2010**, *114*, 4245.
- (115) Tan, B.; Toman, E.; Li, Y.; Wu, Y. *J. Am. Chem. Soc.* **2007**, *129*, 4162.
- (116) Zhang, F.; Chen, S.; Yin, Y.; Lin, C.; Xue, C. *J. Alloys Compd.* **2009**, *490*, 247.
- (117) Kadar, M.; Tokats, Z.; Karancsi, T.; Farsang, G. *Electroanalysis* **1999**, *11*, 809.

- (118) Knizhnikov, V. A.; Borisova, N. E.; Yurashevich, N. Y.; Popova, L. A.; Chernyad'ev, A. Y.; Zubreichuk, Z. P.; Reshetova, M. D. *Russ. J. Org. Chem.* **2007**, *43*, 855.
- (119) Voloshchuk, R.; Galezowski, M.; Gryko, D. T. *Synthesis* **2009**, 1147.
- (120) Kim, D.-S.; Ahn, K. H. *J. Org. Chem.* **2008**, *73*, 6831.
- (121) Jasat, A.; Dolphin, D. *Chem. Rev.* **1997**, *97*, 2267.
- (122) Saito, S.; Osuka, A. *Angew. Chem. Int. Ed.* **2011**, *50*, 4342.
- (123) Sessler, J. L.; Seidel, D. *Angew. Chem. Int. Ed.* **2003**, *42*, 5134.
- (124) Stępień, M.; Sprutta, N.; Latos-Grażyński, L. *Angew. Chem. Int. Ed.* **2011**, *50*, 4288.
- (125) Eller, L. R.; Stępień, M.; Fowler, C. J.; Lee, J. T.; Sessler, J. L.; Moyer, B. A. *J. Am. Chem. Soc.* **2007**, *129*, 11020.
- (126) Baker, E. S.; Lee, J. T.; Sessler, J. L.; Bowers, M. T. *J. Am. Chem. Soc.* **2006**, *128*, 2641.
- (127) Yoon, Z. S.; Kwon, J. H.; Yoon, M.-C.; Koh, M. K.; Noh, S. B.; Sessler, J. L.; Lee, J. T.; Seidel, D.; Aguilar, A.; Shimizu, S.; Suzuki, M.; Osuka, A.; Kim, D. *J. Am. Chem. Soc.* **2006**, *128*, 14128.
- (128) Stępień, M.; Donnio, B.; Sessler, J. L. *Angew. Chem. Int. Ed.* **2007**, *46*, 1431.
- (129) Xu, H.; Yu, G.; Xu, W.; Xu, Y.; Cui, G.; Zhang, D.; Liu, Y.; Zhu, D. *Langmuir* **2005**, *21*, 5391.
- (130) Xu, H.; Wang, Y.; Yu, G.; Xu, W.; Song, Y.; Zhang, D.; Liu, Y.; Zhu, D. *Chem. Phys. Lett.* **2005**, *414*, 369.
- (131) Melfi, P. J.; Kim, S. K.; Lee, J. T.; Bolze, F. d. r.; Seidel, D.; Lynch, V. M.; Veauthier, J. M.; Gaunt, A. J.; Neu, M. P.; Ou, Z.; Kadish, K. M.; Fukuzumi, S.; Ohkubo, K.; Sessler, J. L. *Inorg. Chem.* **2007**, *46*, 5143.
- (132) Köhler, T.; Ou, Z.; Lee, J. T.; Seidel, D.; Lynch, V.; Kadish, K. M.; Sessler, J. L. *Angew. Chem. Int. Ed.* **2005**, *44*, 83.
- (133) Sessler, J. L.; Lee, J. T.; Ou, Z.; Köhler, T.; Hargrove, A. E.; Cho, W.-S.; Lynch, V.; Kadish, K. S. *J. Porphyr. Phthalocyan.* **2006**, *10*, 1329.

- (134) Gorski, A.; Köhler, T.; Seidel, D.; Lee, J. T.; Orzanowska, G.; Sessler, J. L.; Waluk, J. *Chem. A Eur. J.* **2005**, *11*, 4179.
- (135) Lim, J. M.; Yoon, Z. S.; Shin, J.-Y.; Kim, K. S.; Yoon, M.-C.; Kim, D. *Chem. Commun.* **2009**, 261.
- (136) Alkorta, I.; Blanco, F.; Elguero, J. *Centr. Eur. J. Chem.* **2009**, *7*, 683.
- (137) Seidel, D.; Lynch, V.; Sessler, J. L. *Angew. Chem. Int. Ed.* **2002**, *41*, 1422.
- (138) Kohler, T.; Seidel, D.; Lynch, V.; Arp, F. O.; Ou, Z.; Kadish, K. M.; Sessler, J. L. *J. Am. Chem. Soc.* **2003**, *125*, 6872.
- (139) Buda, M.; Iordache, A.; Bucher, C.; Moutet, J.-C.; Royal, G.; Saint-Aman, E.; Sessler, J. L. *Chem. A Eur. J.* **2010**, *16*, 6810.
- (140) Iordache, A.; Melfi, P.; Bucher, C.; Buda, M.; Moutet, J.-C.; Sessler, J. L. *Org. Lett.* **2008**, *10*, 425.
- (141) Bucher, C.; Devillers, C. H.; Moutet, J.-C.; Pecaut, J.; Sessler, J. L. *Chem Commun.* **2006**, 3891.
- (142) Sessler, J. L.; Seidel, D.; Vivian, A. E.; Lynch, V.; Scott, B. L.; Keogh, D. W. *Angew. Chem. Int. Ed.* **2001**, *40*, 591.
- (143) Setsune, J.-i.; Toda, M.; Watanabe, K.; Panda, P. K.; Yoshida, T. *Tetrahedron Lett.* **2006**, *47*, 7541.
- (144) Andrieux, C. P.; Hapiot, P.; Audebert, P.; Guyard, L.; Dinh An, M. N.; Groenendaal, L.; Meijer, E. W. *Chem. Mat.* **1997**, *9*, 723.
- (145) Pavlishchuk, V. V.; Addison, A. W. *Inorg. Chim. Acta* **2000**, *298*, 97.
- (146) van Haare, J. A. E. H.; Groenendaal, L.; Havinga, E. E.; Janssen, R. A. J.; Meijer, E. W. *Angew. Chem. Int. Ed.* **1996**, *35*, 638.
- (147) Furhop, J. H.; Kadish, K. M.; Davis, D. G. *J. Am. Chem. Soc.* **1973**, *95*, 5140.
- (148) van Haare, J. A. E. H.; Groenendaal, L.; Peerlings, H. W. I.; Havinga, E. E.; Vekemans, J. A. J. M.; Janssen, R. A. J.; Meijer, E. W. *Chem. Mat.* **1995**, *7*, 1984.

Vita

Vladimir Roznyatovskiy was born in Moscow, Russia, on March 14, 1983 the son of Dr. Raisa Vinnik and Dr. Vitaliy Roznyatovskiy. After graduating from “Lycee Vtoraya Shkola” High School, Moscow, Russian with advanced courses in chemistry and biology in 2000, he entered M. V. Lomonosov Moscow State University, Department of Chemistry, Moscow, Russia. He received Diplom in Chemistry in 2005 under the supervision of Prof. Yuri Ustynuk. In June of 2006, he entered the Graduate School of the University of Texas at Austin.

Permanent address: 55/7 Vavilova str, apt 7, Moscow, Russia, 117312

This dissertation was typed by Vladimir Roznyatovskiy.